

The interaction of phenelzine with human monoamine oxidase B: characterization and  
consequences

by

Morganne Held

A thesis submitted in partial fulfillment of the requirements for the degree of

Master of Science

Department of Psychiatry

University of Alberta

© Morganne Held, 2022

## ABSTRACT

Phenelzine (PLZ) is a monoamine oxidase (MAO) inhibitor developed in the 1960s which has been used clinically for psychiatric conditions such as depression and anxiety disorders. However, despite over 60 years of research, the mechanism by which PLZ exerts its effects on MAO has yet to be satisfactorily described. The work presented in this thesis has investigated the mechanism of inhibition of human MAO-B by PLZ and discussed these findings in the context of two mechanisms: the forked mechanism and the stepwise mechanism.

First of all, the formation of  $\beta$ -phenylethylidenehydrazine (PEH) from the metabolism of PLZ by MAO-B was examined through high pressure liquid chromatography-mass spectrometry (LC-MS) analysis of deuterated incubations of MAO-B and PLZ. This provided evidence for the intramolecular rearrangement of the diazene intermediate  $\beta$ -phenylethyldiazene (PEDz) to PEH in bulk solvent, contrary to the forked mechanism which states that inactivation of MAO-B occurs *in situ*.

Secondly, the role of oxygen in the covalent modification of the flavin cofactor of MAO-B by PEDz was examined through inclusion of the redox dye 2,6-dichlorophenolindophenol (DCPIP) in anaerobic incubations of MAO-B and PLZ. These results suggest that oxygen may be necessary for both re-oxidation of the flavin cofactor and radicalization of PEDz to form a phenylethyl radical.

Chapter 4 further examined the dissociation of PEDz from the active site, building on the indirect evidence detailed in Chapters 2 and 3, through use of the free radical scavenger ascorbate and chelating agent diethylenetriaminepentaacetic acid (DTPA). These findings suggest a stabilizing effect for PEDz by ascorbate, preventing loss of the inhibiting compound to PEH formation before rebinding to and inhibiting oxidized enzyme.

Finally, the characteristics of irreversible inhibition of MAO-B by a range of PLZ concentrations were compared by utilizing a membrane particle centrifugation protocol which was optimized in Chapter 5. At a single concentration of MAO-B, inhibition by PLZ differed significantly, and in an unexpected manner, in half-life and extent of inactivation depending on whether the concentration of PLZ was in the low-mid micromolar range, or at a super-saturating mid-millimolar concentration. While increased half-lives at high PLZ concentrations were consistent with dissociation of PEDz from the reduced active site and with competition between PEDz, PEH, and PLZ for reassociation, the magnitude and nature of the effect implicated a role for inter-subunit communication. Results are consistent with the idea that the redox state of one monomer may be sensed by the opposing monomer through movement of gating loops, and that this communication may be disrupted by binding of PLZ at high concentrations to a site distinct from the active site - possibly the I<sub>2</sub> site in the entrance channel of the inactivated monomer.

The findings in this thesis suggest that the mechanism by which MAO is inhibited by PLZ is rather more complex than first thought. Indeed, elucidation of the complete mechanism may provide much insight into the role of gating loops in communication within the dimer, information invaluable for development of novel drug therapies targeting dimeric flavin-containing amine oxidases.

## ACKNOWLEDGEMENTS

I would like to take this opportunity to sincerely thank my supervisor, Dr. Andrew Holt, for providing me the opportunity to work on this project and for his continuous patience and advice. I am also grateful to my supervisory committee members, Drs. Glen Baker and Dmitriy Matveychuk, whose thesis my own follows, for their guidance, suggestions, and support in my program.

Endless thanks to Tricia Kent, the lab tech/mom of the Neurochemical Research Unit, for her friendship and constant source of humor over the years, and special thanks to the late Gail Rauw for her invaluable knowledge and guidance in the use of the LC-MS technique utilized in Chapter 2 of this thesis. We also thank Professor Dale Edmondson (Emory University, Atlanta, GA) for providing *Pichia pastoris* yeast over-expressing human MAO-B, as well as batches of purified and mitochondrial membrane-bound human MAO-B derived from yeast fermentations.

Funding was provided by TRIP funding to Dr. G. Baker from the Faculty of Medicine & Dentistry. This work was also supported by a FoMD 75<sup>th</sup> Anniversary Award, an Alberta Graduate Excellence Scholarship, a COVID-19 Graduate Student Support Grant, and a Graduate Completion Scholarship awarded by the University of Alberta.

Last but not least, to my friends and family, none of this would have been possible without your constant support. To my parents, Steve and Andrea Held, and my brother, Jason Held, thank you for rooting for me despite not having a clue what I was doing. And finally, to my wonderful partner, Nicholas Batty, you are my favorite human and your constant belief in me, especially when I did not believe in myself anymore, will not be forgotten.

## TABLE OF CONTENTS

1. Chapter One: General Introduction.....	1
1.1. Monoamine Oxidase .....	1
1.1.1. Amine Oxidases .....	1
1.1.2. MAO: Two Isozymes .....	4
1.1.3. Structural Information .....	6
1.1.4. Substrate Metabolism by Oxidative Deamination .....	10
1.2. Inhibition of MAO .....	14
1.2.1. Reversibility and Selectivity of Monoamine Oxidase Inhibitors (MAOIs) ....	14
1.2.2. Side Effects of MAOIs .....	14
1.3. Phenelzine and its Metabolites .....	18
1.3.1. Phenelzine.....	18
1.3.2. Phenylethylidenehydrazine (PEH).....	21
1.3.3. Phenylethyldiazene (PEDz).....	21
1.4. Thesis Overview .....	23
1.4.1. Currently Proposed Mechanism of Inhibition of MAO by Phenelzine.....	23
1.4.2. Hypotheses and Specific Aims .....	26
2. Chapter Two: An Examination of the Source of PEH Formed During the Metabolism of PLZ by MAO-B .....	28
2.1. Introduction .....	28
2.1.1. Hypotheses.....	33
2.1.2. Specific Aims.....	33
2.2. Materials and Methods.....	33
2.2.1. Materials .....	33
2.2.2. Buffer.....	34
2.2.3. Benzaldehyde Assay .....	34
2.2.4. LC-MS.....	35
2.2.5. Analysis and Statistics.....	35
2.3. Results and Discussion.....	37

2.3.1. Determination of MAO-B Concentration.....	37
2.3.2. pH Determination.....	38
2.3.3. LC-MS .....	40
2.3.4. Controls .....	41
2.4. Conclusions .....	43
3. Chapter Three: Use of the Redox Dye DCPIP to Explore the Role of Oxygen in the Inhibition of MAO-B by PLZ .....	44
3.1. Introduction .....	44
3.1.1. The Role of O <sub>2</sub> in Inhibition of MAO-B by PLZ.....	44
3.1.2. Hypotheses.....	46
3.1.3. Specific Aims.....	46
3.2. Materials and Methods .....	47
3.2.1. Materials .....	47
3.2.2. Anaerobic Experiments .....	47
3.2.3. MAO-B Incubation .....	48
3.2.4. Benzaldehyde Assay .....	48
3.2.5. Analysis and Statistics.....	48
3.3. Results and Discussion.....	49
3.3.1. Spectral Properties of DCPIP .....	49
3.3.2. Interactions .....	51
3.3.3. Aerobic MAO-B Incubation.....	55
3.3.4. Anaerobic MAO-B Incubation .....	59
3.4. Conclusion.....	64
4. Chapter Four: Evidence for the Dissociation of PEDz From the Active Site of Reduced MAO-B .....	66
4.1. Introduction .....	66
4.1.1. Hypotheses.....	68
4.1.2. Specific Aims.....	68
4.2. Materials and Methods.....	69

4.2.1. Materials .....	69
4.2.2. MAO-B Incubation .....	70
4.2.3. Spectrophotometry .....	70
4.2.4. Benzaldehyde Assay .....	71
4.2.5. Amplex Red Peroxidase Assay .....	71
4.2.6. Ascorbate Oxidation.....	72
4.2.7. Membrane Particle Preparations .....	72
4.2.8. Analysis and Statistics.....	73
4.3. Results and Discussion.....	74
4.3.1. Ascorbate Redox Profile.....	74
4.3.2. Chelating Iron Contaminants in Buffer .....	75
4.3.3. Interactions with PEH or PLZ .....	75
4.3.4. MAO-B Test .....	76
4.3.5. Diazene Sequestering Agents .....	78
4.3.6. Membrane Particles.....	81
4.3.7. Influence of DTPA and Ascorbate Together on Inhibition .....	84
4.3.8. Is Ascorbate Reducing PEH to PEDz, Thereby Increasing the Rate of Inhibition by PLZ?.....	87
4.3.9. Ascorbate Concentration Response.....	88
4.3.10. DTPA Concentration Response .....	91
4.5. Conclusion.....	92
5. Chapter Five: Unexpected Mechanistic Insights From a Study of the Concentration- Dependence of MAO-B Inhibition by PLZ .....	94
5.1. Introduction .....	94
5.1.1. Hypotheses.....	95
5.1.2. Specific Aims.....	96
5.2. Materials and Methods.....	96
5.2.1. Materials .....	96
5.2.2. MAO-B Incubation .....	97
5.2.3. Membrane Particle Preparation.....	98

5.2.4. Benzaldehyde Assay .....	99
5.2.5. Amplex Red Assay.....	99
5.2.6. Analysis and Statistics.....	100
5.3. Results .....	100
5.3.1. Effects of MAO-B Concentration on Rate of Inactivation by PLZ .....	100
5.3.2. Inhibitor Plots for Mofegiline, Pargyline, and Phenelzine .....	103
5.3.3. Membrane Particle Protocol Development.....	107
5.3.4. Can We Reach Complete Inhibition of MAO-B by PLZ? .....	111
5.3.5. Effects of High PLZ Concentrations on MAO-B Inactivation .....	114
5.3.6. Effects of Low PLZ Concentrations on MAO-B Inactivation.....	116
5.3.7. Comparison of Inhibition of MAO-B by High and Low Concentrations of PLZ .....	118
5.4. Discussion & Conclusion .....	122
6. Chapter Six: General Discussion and Future Directions .....	130
6.1. Summary of Novel Findings .....	130
6.1.1. What We Have Learned About PLZ.....	130
6.1.2. What We Have Learned About MAO-B .....	132
6.2. Limitations and Future Directions .....	133
6.2.1. Chapter 2.....	133
6.2.2. Chapter 3.....	134
6.2.3. Chapter 4.....	135
6.2.4. Chapter 5.....	136
Bibliography.....	138

## LIST OF FIGURES

Figure 1.1 Differences between classes of amine oxidase.....	3
Figure 1.2 Structures of MAO-A and MAO-B inhibitors and substrates.....	5
Figure 1.3 Active site domain structural differences between human MAO-A and -B. ....	9
Figure 1.4 Oxidative deamination of the amine benzylamine (BZ) by MAO-B. ....	11
Figure 1.5 Proposed mechanisms for the removal of H from C <sub>α</sub> of amine substrates. ....	12
Figure 1.6 Re-oxidation of reduced FAD by binary or ternary complex formation. ....	13
Figure 1.7 Structures of PLZ and its metabolites compared to the structure of PEA. ....	19
Figure 1.8 Proposed mechanisms for the metabolism of phenelzine and the inhibition of MAO-B by its metabolites. ....	24
Figure 1.9 Inconsistencies in observations under current proposed mechanism. ....	25
Figure 2.1 Examples of substrates of MAO which contain a phenylethylamine (PEA) backbone. ....	29
Figure 2.2 Intramolecular rearrangement of PEDz to PEH and incorporation of deuterium.....	32
Figure 2.3 Representative chromatographs for PEH in deuterated buffer.....	36
Figure 2.4 Representative change in absorbance due to benzaldehyde formation over time. ....	37
Figure 2.5 Determination of optimal pH for MAO-B activity.....	39
Figure 2.6 Determination of pD for least background hydrogen deuterium exchange. ....	40
Figure 2.7 Comparison of deuterium incorporation into PEH by two distinct pathways. ....	41
Figure 2.8 Comparison of %HDX values for deuterated and non-deuterated samples. ....	42
Figure 3.1 Spectral characteristics of DCPIP.....	50
Figure 3.2 Calculation of molar absorption coefficient of benzaldehyde.....	52
Figure 3.3 Spectral interaction between DCPIP and PLZ and its metabolites. ....	53
Figure 3.4 Interaction between 50 μM DCPIP and PLZ in 0.1 M KP buffer at 30°C. ....	54
Figure 3.5 Re-oxidation of MAO-B by DCPIP during incubation with PLZ.....	55
Figure 3.6 Aerobic incubation of 2.8 nM MAO-B and PLZ with or without DCPIP.....	56
Figure 3.7 Aerobic incubation of 6 nM MAO-B and PLZ with or without DCPIP.....	58
Figure 3.8 Influence of DCPIP on inhibition of MAO-B by PLZ with or without O <sub>2</sub> present. ....	61

Figure 3.9 Comparisons between $\pm$ DCPIP for aerobic and anaerobic reactions. ....	63
Figure 4.1 Reaction mechanism for ascorbate. ....	67
Figure 4.2 Absorbance of ascorbate in presence or absence of excess antioxidants.....	74
Figure 4.3 Ascorbate autoxidation in NaP buffer $\pm$ chelator. ....	77
Figure 4.4 Soluble MAO-B inhibition by PLZ in the presence of ascorbate.....	79
Figure 4.5 Interaction between ascorbate and free radical scavengers.....	80
Figure 4.6 Influence of ascorbate on inhibition of MAO-B by PLZ.....	83
Figure 4.7 Influence of ascorbate and DTPA on inhibition of MAO-B by PLZ. ....	85
Figure 4.8 Inhibition of MAO-B by PEH in the presence of ascorbate and/or DTPA.....	88
Figure 4.9 Inhibitor plots for inhibition of MAO-B by ascorbate, $\pm$ PLZ, $\pm$ DTPA.....	90
Figure 4.10 Inhibitor plot for MAO-B and PLZ incubated in a range of DTPA concentrations.....	91
Figure 5.1 Impact of MAO-B concentration on inhibition by PLZ. ....	102
Figure 5.2 Inhibitor plots for the inhibition of a range of MAO-B concentrations by mofegiline, pargyline, and phenelzine.....	106
Figure 5.3 Mofegiline titration of MAO-B activity to determine stock concentration. ..	107
Figure 5.4 Influence of centrifuge rotor size and speed on PLZ removal from incubation. ....	109
Figure 5.5 Extent of PLZ removal by centrifugation. ....	110
Figure 5.6 Inhibition of membrane particle-bound MAO-B by PLZ.....	113
Figure 5.7 High [PLZ] inhibition of MAO-B followed by mofegiline titration. ....	115
Figure 5.8 Initial rate of activity remaining in MAO-B plotted against log[PLZ].....	117
Figure 5.9 Initial rate of activity remaining in MAO-B versus incubation time.....	117
Figure 5.10 Inhibition of 16 nM MAO-B by low PLZ (25 $\mu$ M) over time. ....	119
Figure 5.11 Inhibition of 16 nM MAO-B by high PLZ (25 mM) over time. ....	121
Figure 5.12 Proposal for mechanism of MAO-B inactivation via inter-subunit communication .....	1275
Figure 5.13 Increase in $K_M$ for BZ after pre-incubation of MAO-B with PLZ.....	127

## LIST OF TABLES

Table 3.1 .....	61
Table 5.1 .....	109

## LIST OF ABBREVIATIONS

%HDX <sub>inc</sub>	percent HDX in incubation
%HDX <sub>PEH</sub>	percent HDX in PEH
μM	micromolar
2-BFI	2-(2-benzofuranyl)-2-imidazoline
5-HT	5-hydroxytryptamine; serotonin
A <sup>•</sup>	ascorbate radical
A/Abs	absorbance
A <sup>-</sup>	ascorbate anion
AA	ascorbic acid
AD	Alzheimer's disease
ANOVA	analysis of variance
AR/P	Amplex Red/peroxidase assay
AUC	area under the curve
AZIPI	2-(3-azido-4-[ <sup>125</sup> I]iodophenoxy)methylimidazoline
BZ	benzylamine
CAO	copper amine oxidase
CI <sub>95</sub>	95% confidence interval
CNS	central nervous system
Cu <sup>2+</sup>	copper cation
D <sub>2</sub> O	deuterium oxide
DA	dopamine
DCPIP	2,4-dichlorophenolindophenol (oxidized)

DCPIPH <sub>2</sub>	2,4-dichlorophenolindophenol (reduced)
DHA	dehydroascorbate
D-NaP	deuterated sodium phosphate buffer
DOPAL	3,4-dihydroxyphenylacetaldehyde
DOPEGAL	3,4-dihydrophenylglycolaldehyde
D-PEH	deuterated PEH
DTPA	diethylenetriaminepentaacetic acid
E.FADox	enzyme containing oxidized cofactor
E.FADred	enzyme containing reduced cofactor
EC (number)	enzyme commission number
EDTA	ethylenediaminetetraacetic acid
FAD	flavin adenine dinucleotide
Fe <sup>2+/3+</sup>	iron cation
FMN	flavin mononucleotide
GABA	γ-aminobutyric acid
GSH	glutathione
H <sub>2</sub> O <sub>2</sub>	hydrogen peroxide
H <sub>2</sub> PO <sub>4</sub> <sup>-</sup>	mono-basic phosphoric acid salt
HCl	hydrochloric acid
HDX	hydrogen deuterium exchange
hMAO	human monoamine oxidase
HPLC	high pressure liquid chromatography
HPO <sub>4</sub> <sup>2-</sup>	di-basic phosphoric acid salt

HRP	horseradish peroxidase
I <sub>2</sub> site	imidazoline binding site on MAO-B
IC <sub>50</sub>	half-maximal inhibitory concentration
KCl	potassium chloride
k <sub>inact</sub>	rate constant for irreversible inactivation by a mechanism-based inhibitor
K <sub>D</sub>	dissociation constant
KP	potassium phosphate buffer
LC-MS	liquid chromatography-mass spectrometry
LTQ	lysine tyrosylquinone
m/z	mass-to-charge ratio
MAO	monoamine oxidase
MAOI	monoamine oxidase inhibitor
mM	millimolar
mOD	milli-optical density
MS	mass spectrometry
NA	noradrenaline
NAcCys	N-acetylcysteine
NaP	sodium phosphate buffer
nM	nanomolar
O <sub>2</sub>	oxygen
OD	optical density
PAcA	phenylacetic acid
pD	-log of deuterium ion concentration

PD	Parkinson's disease
PEA	$\beta$ -phenylethylamine
PEDz	$\beta$ -phenylethyldiazene
PEH	$\beta$ -phenylethylidenehydrazine
pH	$-\log$ of hydrogen ion concentration
PLZ	phenelzine; $\beta$ -phenylethylhydrazine
PrAO	primary amine oxidase
RIMA	reversible inhibitor of monoamine oxidase-A
RT	retention time
S	substrate
SEM	standard error of the mean
SIM	single ion monitoring
SSRI	selective serotonin reuptake inhibitor
$t_{1/2}$	half-life (of inactivation)
TCP	tranylcypromine
TPQ	topaquinone
UV	ultraviolet
$v$	initial rate of enzyme activity (absorbance/time)
$V_{\max}$	maximum rate of enzyme activity (absorbance/time)
$\epsilon$	molar absorption coefficient

# Chapter One

## General Introduction

### 1.1. Monoamine Oxidase

#### 1.1.1. Amine Oxidases

Monoamine oxidase (MAO) (EC [Enzyme Commission number] 1.4.3.4) is a member of the amine oxidase family and is responsible for the oxidative deamination of many important biogenic and dietary amines in almost every tissue in mammals (Tipton et al., 2004). Discovered in 1928 (Hare), it was originally given the name tyramine oxidase (EC 1.4.3.9) and assumed to be one enzyme. It was renamed in 1938 as monoamine oxidase (Zeller). Eventually, inconsistencies in inhibition across multiple tissues and species led to the hypothesis that what was thought to be one enzyme might actually be two separate enzymes (Fowler et al., 1978; Johnston, 1968). This hypothesis was confirmed when Bach et al. (1988) located two similar but distinct X-linked genes for MAO.

MAO is just one of many families of amine oxidases, which have historically been categorized into two groups (within EC 1.4.3): copper-containing enzymes (CAO) and flavin-containing enzymes (to which MAO belongs). While CAOs do utilize copper as a secondary cofactor, the primary cofactor in amine oxidation is a quinone (Janes et al., 1990). For example, primary amine oxidase (PrAO; EC 1.4.3.21) utilizes topaquinone (TPQ; Figure 1.1a) (Holt et al., 1998), as do plasma amine oxidase (EC 1.4.3.6; Janes et al., 1990) and diamine oxidase (EC 1.4.3.22; Steinebach et al., 1995). Lysyl oxidase (EC 1.4.3.13; Wang et al., 1996) on the other hand contains a lysine tyrosylquinone (LTQ; Figure 1.1a). A quinone is a species or functional group with extensive conjugation, creating a resonance delocalized structure that makes them

effective redox centers (Moenne-Loccoz et al., 1995; Klinman, 1996). Indeed, flavin cofactors such as flavin mononucleotide (FMN) and flavin adenine dinucleotide (FAD) also contain quinone groups which aid in accepting and redistributing electrons from the donor (Figure 1.1a).

As well, this categorization is a little misleading as it leaves out such amine oxidases as the flavin-containing polyamine oxidases (EC 1.5.3.13–1.5.3.17), as these enzymes are within a separate subclass. In EC nomenclature, the second value denotes the functional group of the donor species acted upon by the enzyme, while the third value denotes the electron acceptor; therefore, enzymes belonging to subclasses EC 1.4.3 versus 1.5.3 only differ by whether the initial electron is donated by a CH-NH<sub>2</sub> or a CH-NH functional group, respectively (Figure 1.1b). This has resulted in much confusion and, as is common in taxonomy, contention about how to properly categorize amine oxidases.

MAO's catalytic activity is mediated through covalently linked FAD. The FAD cofactor is involved in oxidation of amines to imines, which are released into the cytosol and non-enzymatically hydrolyzed to aldehydes and ammonia (primary amines) or substituted amines (secondary amines) (Binda et al., 2002; Tipton et al., 2004; Youdim et al., 2006). The now-reduced cofactor is then re-oxidized by molecular oxygen, releasing hydrogen peroxide.

MAO serves many roles in the body, depending on its location and abundance: regulation of vesicular concentrations of neurotransmitters through biogenic amine deamination in the central and peripheral nervous systems, metabolism of dietary amines in the liver, and modulation of exogenous amine levels in the peripheral nervous system (Youdim et al., 2006).

MAO exists predominantly as two isozymes, MAO-A and MAO-B, which are expressed in nearly every tissue in the mammalian body. MAO-A and -B are coded by separate genes which

share 70% sequence homology in humans (Bach et al., 1988) and are thought to be the result of a gene duplication event (Grimsby et al., 1991). In the interest of narrowing the scope of this thesis, specifics contained within will pertain to human MAO, unless otherwise indicated, and may not reflect non-human species.

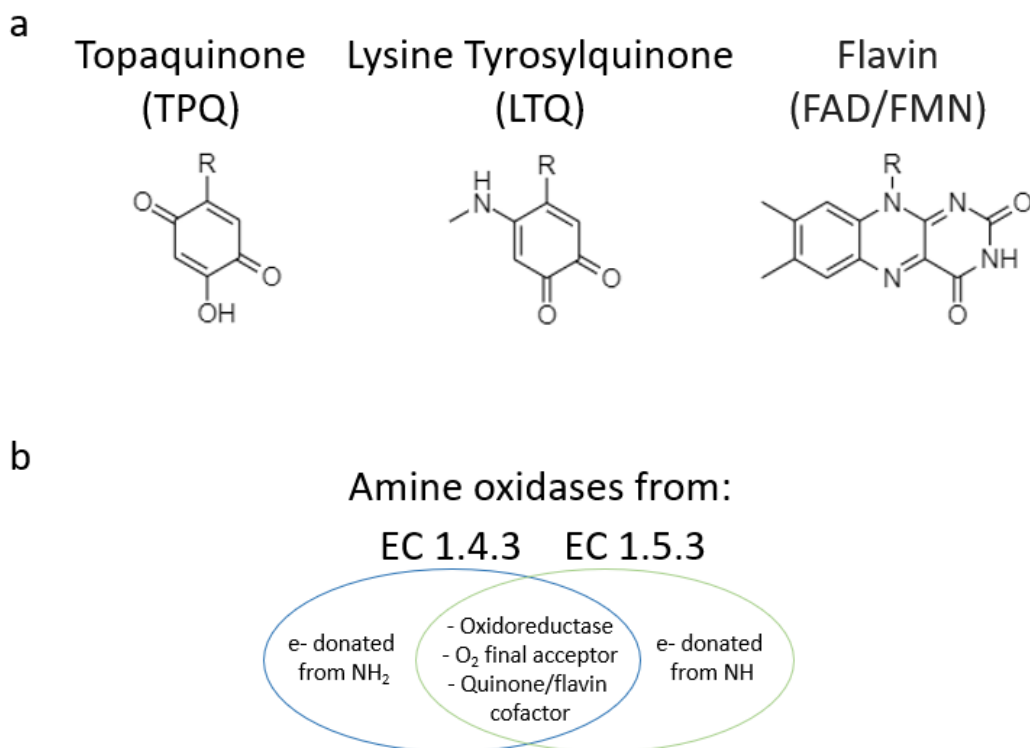


Figure 1.1 Differences between classes of amine oxidase.

(a) Quinone cofactors in amine oxidases. Topoquinone (TPQ) is in primary amine oxidase (PrAO), diamine oxidase, and plasma amine oxidase; lysyl oxidase contains a lysine tyrosylquinone (LTQ); and flavin cofactors such as FMN and FAD are found in amine oxidases from groups EC 1.4.3 and 1.5.3. R = alanine (TPQ) or lysine (LTQ), within the protein's amino-acid backbone, D-ribitol and adenosine monophosphate (FAD), and D-ribitol (FMN). (b) Overlap in features of amine oxidases from groups EC 1.4.3 (blue circle) and 1.5.3 (green circle). Despite this overlap in function, amine oxidases are commonly only classified within EC 1.4.3, where they are further split into copper-containing and flavin-containing. This is despite the fact that the amine oxidases represented in this Venn diagram utilize a quinone/flavin cofactor primarily to oxidize amine substrates, and not solely copper, as the name suggests.

### 1.1.2. MAO: Two Isozymes

Each gene produces its own globular protein (59.7 kDa for A and 58.0 kDa for B); these monomers dimerize before mitochondrial membrane insertion, resulting in homo-dimeric transmembrane proteins of about 120kDa (Bach et al., 1988). Each subunit is composed of the greater globular domain, a membrane binding domain, and an active site. A transmembrane C-terminal alpha helix embedded perpendicular to the plane of the membrane anchors each monomer to the cytosolic face of the outer mitochondrial membrane. The active site is a cavity that extends into the middle of the subunit, ending with a FAD molecule covalently bound by a thioether link to cysteine 397 (in MAO-B; Bach et al., 1988), creating the substrate binding domain. The two monomers are believed to operate independently of one another. Although communication between monomers occurs in many homodimers, including in copper amine oxidases (Frébert et al., 1995; Klinman, 1996), no kinetic evidence has been presented that suggests this to be the case with MAO.

Although they share a lot of similarities and are co-expressed in most mammalian tissues, MAO-A and MAO-B are still distinct and separate enzymes, differing in expression (depending on tissue type and age), substrate binding, and pharmacological inhibition. For example, in primates, MAO-B is not found in the placenta as MAO-A develops first in the fetus, but platelets only express MAO-B. MAO-A is highly expressed in the heart and catecholaminergic neurons, preferentially metabolizes 5-hydroxytryptamine (5-HT, serotonin) and noradrenaline (NA), and is inhibited by clorgyline. MAO-B is found predominantly in glial cells, preferentially metabolizes benzylamine (BZ) and  $\beta$ -phenylethylamine (PEA), and is inhibited by l-deprenyl (selegiline) and mofegiline (Westlund et al., 1985; Westlund et al., 1988). Dopamine (DA), adrenaline, and tyramine are metabolized by both enzymes with similar efficiency (Youdim et al., 2006). These

are not hard divisions however, as most tissues in the body contain differing ratios of the two isozymes, and both forms have the flexibility to catalyze the metabolism of at least some of the other's preferred substrates, given high enough concentration of the ligand (Figure 1.2).

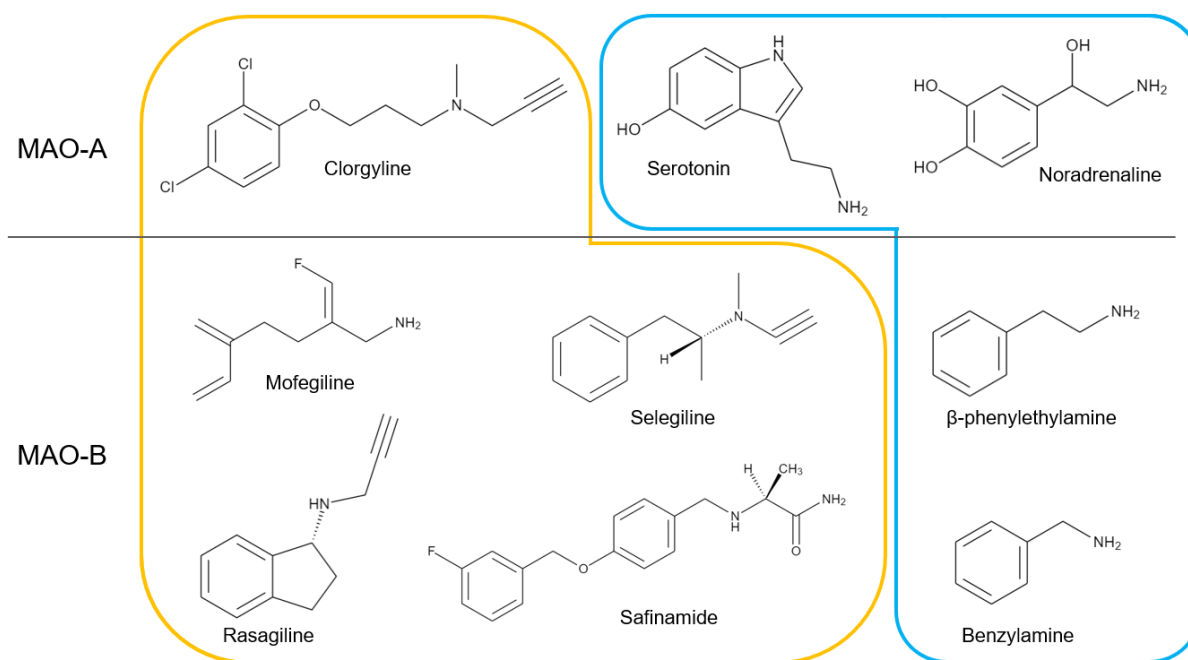


Figure 1.2 Structures of MAO-A and MAO-B inhibitors and substrates. Yellow box contains inhibitors and blue box contains substrates.

Although these enzymes are found across mammalian species, the activity and localization of the isozymes vary, sometimes greatly, between species. This, and slight protein structure differences, results in altered affinities and turnover rates for substrates and effects of inhibitors between species, which must be considered when the source of enzyme in an experiment is non-human. For instance, rat brains have a greater amount of MAO-A than MAO-B, and MAO-A predominates in dopamine metabolism. Dopamine preservation in rat brains would therefore be through MAO-A inhibition (Willis & Kennedy, 2004). However, in human brains, neither isozyme

predominates in expression, and the MAO-B inhibitor safinamide has recently been FDA-approved for early-stage Parkinson's disease (Fabbri et al., 2015).

### 1.1.3. Structural Information

Other differences between MAO-A and -B lie in their structures; the active site cavities are markedly different, resulting in many of the substrate and inhibitor differences seen between the two isozymes (Figure 1.3). MAO-A has an active site that is shallow in depth but wide and flexible, with a volume of  $\sim 400 \text{ \AA}^3$  (De Colibus et al., 2005). MAO-B, on the other hand, has an active site which is narrow and extends further into the middle of the enzyme, with a volume of  $\sim 710 \text{ \AA}^3$  (Binda et al., 2002). These structural differences, along with other key active site structures, contribute to the specificity of clorgyline for MAO-A and of selegiline for MAO-B (Milczek et al., 2011).

The active site of MAO-B is functionally and structurally dipartite (Binda et al., 2002; Figure 1.3). The active site begins with the first cavity, the entrance channel ( $\sim 290 \text{ \AA}^3$ ), which is physically separated from the second cavity, the FAD-containing substrate binding cavity ( $\sim 420 \text{ \AA}^3$ ), by the side chains of Ile199 and Tyr326 (Figure 1.3). These “gating” residues can easily move to an “open” conformation in order to accommodate binding of molecules with an extended conformation, such as farnesol (Milczek et al., 2011), while the “closed” conformation prevents substrate access to or product dissociation from the active site, observable when tranylcypromine (TCP) or PEA are bound (McDonald et al., 2010).

The 3D crystal structure of TCP-bound MAO-B further incubated with 2-(2-benzofuranyl)-2-imidazoline (2-BFI) confirmed the existence of an allosteric binding site within the entrance channel. This site, termed the  $I_2$  binding site, is formed when the Ile199 “gate” residue changes its conformation from open to closed, physically dividing the binding cavity into two separate areas.

It is thought that residues near the entrance of the binding cavity (residues 99-112) contribute to further stabilization of the I<sub>2</sub> site, creating an environment in which I<sub>2</sub> ligands bind tightly and for much longer (Basile et al., 2014; Milczek et al., 2011).

The existence of this site had been postulated for years, after it was noted by Renouard et al. (1993) that MAO-B showed micromolar affinity for imidazoline compounds. Experiments with the radiolabeled imidazoline compound 2-(3-azido-4-[<sup>125</sup>I]iodophenoxy)methylimidazoline (AZIPI) located the postulated I<sub>2</sub> binding site near the active site (Raddatz et al., 1997). Shortly after the 3D crystal structure of human MAO-B (hMAO-B) was resolved (Binda et al., 2004), the exact location of the I<sub>2</sub> binding site was determined to be in the entrance channel of the dipartite cavity, near the gating residues (McDonald et al., 2010).

I<sub>2</sub> ligands inhibit hMAO-B at the same micromolar concentrations at which they bind to this allosteric site, the result of a mixed mechanism rather than a competitive inhibition. These ligands bind and block the entrance channel, preventing access of substrate and/or departure of product, depending on whether binding of the I<sub>2</sub> ligand occurs before or after substrate binding, respectively. Raddatz et al. (1995) observed inhibition of MAO at mid-micromolar concentrations of AZIPI, despite a low-nanomolar binding affinity. While there is no evidence for inhibition of MAO-B at nM concentrations of these ligands alone, data from our laboratory suggest nM binding of 2-BFI that increases the rate at which PEA inactivates the enzyme (McDonald et al., 2010).

Further into the cavity, separated by the gating residues Tyr326 and Ile199, is the substrate binding site, in which the FAD cofactor is tethered to the enzyme via a thioether link between the C(8 $\alpha$ ) position of FAD and the MAO-B residue Cys397 (Bach et al., 1988). FAD is a planar aromatic isoalloxazine ring molecule in solution as well as in enzymes such as D-amino acid oxidase (EC 1.4.3.3; DAAO); however, in MAO as well as in some other flavoenzymes, the

molecule is bent  $\sim 30^\circ$  along the N(5)–N(10) axis (Binda et al., 2002). This is believed to influence the mechanisms by which the cofactor both catalyzes deamination of substrates and is irreversibly inhibited by various compounds by making the C(4a) atom of FAD more electrophilic and the N(5) atom beside it more nucleophilic.

Substrate binding in the active site is further facilitated by the “aromatic cage” (Li et al., 2006), composed of two tyrosine residues (Tyr398 and Tyr435 in human MAO-B), the phenolic rings of which are parallel to each other and located on the *re* face of the flavin molecule. This creates an environment which may help to orient the substrate near the flavin and/or to increase the nucleophilicity of the amine functional group (Geha et al., 2002). A highly conserved water molecule in the mostly hydrophobic substrate cavity is immobilized by hydrogen bonds to a conserved lysine residue (in humans, Lys 296) and the N(5) atom of the flavin and is displaced on substrate binding (Binda et al., 2003).

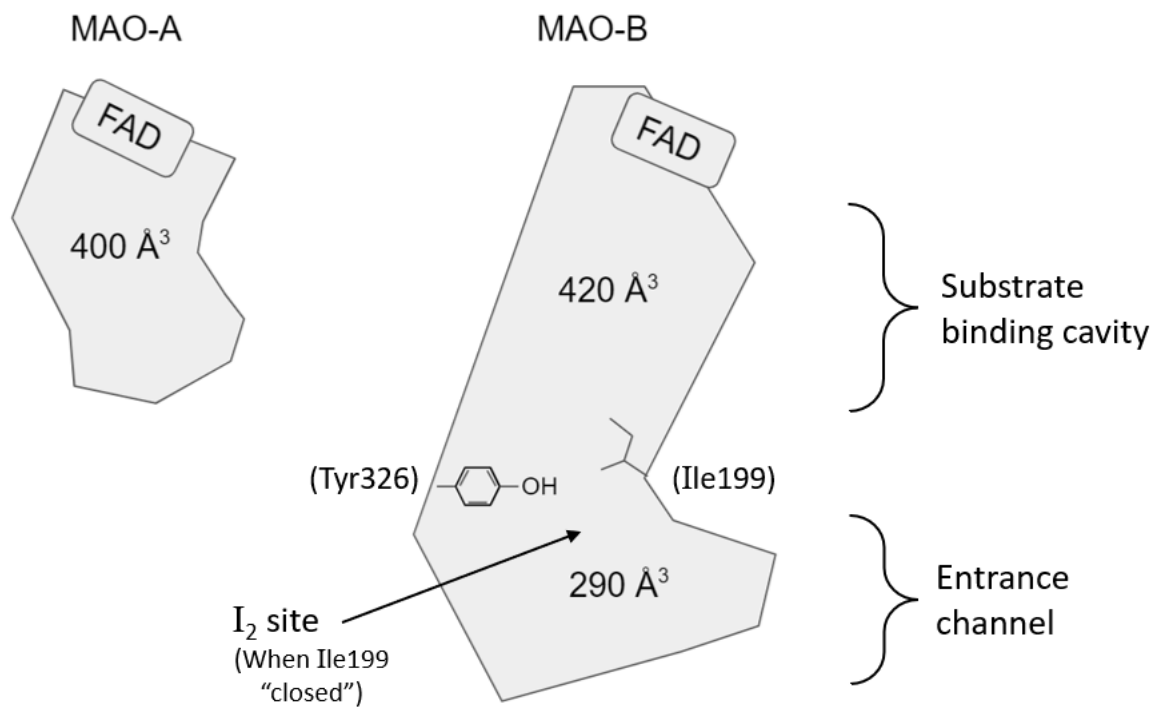


Figure 1.3 Active site domain structural differences between human MAO-A and -B. MAO-A has a shallow but flexible substrate cavity with a volume of about 400 Å<sup>3</sup>. MAO-B has a larger, narrower, and more rigid cavity which is structurally and functionally dipartite, with an entrance channel volume of ~290 Å<sup>3</sup> preceding the substrate binding cavity (~420 Å<sup>3</sup>). These cavities are physically separated by “gating” residues Ile199 and Tyr326 which undergo conformational changes to allow or prevent access to the FAD. (Figure adapted from De Colibus et al., 2005)

#### 1.1.4. Substrate Metabolism by Oxidative Deamination

MAO-B is a redox enzyme which utilizes an FAD cofactor as the initial electron acceptor and oxygen as the final electron acceptor (Figure 1.4). FAD catalyzes the reductive half-reaction, in which primary amines are oxidized to their imine via reduction of FAD. The oxidative half-reaction is initiated by a proton acceptor, usually molecular oxygen, re-oxidizing the cofactor and producing hydrogen peroxide (Rojas et al., 2015).

The flavin gains two electrons by breaking a C<sub>α</sub>-H bond in the amine substrate to form a protonated imine via a mechanism that remains debated. Three mechanisms have been proposed for the initial bond-breaking step in the reductive half reaction: the polar nucleophilic mechanism (Figure 1.5a), the hydride transfer mechanism (Figure 1.5b), and the single electron transfer mechanism (Figure 1.5c). Countless studies and multiple experimental approaches have yet either to exclude fully or to confirm one mechanism over the others (see Fitzpatrick, 2010 for review). It has even been suggested that the reduction mechanism may depend on the substrate to be metabolized (Zapata-Torres et al., 2015); how the substrate fills the enzyme cavity and interacts with the flavin, residues, and water molecules therein influences how the electrons are distributed around the substrate, and therefore how they are removed, making the existence of a one-size-fits-all mechanism less likely.

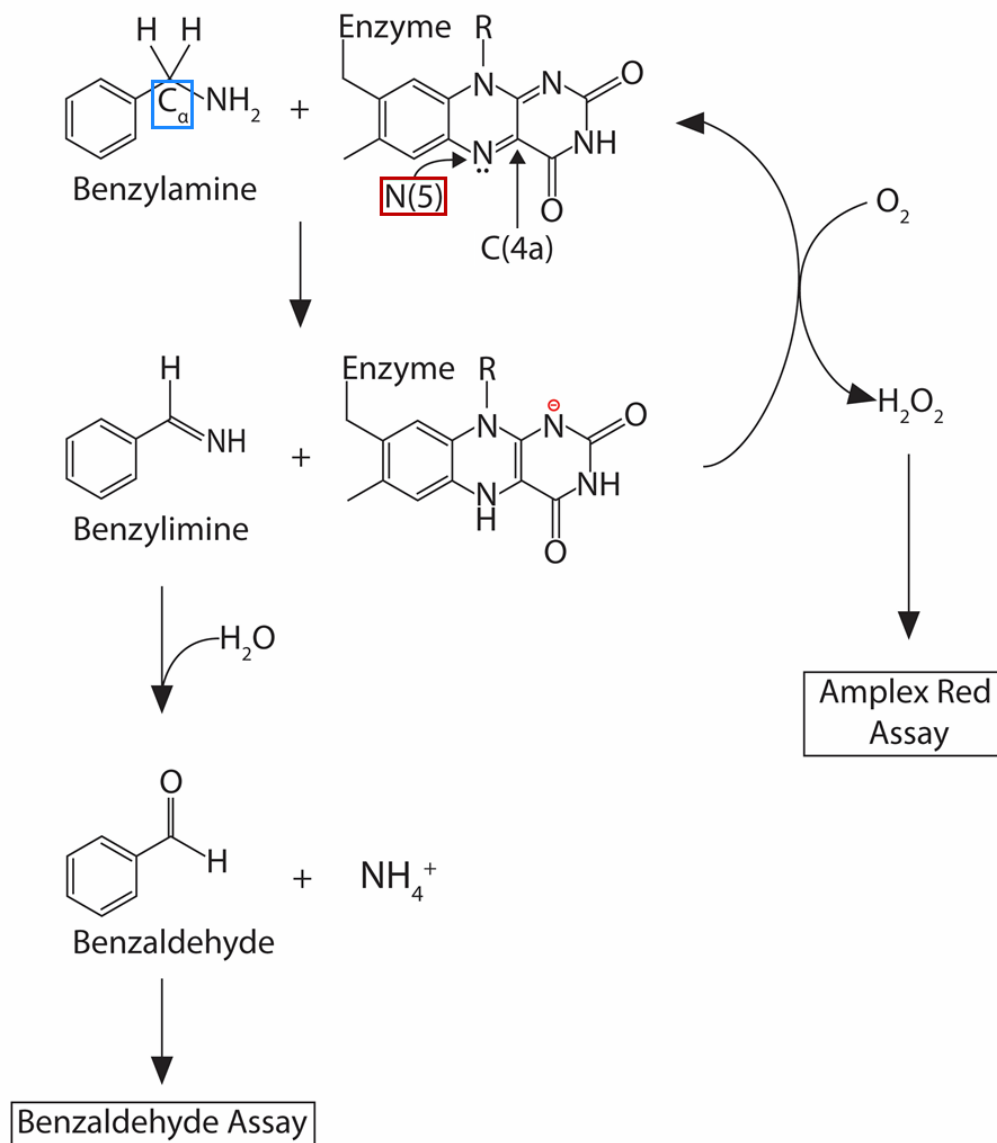


Figure 1.4 Oxidative deamination of the amine benzylamine (BZ) by MAO-B. Removal of a hydrogen from C<sub>α</sub> (blue box) of BZ by the N(5) atom of FAD (red box) produces benzylimine and reduced FAD. Molecular oxygen (O<sub>2</sub>) re-oxidizes FAD to produce H<sub>2</sub>O<sub>2</sub> and catalytically active enzyme. Benzylimine is short lived and hydrolyzes non-enzymatically to benzaldehyde and ammonia. H<sub>2</sub>O<sub>2</sub> production is measured by monitoring absorbance change at 571 nm by a spectrophotometer (Amplex Red assay) while benzaldehyde is monitored similarly at 254 nm (benzaldehyde assay). FAD R-group is adenosine monophosphate linked by D-ribose; FAD covalently attached to MAO-B by thioether linkage to Cys397.

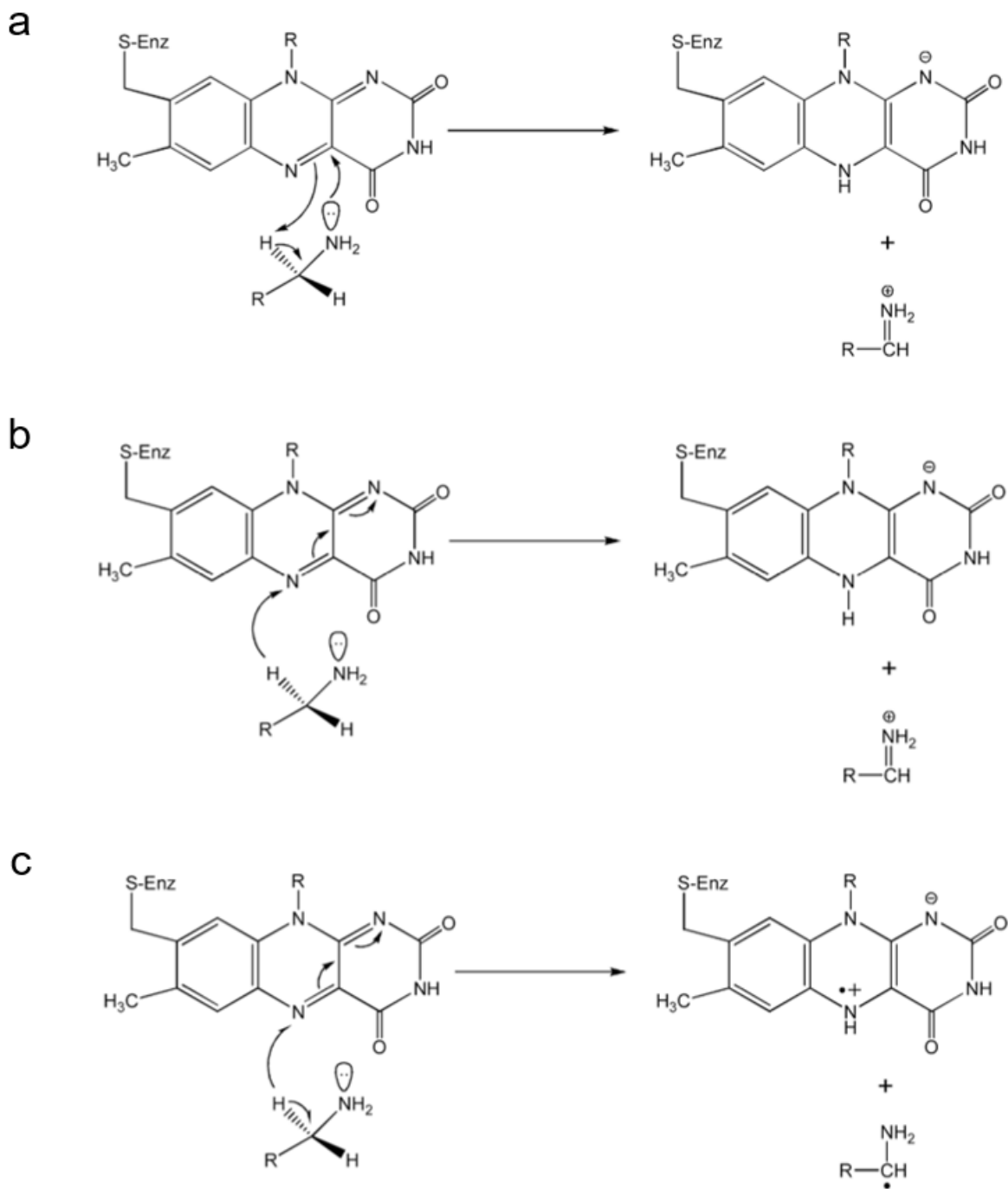


Figure 1.5 Proposed mechanisms for the removal of H from  $C_{\alpha}$  of amine substrates. **(a)** The polar nucleophilic mechanism, **(b)** the hydride transfer mechanism, and **(c)** the single electron transfer mechanism. (Figure adapted from Edmondson et al., 2009)

After substrate deamination and product release, the reduced FAD cofactor (E.FAD<sub>red</sub>) is re-oxidized. Stopped-flow analysis of the oxidative half-reaction of MAO reduced by various substrates shows evidence that suggests the amine substrate (S) may bind either to oxidized or to reduced MAO-B (Figure 1.6) (Ramsay et al., 1987). In the latter case, oxygen would bind to E.FAD<sub>red</sub>-S, generating a ternary complex and enhancing the rate of cofactor reoxidation (Figure 1.6b), compared to the rate at which flavin is re-oxidized in the binary complex between E.FAD<sub>red</sub> and oxygen (Figure 1.6a) (Ramsay, 1991; Ramsay et al., 1987; Tan & Ramsay, 1993). As the concentration of substrate increases, so too does the formation of the E.FAD<sub>red</sub>-S complex, pushing an increasing proportion of the oxidative half-reaction through the ternary pathway (Ramsay et al., 2011). The affinity with which oxygen binds in the ternary pathway is also dictated by the specific substrate being metabolized. Therefore, the catalytic rate depends upon the substrate being metabolized, as well as its concentration.

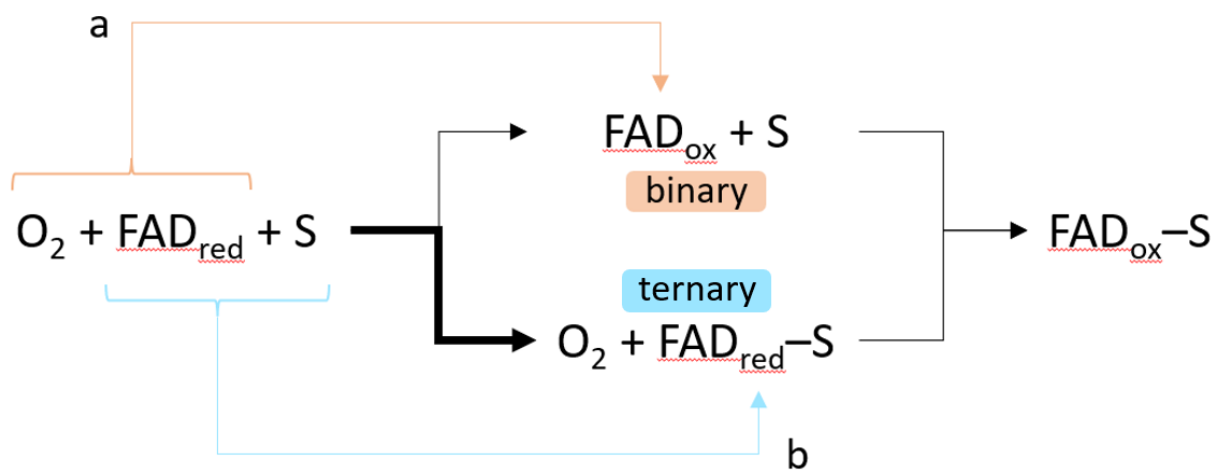


Figure 1.6 Re-oxidation of reduced FAD by binary or ternary complex formation. Oxygen can either bind to (a) a reduced flavin before binding of the substrate, resulting in a binary complex (orange), or to (b) a reduced flavin-substrate complex to form a ternary complex (blue). The affinity with which  $O_2$  binds  $FAD_{red}$  depends upon the specific substrate's  $K_D$ , with a preference for the ternary complex as substrate concentration increases (thicker arrow) and formation of the reduced flavin-substrate complex increases.

## **1.2. Inhibition of MAO**

### 1.2.1. Reversibility and Selectivity of Monoamine Oxidase Inhibitors (MAOIs)

Enzyme inhibition can be transient or permanent, depending on the ligand-enzyme interaction. Reversible inhibitors utilize hydrogen bonding and van der Waals interactions to occupy the active site and prevent substrate turnover for the duration of their stay in the active site. Tightness of ligand binding influences how long the reversible inhibitor stays in the active site, while the inhibitor concentration and competition with substrates determine how often a binding event happens. Irreversible inhibitors form very strong bonds within the active site, permanently rendering the enzyme non-functional and thus reducing activity until new enzyme can be synthesized, often taking up to 2 weeks in humans after cessation of MAOIs (Fowler et al., 1994).

The originally developed MAOIs were irreversible and non-selective, i.e., they inhibited both MAO-A and MAO-B. Several of these original MAOIs, namely phenelzine, tranylcypromine, and isocarboxazid, are still being used clinically as antidepressants. Selegiline (reviewed in Ebadi et al., 2002), which was developed later, is an MAO-B-selective, irreversible inhibitor and is used in treating early Parkinson's disease patients and, in a transdermal patch formulation at high, MAO non-selective doses, to treat depression. Moclobemide, a reversible inhibitor of MAO-A (RIMA), was developed as an MAOI which would have an improved side effect profile over the original non-selective, irreversible MAOIs (see next section).

### 1.2.2. Side Effects of MAOIs

Side effects, or adverse events, can be due to the promiscuity of the drug, resulting in so-called off-target effects, or to downstream ramifications of altering enzyme activity. Perhaps the most infamous MAOI adverse reaction is the so-called "cheese effect" resulting from the ingestion of certain tyramine-containing foods, such as aged cheeses, by patients taking the older irreversible

MAOIs. Tyramine, a strong sympathomimetic amine, is a dietary amine sometimes present in large amounts in fermented or aged foods, such as Chianti wine, soy sauce, and, of course, aged cheese. Normally, ingested tyramine is metabolized by MAO-A in the intestinal walls and liver, but when MAO-A is inhibited, tyramine in the systemic circulation can reach concentrations high enough to displace NA from sympathetic varicosities innervating vascular smooth muscle and produce a sympathomimetic pressor response (Anderson et al., 1993). This pressor response reportedly causes blood pressure increases that can result in symptoms ranging from headaches to a hypertensive crisis and death. Therefore, patients taking MAOIs receive from their pharmacist a list of foods that should be avoided while taking these drugs.

Experiments on tyramine toxicity thresholds in humans have set the limit at 50 mg tyramine before hypertensive urgency sets in (Goren et al., 2010), and research in the 1960s and 70s stated that some foods had levels as high as 3,500 mg/kg (Bullock & Irvine, 1956). Based on such information, there was grave concern from physicians about prescribing MAOIs, and they are under-prescribed to this day. However, advances in food chemistry have resulted in more sophisticated analytical techniques and better estimations of levels of tyramine and other sympathomimetic amines in foods. As well, most starter cultures needed for foods have now been engineered to contain no decarboxylating microorganisms, preventing the conversion of tyrosine to tyramine, and producing few cheeses with tyramine levels greater than 250mg/kg (Latorre-Moratalla et al., 2012). Therefore, except for a few high-tyramine foods, most of what we eat would not result in a pressor response for those taking the old irreversible MAOIs, and the lists of foods to be avoided by patients has been reduced in size (Gillman, 2018; Grady & Stahl, 2012; Meyer, 2017).

However, the concern about this side effect resulted in the testing of selegiline as an antidepressant. Selegiline had been available as a “psychic energizer” since the 1960s, and later studies showed that it was an irreversible inhibitor of MAO-B (at relatively low doses) (Knoll & Magyar, 1972), suggesting that it might be a useful antidepressant without the cheese effect. However, clinical studies indicated that inhibition of MAO-A was necessary for antidepressant activity and that oral selegiline did not have antidepressant activity until higher doses were reached (Mann, 1989); at those doses, it loses its selectivity and inhibits both MAO-A and B, making the cheese effect a potential problem. However, it has proved to be a useful drug for treating some of the symptoms of Parkinson’s disease (Riederer et al., 2004) and is also used as a transdermal patch to treat depression (Bodkin & Amsterdam, 2002). When administered as a patch, it inhibits both MAO-A and -B, but the peripheral effect on tyramine in the gut and liver is largely avoided (Bodkin & Amsterdam, 2002).

Another development resulting from concern about the cheese effect was the synthesis and testing of the RIMA moclobemide. It provides the inhibition of MAO-A necessary for antidepressant activity, but since it is a reversible inhibitor, tyramine is still metabolized by the enzyme and the “cheese effect” is avoided (Riederer et al., 2004; Waldmeier et al., 1994). Another advantage of moclobemide over the old irreversible MAOIs is the ease with which it may be withdrawn if patients do not react well to it (Nair et al., 1993). With the older, irreversible MAOIs, if patient tolerability is an issue, it takes up to 2 weeks before there is full recovery of MAO activity since new enzyme must be synthesized. With moclobemide, enzyme recovery occurs as soon as the drug is metabolized and removed from the body, usually taking 2-3 days. Moclobemide is used in many countries worldwide, but interestingly has never been approved by the FDA for use in the USA.

Although hypertension can be a problem with the older MAOIs in combination with foods containing sympathomimetic substances or with certain sympathomimetic drugs like amphetamine, when given on their own, MAOIs are much more likely to produce hypotension (Fiedorowicz & Swartz, 2004; Ricken et al., 2017).

Regarding other potential adverse effects of MAOIs, hepatotoxicity can be a problem with hydrazine-containing drugs, as the hydrazine moiety is prone to N-hydroxylation by microsomal hydroxylases in the liver, forming toxic metabolites, such as diazenes, that may wreak havoc on liver cells (Nelson et al., 1976). Iproniazid was removed from the market because of this side effect, but phenelzine has been used clinically for over 6 decades now and reports of hepatotoxicity are rare. The MAOIs can cause a large increase in concentrations of 5-HT in the body. If taken with other serotonergic medications, such as selective serotonin reuptake inhibitors (SSRIs), MAOIs can elicit a serotonin syndrome (Grady & Stahl, 2012). This response is characterized by central nervous system (CNS) disruption leading to adverse somatic (tremor), cognitive (agitation, confusion), and autonomic (hyperthermia, tachycardia) effects and is due to an increase in synaptic serotonin concentrations in the brain (reviewed in Gillman, 2011 and Buckley et al., 2014).

Despite the adverse effects mentioned above, the older MAOIs like phenelzine and tranylcypromine are still effective antidepressants, and it is considered by many clinicians and researchers that the safety issues with them have been exaggerated (see Gillman, 2011 and Gillman et al., 2020). Phenelzine and tranylcypromine continue to be used over 60 years after they were first introduced. Despite this continued use, it is interesting that much is still not known about the metabolism of phenelzine and about how it actually interacts with MAO-B to inhibit it. The studies described in this thesis were designed to increase our knowledge in these areas.

### 1.3. Phenzine and its Metabolites

#### 1.3.1. Phenzine

Phenzine ( $\beta$ -phenylethylhydrazine; Figure 1.7a) is an irreversible, non-selective inhibitor of both MAO-A and MAO-B, despite being a structural analogue of MAO-B's preferred substrate,  $\beta$ -phenylethylamine (PEA) (Figure 1.7d). It was developed as an antidepressant after the anti-tuberculosis drug iproniazid, a hydrazine-containing molecule, was found to have the unexpected effect of mood elevation in patients (Kline, 1958). Phenzine has proven to be effective in depression with an atypical mood reactivity component (so-called atypical depression) and depression that does not respond to other antidepressant treatment (treatment-resistant or treatment-refractory depression) (see Meyer et al., 2021 for review). Phenzine has also been reported to be effective in anxiety disorders including social anxiety disorder and panic disorder (Sheehan, 1980; Stein et al., 2002; Williams et al., 2020). Phenzine's use clinically has waned due to exaggerated fears regarding the "cheese effect" and hepatotoxicity, as well as other adverse effects such as weight gain and sexual dysfunction that may reduce patient compliance (Gillman et al., 2020; Meyer et al., 2021).

Recently, interest has been renewed in phenzine due to its documented neuroprotective properties. Of note, administration of phenzine after neurological damage reduced the extent of trauma in a gerbil model of stroke (Wood et al., 2006), a rat model of traumatic brain injury (Singh et al., 2013), and a mouse model of multiple sclerosis (Benson et al., 2013; Musgrave et al., 2011). Phenzine also inhibits GABA transaminase (Baker et al., 1991; MacKenzie, 2009; Popov & Matthies, 1969), significantly increasing  $\gamma$ -aminobutyric acid (GABA) concentrations in the brain, which may account for its anxiolytic properties (Paslowski et al., 1996) and its effectiveness in reducing neuronal damage in the gerbil stroke model (Matveychuk et al., 2021).

Phenelzine is also an inhibitor of primary amine oxidase (PrAO) (Lyles & Callingham, 1982), an enzyme associated with vascular smooth muscle and adipocytes and over-expressed in Alzheimer's disease (Chen et al., 2006; Yu et al., 2003). PrAO is responsible for formation of toxic aldehydes such as formaldehyde from methylamine (Lyles, 1996; Precious & Lyles, 1988), acrolein from allylamine (Nelson & Boor, 1982), and methylglyoxal from aminoacetone (Lyles & Chalmers, 1992). Since phenelzine has a free hydrazine group, it is also capable of sequestering reactive aldehydes such as acrolein and 3-aminopropanal that have been suggested to be involved in the etiology of a variety of neurologic and psychiatric disorders, including traumatic brain injury and multiple sclerosis (Hill et al., 2017; Leung et al., 2011; Singh et al., 2013; Wood et al., 2006).

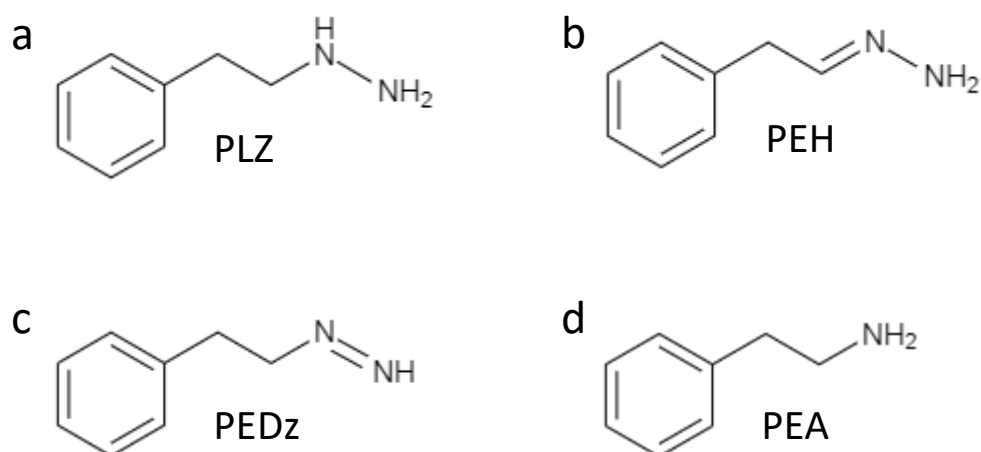


Figure 1.7 Structures of PLZ and its metabolites compared to the structure of PEA. (a) Phenelzine (PLZ) contains a hydrazine (C-HN-NH<sub>2</sub>) instead of an amine (C-NH<sub>2</sub>) functional group. (b) Phenylethylenedihydrazine (PEH) contains a double bond between C $\alpha$  and the internal nitrogen. (c) Phenylethyldiazene (PEDz) has a diazene functional group (HN=NH) and is theorized to be the inhibiting species in the inhibition of MAO-B by PLZ. (d) Structure of the endogenous MAO-B substrate  $\beta$ -phenylethylamine (PEA).

Phenelzine's inhibition of MAO also serves a neuroprotective purpose, in addition to its antidepressant effect, due to its effect of reducing the levels of the metabolites produced as a result of MAO activity. Metabolism catalyzed by MAO produces hydrogen peroxide and an imine, which then hydrolyzes either to an aldehyde and ammonia (primary amines) or to a substituted amine (secondary and tertiary amines). Hydrogen peroxide and ammonia are well known as sources of oxidative stress in cells and can be neurotoxic in large amounts (Wang et al., 2004; Wood et al., 2006; Yang et al., 2003; 2004). In addition, the neurotoxic aldehyde metabolites of dopamine (3,4-dihydroxyphenylacetaldehyde, DOPAL), of adrenaline and noradrenaline (3,4-dihydroxyphenylglycolaldehyde, DOPEGAL), and of 5-HT (5-hydroxyindoleacetaldehyde) have been implicated in contributing to the development of Parkinson's disease (PD) and Alzheimer's disease (AD) (Burke, 2004; Burke et al., 2003; Panneton et al., 2010). Thus, by inhibiting MAO, not only do substrate neurotransmitter levels increase, but levels of toxic metabolites of those substrates also decrease.

It has been reported by several researchers that MAO-B activity increases in old age and that this increase is more marked in Alzheimer's disease (AD) than in controls (Fowler, 2002; Fowler et al., 1997; Sherif et al., 1992; Sparks et al., 1991). It has been proposed that this increase may be the result of increased proliferation of glial cells since MAO-B is expressed in glia (Riederer et al., 1987). As such, there may be potential uses of phenelzine as an adjunctive treatment in AD as it would reduce MAO-B activity, and through its inhibition of MAO-A would increase brain levels of 5-HT, which have been reported to be reduced in AD (Baker & Reynolds, 1989).

### 1.3.2. Phenylethylidenehydrazine (PEH)

As well as being an inhibitor of MAO, phenelzine is a substrate for the enzyme, and the result is the production of pharmacologically active metabolites; thus, phenelzine could be considered a prodrug. A product of the reaction between MAO and phenelzine is  $\beta$ -phenylethylidenehydrazine (PEH) (Figure 1.7b), which is produced almost stoichiometrically as phenelzine is oxidized (Matveychuk, 2015). Many of the effects seen with phenelzine, such as neuroprotection, GABA increases in the brain, and reactive aldehyde sequestering, are also seen with PEH administration (Baker et al., 2019). In fact, it is hypothesized that phenelzine's effect on GABA levels is actually due to PEH-mediated GABA transaminase inhibition, as MAO pre-inhibition by another MAOI before administering phenelzine reduces markedly the increase in GABA levels in brain seen with phenelzine (Baker et al., 2019; Popov & Matthies, 1969; Todd & Baker, 1995).

Despite these pharmacological similarities, PEH is only a weak, reversible inhibitor of both MAO isoforms and thus does not have the capacity of phenelzine to increase amine concentrations in the brain (MacKenzie et al., 2008a,b; Paslawski et al., 2001). This factor is important, however, in that it means that PEH is not associated with the cheese effect.

### 1.3.3. Phenylethyldiazene (PEDz)

Despite being a metabolite of phenelzine oxidation by MAO, PEH is only a weak reversible inhibitor of MAO, and therefore is not the species which irreversibly inactivates the enzyme. The inhibitory species could instead be a putatively-minor metabolite,  $\beta$ -phenylethyldiazene (PEDz) (Figure 1.7c), which has been proposed to modify covalently the FAD cofactor in MAO-B, resulting in permanently inhibited enzyme (Binda et al., 2008; Patek & Hellerman, 1974; Yu & Tipton, 1989). The mechanism by which MAO-B oxidizes phenelzine predominantly to PEH, and

only occasionally to PEDz, and by which PEDz then inactivates MAO-B, has yet to be clearly elucidated.

## 1.4. Thesis Overview

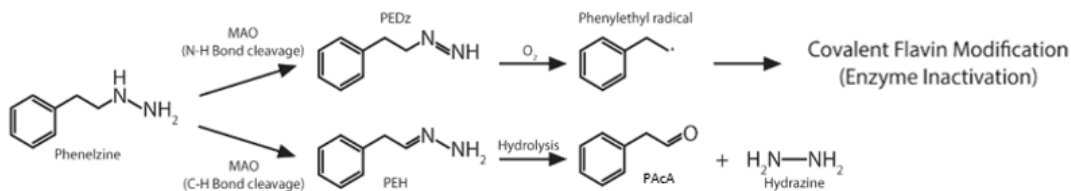
### 1.4.1. Currently Proposed Mechanism of Inhibition of MAO by Phenelzine

It has been theorized that MAO oxidizes phenelzine to produce PEH and PEDz via different catalytic mechanisms (see Binda et al., 2008 for detailed discussion). This theory proposes that PEH is formed via a C $\alpha$ -H bond cleavage and is released into the cytosol as a metabolite. Once every (approximately) 40 phenelzine turnovers, PEDz is produced via internal N-H bond cleavage. Oxygen then radicalizes PEDz *in situ*, producing an arylalkyl radical which binds covalently at the N(5) position of the reduced FAD (Binda et al., 2008), resulting in a permanently inhibited enzyme (Figure 1.8a, adapted from Matveychuk, 2015). This mechanism throughout this thesis will be referred to as the “forked mechanism”.

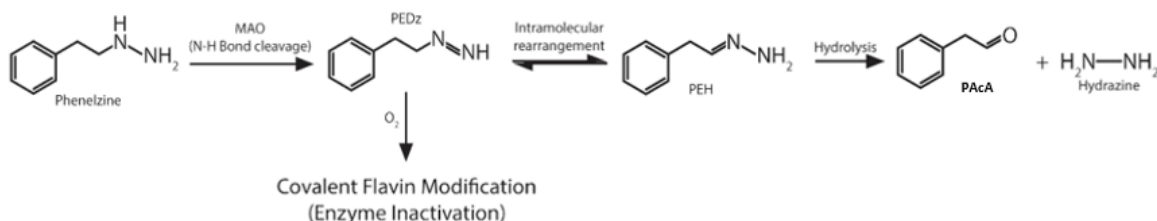
However, a growing body of experimental data obtained in our laboratory is inconsistent with this theory and has led us to propose an alternative mechanism (Figure 1.8b). Inconsistencies include variations in the partition ratio, in the half-life of inactivation, and in the rate of onset and the extent of irreversible inhibition observed across various concentrations of MAO-B and phenelzine. The average number of catalytic cycles resulting in product release per inhibition event, referred to as the partition ratio, was determined to be 36-40 (Binda et al., 2008), but we have found that the turnover number actually varies from around 20 up to several thousand turnovers per inactivation event (Figure 1.9a; A. Holt, unpublished results), and is dependent upon the concentration of both MAO and PLZ. In a similar fashion, the half-life of formation of PEH varies from 10 minutes to 20 minutes, decreasing as MAO-B concentration increases before reaching a plateau (Figure 1.9b, Matveychuk, 2015). This is consistent with faster enzyme inactivation at higher concentrations of MAO-B, as opposed to depletion of PLZ. These variable pharmacological constants make it very difficult to achieve 100% inhibition of MAO-B by

phenelzine unless very specific concentrations of the two reactants are used.

**a**



**b**



**c**

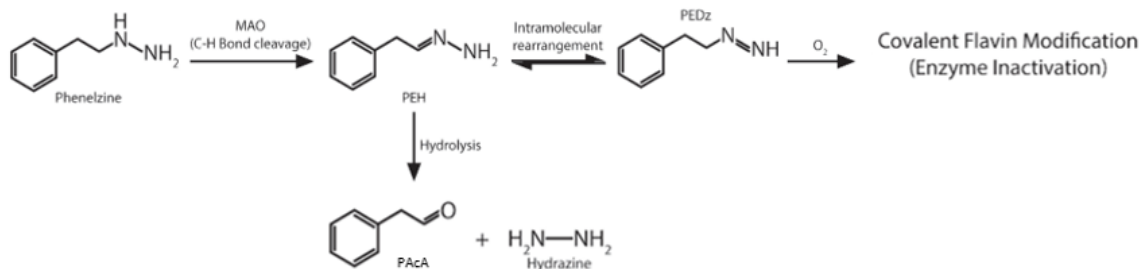


Figure 1.8 Proposed mechanisms for the metabolism of phenelzine and the inhibition of MAO-B by its metabolites.

(a) The forked mechanism suggests two different bond cleavage events which produce PEH and PEDz separately. PEH then hydrolyzes non-enzymatically to PAcA (phenylacetaldehyde) and hydrazine, while PEDz is radicalized by  $O_2$  in the active site, allowing it to covalently modify the still-reduced FAD *in situ*. (b) The stepwise mechanism suggests only one initial product forms from PLZ metabolism, PEDz. PEDz then undergoes intramolecular rearrangement to form PEH, or it inactivates the enzyme by covalent flavin modification. (c) In a variation of the stepwise mechanism, PLZ metabolism produces PEH, which then either hydrolyzes to PAcA and hydrazine, as in the forked mechanism, or it undergoes molecular rearrangement to form PEDz. PEDz then inactivates MAO-B. This mechanism is unlikely to occur, as incubation of MAO-B with PEH does not result in irreversible, time-dependent inhibition. Figure adapted from Matveychuk, 2015 with permission.

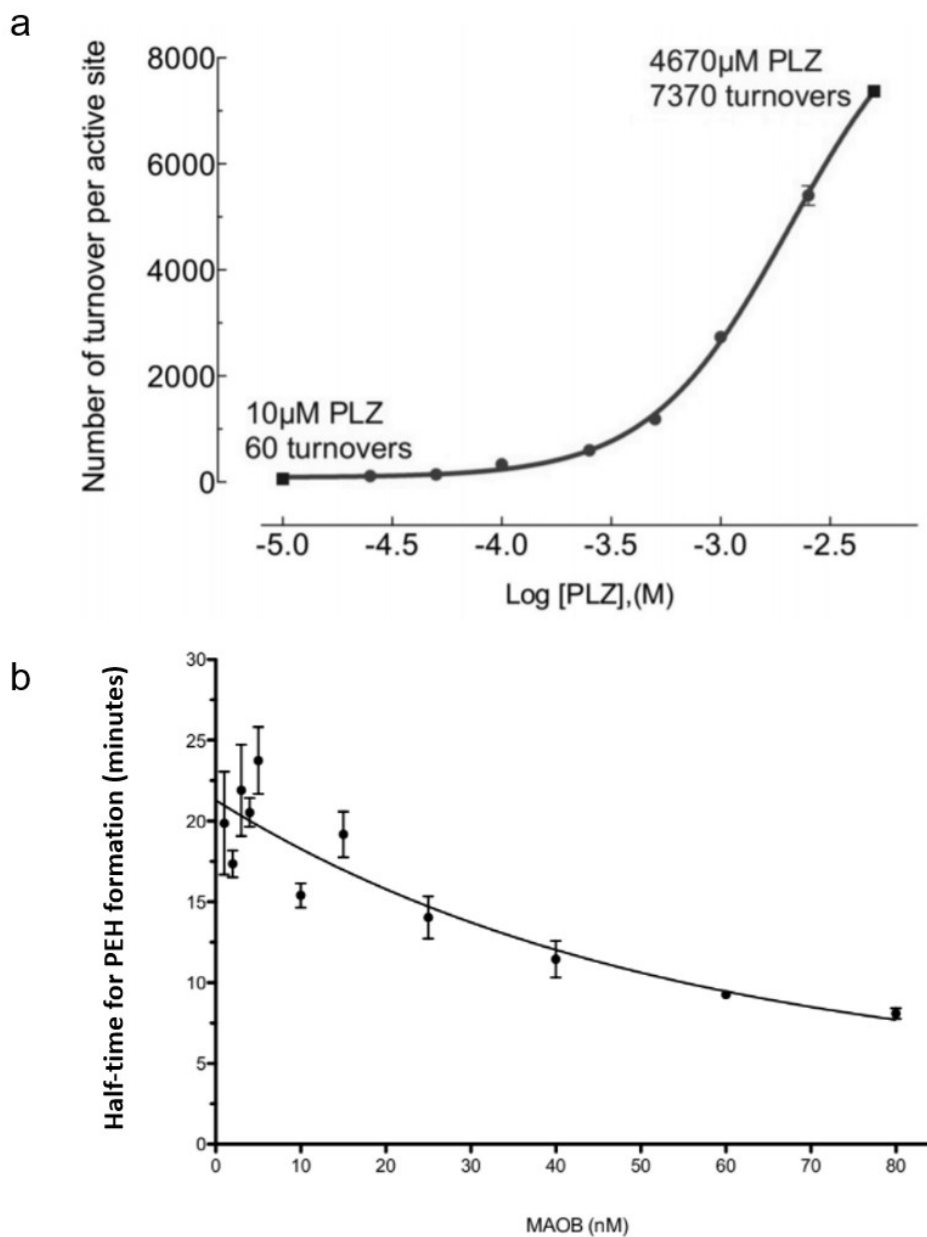


Figure 1.9 Inconsistencies in observations under current proposed mechanism.

(a) Effect of phenelzine concentration on the number of catalytic cycles prior to MAO-B (50 nM) inactivation, measured using the aldehyde dehydrogenase assay. Figure used with permission from Dr. Andrew Holt (Department of Psychiatry, University of Alberta). (b) Relationship between increasing MAO-B concentration and half-time for PEH formation when incubated with 100 μM phenelzine. The half-life of formation of PEH decreased with increasing concentrations of MAO-B, appearing to head towards a plateau; this plateau may be the result of more rapid inhibition of MAO-B preventing formation of PEH, as opposed to being the result of depletion of PLZ from the incubation. Data (n=3) are expressed as means ± SEM. Figure adapted from Matveychuk, 2015 with permission.

Figure 1.8c outlines another possible iteration of the stepwise mechanism, in which PLZ is metabolized to PEH, which then leaves the active site. As with the previous mechanism (Figure 1.8b), either intramolecular rearrangement or non-enzymatic hydrolysis then occurs in bulk solvent, producing either PEDz or phenylacetic acid (PAcA) and hydrazine, respectively. This would result in a time-dependent, irreversible inactivation of MAO-B, as PEDz is formed over time before reaching inhibitory concentrations. However, incubation of MAO-B with PEH results in a weak, reversible inhibition of enzyme activity (Matveychuk, 2015).

#### 1.4.2. Hypotheses and Specific Aims

The studies reported in this thesis aimed to seek evidence for an alternative to the accepted forked mechanism of action for the irreversible inhibition of MAO-B by phenelzine, herein referred to as the “stepwise mechanism”. This mechanism differs from the forked mechanism in two major ways. First, rather than the oxidation of phenelzine by MAO-B producing both PEH and PEDz via separate mechanisms, PEDz is instead the sole metabolite. Second, after formation, PEDz is released into the cytosol, where it then either competes with reactants and metabolites for access to the active site in order to form a covalent bond at the N(5) position of the oxidized flavin, or undergoes intramolecular rearrangement to form PEH, the measured end product of the reaction (Figure 1.8b).

The focus of this thesis will be to present evidence addressing the following hypotheses, based on previous findings reported in the literature and from preliminary experiments, regarding the mechanism by which phenelzine inhibits MAO:

- That phenelzine is oxidized by MAO to yield PEDz, the majority of which undergoes a bond rearrangement to generate PEH. (Chapter 2)
- That reoxidation of reduced flavin by oxygen is necessary before PEDz, or a PEDz-derived arylalkyl radical, can react with the flavin and inactivate the enzyme. (Chapter 3)
- That PEDz can dissociate from the active site of MAO-B and can return to inactivate the enzyme. (Chapters 4 and 5)

These experiments aim to characterize phenelzine's effects in the body so that we can make more informed decisions regarding the use of phenelzine, be it as an antidepressant or anxiolytic, or in new ways that take advantage of these mechanistic insights.

## Chapter Two

### **An Examination of the Source of PEH Formed During the Metabolism of PLZ by MAO-B**

#### **2.1. Introduction**

MAO-B catalyzes the oxidative deamination of mostly primary and secondary amines through a redox reaction in which a covalently bound flavin cofactor is the initial electron acceptor and molecular oxygen ( $O_2$ ) is the final electron acceptor, as shown in Figure 1.4 using benzylamine as an example substrate. In the active site, FAD oxidizes bound substrate by hydrogen removal from  $C_\alpha$  (Figure 1.4, blue box), the carbon adjacent to the terminal amine group (Dostert et al., 1989). The resulting imine is then released from the active site, and hydrolyzes non-enzymatically to produce aldehyde and ammonium, the final products of amine oxidation by MAO-B. The flavin cofactor, reduced at the N(5) position of the isoalloxazine ring (Figure 1.4, red box; Binda et al., 2008), is then re-oxidized by  $O_2$ , resulting in formation of hydrogen peroxide ( $H_2O_2$ ).

The structure of the endogenous amine  $\beta$ -phenylethylamine (PEA; Figures 1.7d and 2.1) is the backbone of many of the substrates which MAO metabolizes, making it a prominent motif in MAO inhibitor (MAOI) design. For example, phenelzine (PLZ; Figure 1.7a), in the hydrazine class of MAOIs, contains a PEA structure with a hydrazine group ( $R-NH-NH_2$ ) replacing the terminal amine ( $R-NH_2$ ), making PLZ both a substrate for and an inhibitor of MAO-B (Yu & Tipton, 1989).

Analysis of the products of oxidation of PLZ by MAO-B identifies phenylethylidenehydrazine (PEH; Figure 1.7b) as a major metabolite (Matveychuk, 2015). As well, MAO-B crystallography of the resulting covalent adduct within the active site reveals a phenylethyl group attached to N(5) of the FAD cofactor (Binda et al., 2008); given that this is the primary detected metabolite, it would make sense that the potential time-dependent inhibitory

species would be PEH. However, incubation of MAO-B with PEH reveals weak, time-independent, reversible inhibition as opposed to the expected time-dependent, irreversible inhibition typically seen with PLZ (Matveychuk, 2015).

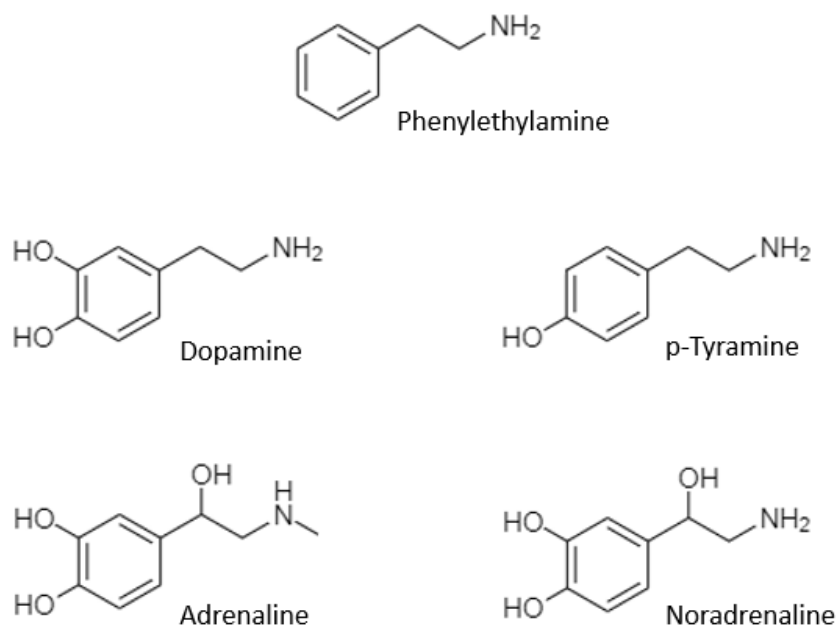


Figure 2.1 Examples of substrates of MAO which contain a phenylethylamine (PEA) backbone.

Instead, it has been proposed that the inhibitory species may be phenylethyldiazene (PEDz; Figure 1.7c), which, in the presence of oxygen, is thought to break down to the phenylethyl radical which covalently binds FAD, as well as to diazene (HN=NH). However, PEDz has yet to be successfully measured during the reaction between MAO-B and PLZ (Patek & Hellerman, 1974), although a spectrum consistent with the transient existence of a diazene species was observed on incubating hMAO-B with PLZ in a 700 MHz nuclear magnetic resonance instrument (A. Holt, unpublished observations). In contrast, PEH can be synthesized from phenylacetaldehyde and hydrazine monohydrate (Pross & Sternhell, 1970), which has allowed for extensive investigation

into this metabolite and its potential pharmacological activity. For instance, PLZ has been reported to be effective in treating anxiety disorders (Sheehan, 1980; Stein et al., 2002; Williams et al., 2020), presumably due to its ability to inhibit GABA-transaminase and increase the concentration of GABA in the brain (Paslawski et al., 1996). Both PEH and PLZ inhibit GABA-transaminase and elevate brain GABA (Baker et al., 1991; MacKenzie et al., 2008; Paslawski et al., 2001; Popov & Matthies, 1969), but prior *in vivo* inhibition of MAO by another MAO inhibitor (e.g., tranylcypromine) before administering phenelzine largely abolishes this effect on GABA (Popov & Matthies, 1969; Todd & Baker, 1995) suggesting that PEH may be responsible for the GABAergic and anxiolytic effects of PLZ.

However, despite all of this research, the mechanism by which PLZ metabolism by MAO-B produces both PEH and PEDz has yet to be satisfactorily elucidated (see Binda et al., 2008; Patek & Hellerman, 1974; and Yu & Tipton, 1989 for reviews). Either each product is formed by its own separate pathway, or only one metabolite is produced from which the other is formed, as outlined in Figure 1.8, adapted from Matveychuk (2015). Given that incubation of MAO-B with PEH does not yield any time-dependent inhibition, it is unlikely that PEDz is formed from PEH (Figure 1.8c). Therefore, either two metabolites are formed independently in a forked mechanism (Figure 1.8a), or PEDz is formed first and rearranges to yield PEH in a stepwise mechanism (Figures 1.8b).

Current opinion favours the forked mechanism (Figure 1.8a), which states that oxidation of PLZ by MAO-B produces PEH and PEDz, depending on which hydrogen is removed from PLZ (Binda et al., 2008). According to this mechanism, PEH is formed when a C $\alpha$ -H bond is broken in the process of oxidation; this is also the mechanism by which MAO-B metabolizes amine substrates to generate imines, as mentioned previously (Figure 1.4). PEDz, on the other hand,

forms when FAD instead breaks the internal N-H bond in PLZ. Following radicalization by oxygen, PEDz then goes on to inactivate the still-reduced enzyme *in situ* by forming a covalent bond to N(5) of the flavin.

This chapter will consider the remaining alternative, outlined in Figure 1.8b. In this proposed stepwise mechanism, the sole product of PLZ metabolism by MAO-B is PEDz, which then undergoes intramolecular rearrangement to become PEH (Figure 1.8b). Inhibition of MAO-B occurs when PEDz (or an alkyl radical generated from PEDz) instead binds the re-oxidized enzyme to form a covalent bond at the N(5) of the flavin.

As illustrated in Figure 2.2b, the process of intramolecular rearrangement would likely involve a water molecule. We can utilize heavy hydrogen (deuterium) to determine how these two separate double bonds are formed in a process known as hydrogen deuterium exchange (HDX; see Huang & Chen, 2014 for review). If PEH is formed from the rearrangement of PEDz, incubation of MAO-B and PLZ in deuterated buffer would result in the incorporation of deuterium into the resulting PEH (D-PEH, Figure 2.2c). If PEH and PEDz are produced via separate mechanisms directly from PLZ oxidation, as stated in the forked mechanism (Figure 1.8a), we would not expect to see incorporation of deuterium in PEH.

Using high-pressure liquid chromatography coupled with mass spectrometry (LC-MS), the amount of D-PEH can be determined. LC separates the target analytes by retention time, and MS measures the signal from each component's mass-to-charge ( $m/z$ ) ratio. Mono-deuterated compounds will be 1  $m/z$  heavier than their non-deuterated counterparts due to incorporation of a heavy hydrogen, which increases the mass by one without increasing the charge (Figure 2.2c).

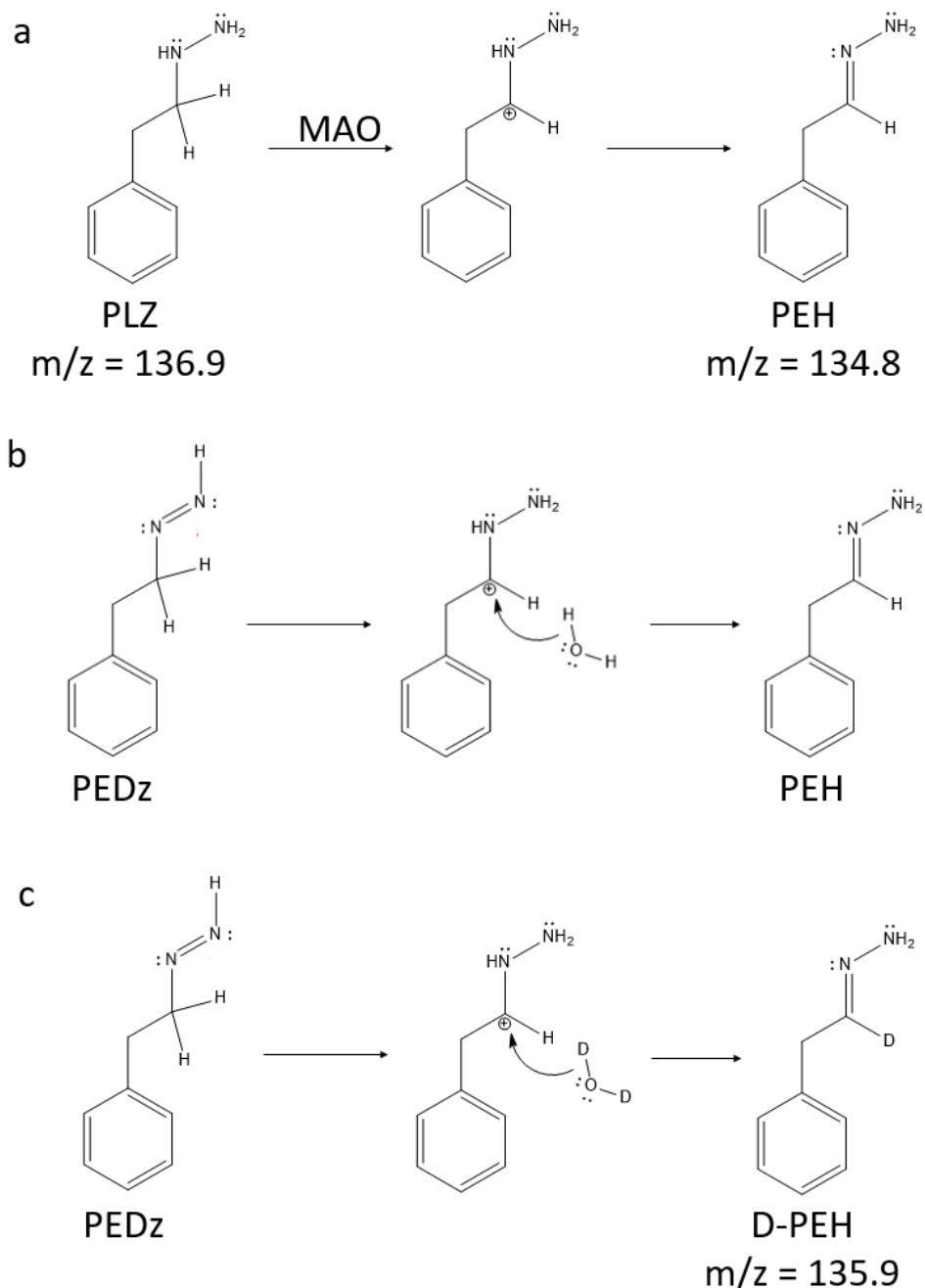


Figure 2.2 Intramolecular rearrangement of PEDz to PEH and incorporation of deuterium. **(a)** Formation of PEH from PLZ according to the forked mechanism does not involve water, thus PEH would not become deuterated. **(b)** A water molecule attacks the  $C_\alpha$  of PEDz, and the resulting rearrangement of electrons forms PEH. **(c)** Deuterium oxide ( $D_2O$ ) is water in which the hydrogens have an extra neutron. Incorporation of a deuterium into the structure of PEH will alter the molecule's  $m/z$  ratio by +1 unit (PEH  $m/z$  increased from 134.8 to 135.9 for D-PEH, and PLZ  $m/z$  increased from 136.9 to 137.9 for D-PLZ). Given the current debate surrounding the mechanism of amine oxidation by MAO-B, as well as the nature of the study and its results, electron-pushing arrows have been largely left out.

### 2.1.1. Hypotheses

- MAO-B oxidizes PLZ to yield PEDz, which leaves the active site and either rebinds to an oxidized active site or undergoes intramolecular rearrangement in bulk solvent to form PEH.
- Incubation of PLZ and MAO-B in deuterated buffer will result in deuterated PEH, formed from deuterated PEDz.

Deuterated PEH will be one m/z unit heavier than non-deuterated PEH, a difference that can be measured with LC-MS. LC will allow for the separation of sample components, while single ion monitoring (SIM) quadrupole MS will allow for resolving 1 mass/charge unit difference.

### 2.1.2. Specific Aims

- Determine background HDX. There is always background HDX of labile hydrogens in deuterated solutions. The extent to which background HDX occurs must be quantified (%HDX<sub>PEH</sub>), and reaction conditions chosen to minimize this process.
- Quantify the extent of deuterium incorporation into PEH following incubation of PLZ with MAO-B in deuterated buffer (%HDX<sub>inc</sub>). In deuterated buffer, we should be able to see evidence of intramolecular rearrangement through LC-MS, by way of a +1 m/z on the PEH due to deuterium incorporation. PEDz incorporates deuterium in the process of rearranging bonds to form PEH, producing D-PEH in amounts exceeding background HDX.

## **2.2. Materials and Methods**

### 2.2.1. Materials

All water used in the experiments was filtered through a Millipore Milli-Q filtration system. BZ hydrochloride, PLZ sulfate, deuterium oxide (D<sub>2</sub>O), and ammonium formate were purchased from Sigma-Aldrich. Acetonitrile, methanol, and monobasic and dibasic sodium

phosphate were obtained from Fisher Scientific. For spectrophotometric experiments, 96-well microplates were obtained from Greiner Bio-One. Full length human MAO-B was expressed in *Pichia pastoris* yeast and purified in our laboratory. PEH was synthesized from phenylacetaldehyde and hydrazine monohydrate in the laboratories of Dr. Velázquez-Martínez in the Faculty of Pharmacy and Pharmaceutical Sciences, University of Alberta. PEH has low solubility in water, therefore 1 mg/mL PEH was prepared in acetonitrile before being diluted 10-fold in buffer as needed. PLZ was prepared in buffer. PLZ, PEH, and BZ were made fresh for each experiment.

### 2.2.2. Buffer

Solutions of monobasic and dibasic sodium phosphate (0.2 M), made up in H<sub>2</sub>O or D<sub>2</sub>O, were combined until the desired pH or pD, respectively, was reached. The pH of the non-deuterated sodium phosphate buffer (NaP) was measured using a pH meter and a KCl-buffered/filled electrode. The pD of the deuterated NaP buffer (D-NaP) was measured by obtaining the pH as above and converting to pD using  $pD = pH + 0.4$  (Glasoe & Long, 1960). Because the buffer is composed of deprotonated phosphoric acid salts (i.e., HPO<sub>4</sub><sup>2-</sup> and H<sub>2</sub>PO<sub>4</sub><sup>-</sup>), there is some contaminating hydrogen in the deuterated buffer, but at low buffer concentrations, the presence of hydrogen is at negligibly low levels (Glasoe & Long, 1960).

### 2.2.3. Benzaldehyde Assay

For measurement of MAO-B activity in some experiments, a spectrophotometric assay for measurement of benzaldehyde production was used. Metabolism of BZ by MAO-B produces benzyldimine, which quickly hydrolyzes to benzaldehyde after formation (Figure 1.4) such that enzymatic turnover of one molecule of BZ generates one benzaldehyde molecule. Benzaldehyde has a characteristic absorbance at a wavelength of 254 nm ( $\epsilon \approx 12,500 \text{ M}^{-1}\text{cm}^{-1}$ ), the change in

which is measured through a continuous kinetic assay during incubation of MAO-B and BZ in physiological buffer. Here, this assay was carried out on a Molecular Devices FlexStation 3 microplate reader at 37°C, unless otherwise indicated.

#### 2.2.4. LC-MS

The LC-MS protocol was adapted from Matveychuk (2015). Briefly, the HPLC instrument was a Waters Alliance 2695 with an Atlantis T3 5  $\mu\text{m}$  (3 x 100 mm) analytical column. The mobile phase consisted of 15% 10 mM ammonium formate in water, 25% methanol, and 60% acetonitrile and was programmed to have a flow rate of 0.3 mL/minute. The MS instrument was a Waters Micromass ZQ-4000 with the following voltages: capillary = 3.31 kV, cone = 21 V, extractor = 2 V, and RF lens = 1 V. The source and desolvation temperatures were 150°C and 350°C, respectively. Nitrogen gas was set at a desolvation flow rate of 350 L/hour and cone flow rate of 90 L/hour.

Samples were prepared for HPLC as follows: 10  $\mu\text{L}$  aliquots were diluted to 1 mL in acetonitrile and centrifuged for 2 minutes at 10,000 rpm. A portion (100  $\mu\text{L}$ ) was put into an HPLC vial with a glass insert and run through the LC-MS system. Using positive electrospray ionization mode, selective ion monitoring (SIM) was used to detect the compounds at the following mass-to-charge ratios ( $m/z$ ): 134.8 for PEH and 135.9 for D-PEH. Representative chromatographs for the analysis of PEH in deuterated buffer are shown in Figure 2.3.

#### 2.2.5. Analysis and Statistics

The area under the curve (AUC) of the response peak was quantified using MassLynx4.1. The %HDX within a sample was calculated as the ratio of D-PEH signal to total PEH signal (PEH+D-PEH). Statistical analysis was done with Prism7 (GraphPad Software Inc., San Diego, CA); all error bars in figures represent  $\pm$  SEM.

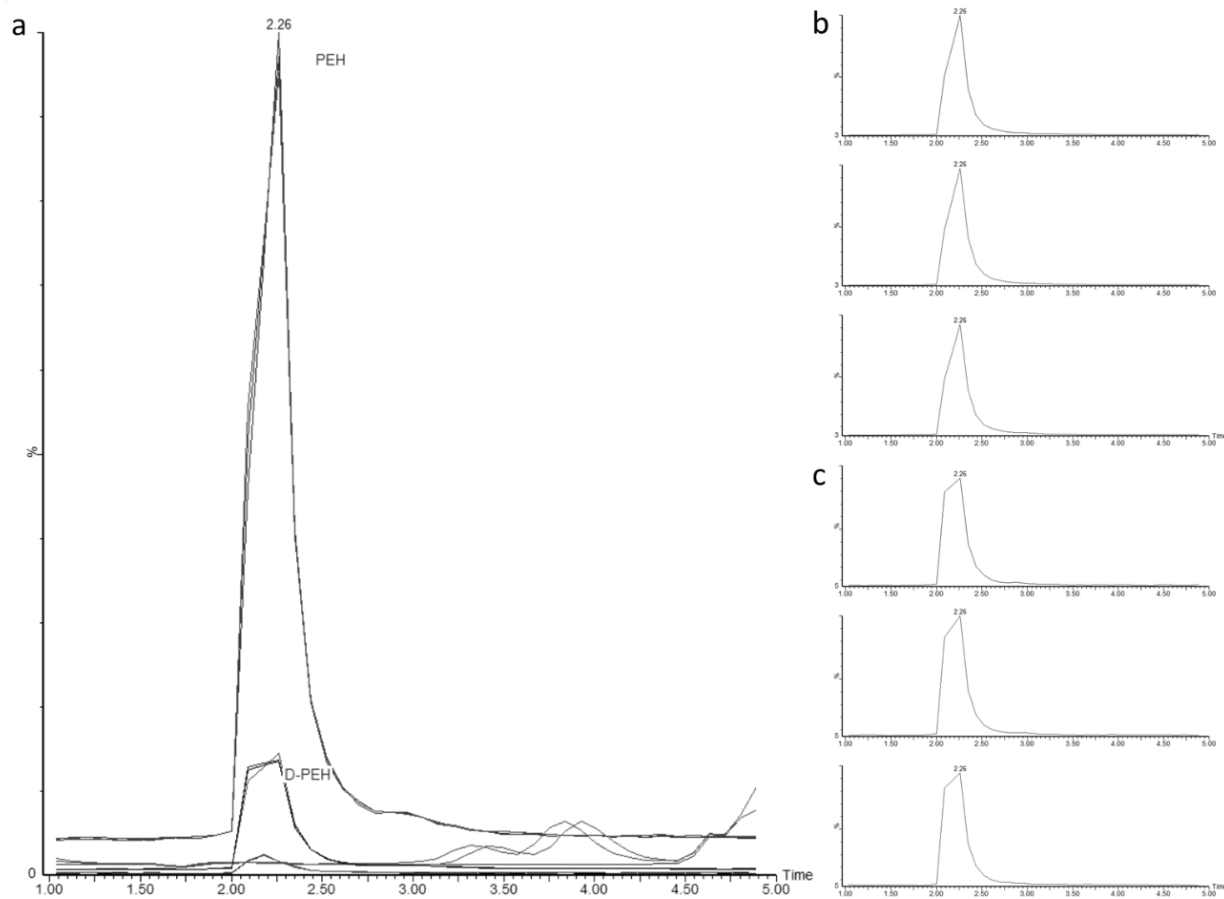


Figure 2.3 Representative chromatographs for PEH in deuterated buffer. PEH ( $2 \mu\text{g/mL}$  or  $15 \mu\text{M}$ ) incubated in D-NaP buffer for 20 minutes at  $21^\circ\text{C}$  ( $n=3$ ). Y-axes (relative signal response (%)) are locked in each panel, but not between panels. (a) Panels b and c stacked and compared against the same axis. The very small peaks shown at the bottom of the chromatogram were not investigated, but probably represent non-specific exchange of deuterium with hydrogen at some sites on PEH other than the  $\text{C}\alpha$ . Inter-replicate consistency and retention time (RT, min) for (b) PEH ( $m/z = 134.8$ ; RT = 2.26) and (c) D-PEH ( $m/z = 135.9$ ; RT = 2.18).

## 2.3. Results and Discussion

### 2.3.1. Determination of MAO-B Concentration

The enzyme concentrations of two purified hMAO-B stocks were estimated as follows: A known volume of MAO-B was incubated with 1 mM BZ in NaP (0.2 M, pH 7.4) for 20 minutes at 37°C. By measuring the change in absorbance at 254 nm (Abs (OD<sub>254</sub>); Figure 2.4) and using the Beer-Lambert equation ( $A = \epsilon bc$ ,  $\epsilon_{254} \approx 12,500 \text{ M}^{-1} \text{ cm}^{-1}$ ), the concentration of BZ metabolized, and therefore benzaldehyde produced, was calculated. From there, the moles of MAO-B needed to metabolize the amount of BZ required to produce that much benzaldehyde was determined, using the estimation that one hMAO-B molecule can perform about 300 catalytic turnovers per minute in these conditions (Milczek et al., 2011). Taking dilution into account, the stock solutions of pure hMAO-B used in these experiments were estimated to be 0.56  $\mu\text{M}$  and 0.77  $\mu\text{M}$ . This calculation was done as follows:

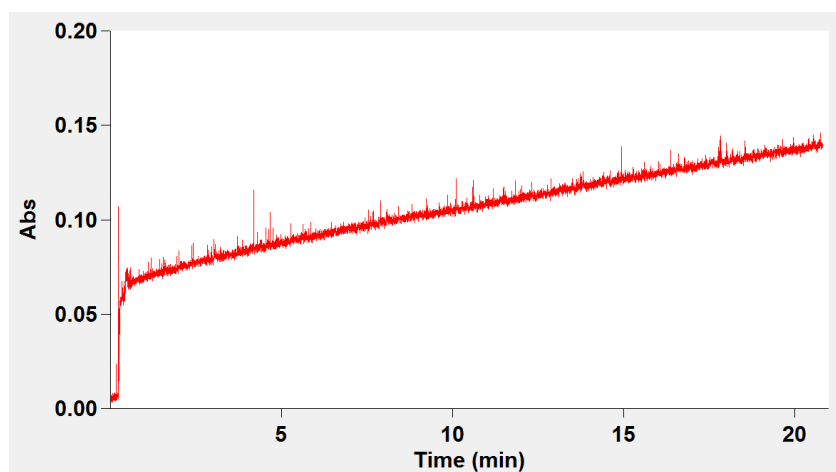


Figure 2.4 Representative change in absorbance due to benzaldehyde formation over time. A known volume of soluble hMAO-B stock (5  $\mu\text{L}$ ) was incubated with BZ (1 mM) in physiological buffer (0.1 M KP, pH 7.4) for 20 minutes in a quartz cuvette (3 mL volume, 37°C). The total change in absorbance at 254 nm (OD) was then used to estimate the stock hMAO-B concentration of 0.56  $\mu\text{M}$ .

A volume of 5  $\mu\text{L}$  of the hMAO-B stock resulted in a change in absorbance over 20 minutes of 77 mOD.

$$c = \frac{0.077 \text{ OD}}{12,500 \text{ M}^{-1}\text{cm}^{-1} \times 1 \text{ cm}} = 5.6 \mu\text{M}$$

Therefore, 5.6  $\mu\text{M}$  benzaldehyde was generated in 20 minutes, corresponding to a rate of change in concentration of 179.0 nM/min in a 3 mL volume, or 0.84 nmol/min. At 300 turnovers/min, this would require 2.8 pmol MAO-B, and since 5  $\mu\text{L}$  of stock were used, the stock concentration of hMAO-B can be estimated as 0.56  $\mu\text{M}$ .

### 2.3.2. pH Determination

For optimal quantification of PEH, conditions must be favourable both for the production of PEH and for its stability in solution, both of which are dependent on pH. The peak catalytic activity of hMAO-B, measured as  $k_{\text{cat}}/K_{\text{D}}$ , is observed at pH values above 9.0 (Milczek et al., 2011), and at higher pH values, the rate of PEH hydrolysis to hydrazine and phenylacetaldehyde is lower (Matveychuk, 2015). On the other hand, HDX is influenced by pD, with hydrogens becoming more labile as pD increases (Bai et al., 1993). Another consideration is background HDX, the passive exchange of labile hydrogens for deuteriums associated with  $\text{D}_2\text{O}$ , which likely occurs within PEH ( $\%\text{HDX}_{\text{PEH}}$ ). The rate of this passive exchange depends on the pKa of the labile hydrogens; if the pD is higher than the pKa, the rate of exchange increases. Therefore, it was necessary to select a pD value at which MAO-B activity was high, while also considering the conditions under which HDX is more likely to occur in order to limit  $\%\text{HDX}_{\text{PEH}}$ .

To determine optimal conditions for enzyme activity, a benzaldehyde assay was used. In quadruplicate, MAO-B (7.5 nM) was incubated with BZ (1 mM) for an hour at 30°C, in NaP buffers (0.2 M) ranging from pH 5.20 to 7.92, and initial rates (mOD/min) plotted against buffer

pH (Figure 2.5;  $\pm$  SEM). As the ideal pD was assumed to be low, pH values higher than 8 were not initially tested. MAO-B had the most activity at the highest tested pH, and the least at pH 5.20, which is consistent with the literature (Milczek et al., 2011).

Next, the pD at which %HDX<sub>PEH</sub> was lowest was determined. PEH (100  $\mu$ g/mL; 750  $\mu$ M) was incubated in D-NaP (0.2 M) for 30 minutes at 21°C; the pD of the buffer was increased in roughly half unit increments from 6.37 to 8.90, based on the threshold of 50% loss in activity from Figure 2.5 at around pH 6.5. In triplicate, samples were then diluted in acetonitrile to 2  $\mu$ g/mL (15  $\mu$ M) and analyzed by direct injection into the MS system. %HDX was calculated by expressing the AUC for the D-PEH signal as a percentage of the combined AUC for PEH and D-PEH signals (Figure 2.6; mean of  $n=4 \pm$  SEM). From pD 6.37 to 7.70, HDX values ranged from  $14.1 \pm 1\%$  to  $22.9 \pm 0.2\%$ , while at pD 8.30 and 8.90, %HDX was  $10.7 \pm 0.1\%$  and  $9.3 \pm 0.04\%$ , respectively. Therefore, given that buffers of higher pH or pD resulted in the highest enzymatic activity and the lowest %HDX<sub>PEH</sub>, subsequent experiments were conducted at pD/pH 8.90.

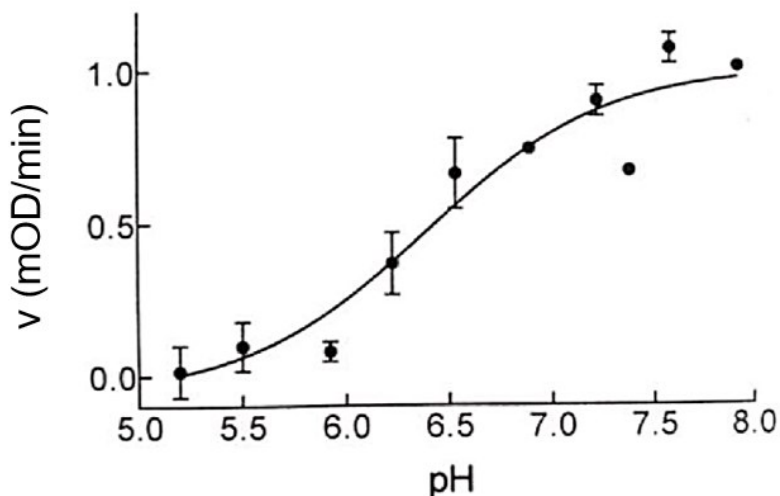


Figure 2.5 Determination of optimal pH for MAO-B activity. Initial rate of absorbance change at 254 nm (mOD/min;  $n=4$ ) due to production of benzaldehyde from metabolism of BZ (1 mM) by MAO-B (7.5  $\mu$ M) in NaP buffers (0.2 M; 30°C) of varying pH.

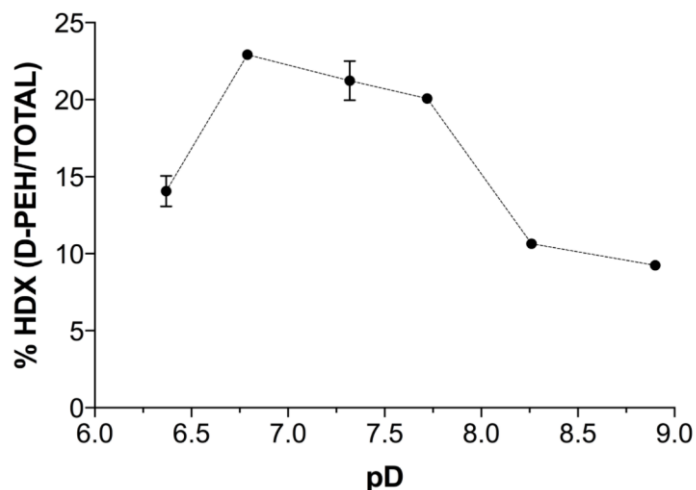


Figure 2.6 Determination of pD for least background hydrogen deuterium exchange. Background %HDX for PEH incubated in a range of pD D-NaP buffer (0.2 M) for 30 min at 21°C (n=3).

### 2.3.3. LC-MS

In triplicate, hMAO-B (2 nM) was incubated with PLZ (1 mM) for 30 minutes at room temperature in 0.2 M D-NaP, after which 5 samples of each replicate, as well as blanks, were prepared and analyzed by LC-MS as detailed above. The area under the curve (AUC) for PEH and D-PEH were obtained from each sample and analyzed to obtain %HDX (Figure 2.7).

Incubation of MAO-B and PLZ in deuterated buffer produced D-PEH to a much greater extent than observed in background samples (%HDX<sub>inc</sub> = 39.7 ± 4.5% vs %HDX<sub>PEH</sub> = 7.8 ± 0.1%, p = 0.0022). There was a clear indication that PEH formed from the metabolism of PLZ by MAO-B had a higher incidence of HDX compared to PEH alone when incubated in deuterated buffer. These observations are consistent with the hypothesis that PEH formed was the result of a rearrangement of PEDz in bulk solvent after release from the active site. The intramolecular rearrangement of PEDz to PEH in the deuterated buffer allows for the increased incorporation of deuterium, and thus an increase in the molecular mass of PEH.

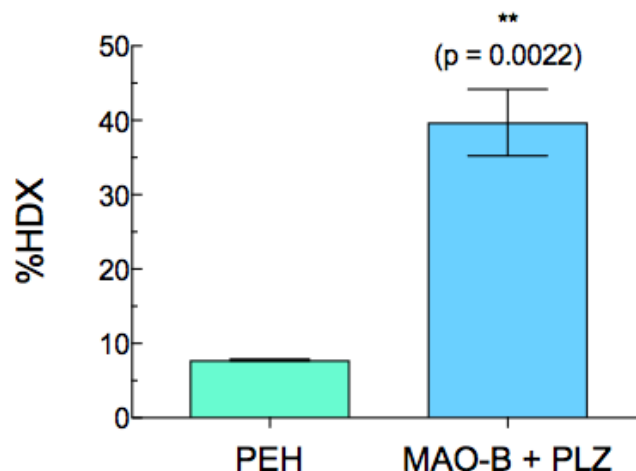


Figure 2.7 Comparison of deuterium incorporation into PEH by two distinct pathways. %HDX in synthesized PEH (%HDX<sub>PEH</sub>; green bar) represented the background rate of HDX due to labile hydrogens in deuterated solution (7.8 ± 0.1%). For PEH generated by hMAO-B from PLZ (%HDX<sub>inc</sub>; blue bar), the extent of HDX (39.7 ± 4.5%) was nearly 500% greater than background (\*p = 0.0022; Mann-Whitney two-tailed parametric unpaired t-test (Prism7)).

#### 2.3.4. Controls

After analysis of preliminary experiments yielded results consistent with the hypothesis that PEDz is the proximal metabolite and that PEH is derived from PEDz, an assessment of %HDX<sub>PEH</sub> was done in non-deuterated NaP, to confirm the absence of a peak corresponding to D-PEH in an LC-MS analysis. Surprisingly, PEH, whether incubated in non-deuterated (NaP) or deuterated (D-NaP) buffer, demonstrated HDX with values around the previously-measured background level (8.9 ± 0.6% in NaP and 9.5 ± 0.6% in D-NaP; p = 0.4619 from Welch’s two-tailed t-test) (Figure 2.8).

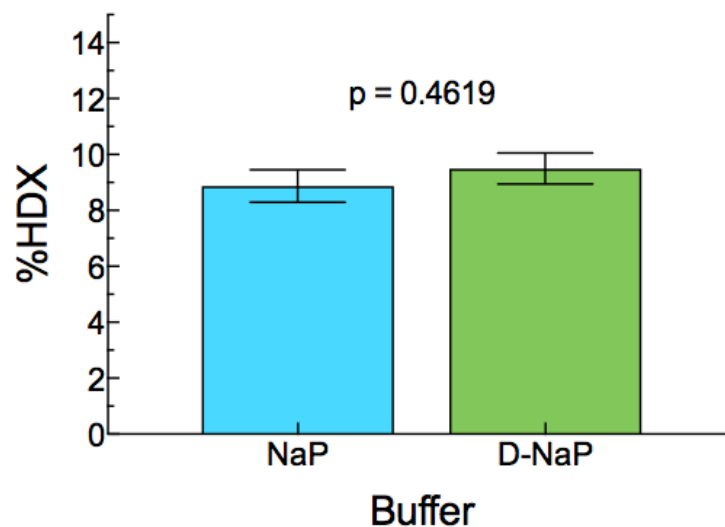


Figure 2.8 Comparison of %HDX values for deuterated and non-deuterated samples. Background %HDX for PEH (1 mg/mL) incubated in non-deuterated (NaP, blue bar) and deuterated (D-NaP, green bar) buffer (0.2 M, pH/pD 8.90), for 30 minutes at 21°C. In NaP, %HDX<sub>PEH</sub> (8.9 ± 0.6%) was not significantly different from that in D-NaP (9.5 ± 0.6%;  $p = 0.4619$ , Welch's two-tailed t-test (Prism7)). These data suggest contamination of the HPLC column by deuterium.

Consultation with Dr. Randy Whittal (Mass Spectrometry Core Facility, Department of Chemistry, University of Alberta) revealed sources of potential complications. The column used in the HPLC was a C<sub>18</sub> column, saturated with labile hydrogens that could potentially exchange with the deuterium in the samples as they were passing through the column. However, deuteration of the column should not influence HDX beyond background for PEH formed from the incubation of MAO-B and PLZ in non-deuterated buffer, as the exchange only occurs while the sample is in the column. Indeed, that is consistent with results here. Therefore, it is unlikely that PEH formed from incubating MAO-B and PLZ in non-deuterated buffer would have any more HDX than background, as the PEH is already formed by the time the sample gets to the column and the opportunity for HDX during intramolecular rearrangement has passed.

## 2.4. Conclusions

In this experiment, preliminary evidence suggested that PEH is formed from the intramolecular rearrangement of PEDz to PEH during the metabolism of PLZ by MAO-B. In deuterated buffer, the amount of HDX that occurred in PEH resulting from PLZ oxidation was greater than the passive exchange which occurs in synthesized PEH ( $39.7 \pm 4.5\%$  vs  $7.8 \pm 0.1\%$ ,  $p = 0.0022$ ). Unfortunately, because of subsequent problems with the LC-MS machine used, including leaks in the system, we were unable to repeat these experiments. The machine was over 17 years old and no longer under a service contract. Costs for repair would have been prohibitive, and we were unable to find anyone else on campus who was able to conduct the experiments for us.

## Chapter Three

### Use of the Redox Dye DCPIP to Explore the Role of Oxygen in the Inhibition of MAO-B by PLZ

#### 3.1. Introduction

During catalytic turnover, reduced FAD must be re-oxidized before it can participate in another catalytic cycle. In the oxidative half-reaction, the C(4a) of the isoalloxazine ring donates electrons to molecular oxygen ( $O_2$ ), re-oxidizing the flavin and producing hydrogen peroxide ( $H_2O_2$ ) (Pizzinat et al., 1999), through a mechanism which has yet to be fully characterized.

Inhibitors such as mofegiline are able to inactivate MAO-B in the absence of  $O_2$ , as their mechanisms of action do not require completion of a full catalytic cycle (Milczek et al., 2008). PLZ, however, acts as a substrate for MAO-B; the production of  $H_2O_2$  over the course of inhibition confirms that  $O_2$  is used as the final electron acceptor in PLZ metabolism by MAO-B (Clineschmidt & Horita, 1969; Tipton & Spires, 1971). This is further exemplified in the inability of PLZ to inhibit MAO-B during anaerobic incubation; the oxidized enzyme is able to perform a single turnover, producing PEDz from PLZ, but the anaerobic environment prevents the last step in inhibition (Binda et al., 2008).

##### 3.1.1. The Role of $O_2$ in Inhibition of MAO-B by PLZ

In the quest to understand the inhibition of MAO-B by PLZ, two competing theories are being evaluated: the forked and the stepwise mechanisms. The forked mechanism states that  $H_2O_2$  is only produced when PEH is formed, as that is when the enzyme is still in a state to be re-oxidized via  $O_2$ . When PEDz is formed, it is argued, inactivation of the enzyme occurs *in situ*; the unstable PEDz reacts with  $O_2$ , resulting in diazene ( $HN=NH$ ) and a phenylethyl radical which covalently modifies the flavin (Binda et al., 2008). The stepwise mechanism differs from that proposed here,

in that PEDz is the sole metabolic product and is released from the active site after formation. The reduced FAD is re-oxidized, allowing PEDz to rebind and inactivate MAO-B, as binding to reduced flavin is generally energetically unfavourable (Nagy et al., 1979). As such, PEDz would compete with PLZ for binding to the oxidized enzyme, this competition being evident in appropriate kinetic studies.

In order to determine whether O<sub>2</sub> is involved only in enzyme re-oxidation, or also in PEDz radicalization, the two mechanisms need to be made mutually exclusive; this might be achieved by replacing O<sub>2</sub> with a compound that can re-oxidize the enzyme in an anaerobic environment that would preclude radicalization of the diazene. 2,6-Dichlorophenolindophenol (DCPIP) is a redox dye, capable of donating or accepting one or two electrons, with associated changes in its absorbance spectrum, changing from dark blue (DCPIP) to bright pink (DCPIPH) to colorless (DCPIPH<sub>2</sub>) as it is reduced in a stepwise manner. DCPIP has been shown to re-oxidize redox flavoenzymes such as xanthine oxidase and D-amino acid oxidase (Brugger et al., 2014) through acting as a final electron acceptor, much like O<sub>2</sub>, in a manner which is measurable by spectrophotometrically monitoring the absorbance change of the dye at 604 nm. Since DCPIP cannot radicalize PEDz, an observation of anaerobic inactivation of hMAO-B by PLZ in the presence of DCPIP, but not in the absence of DCPIP, would confirm flavin reoxidation rather than PEDz radicalization as the only role played by O<sub>2</sub> in the inactivation process.

The previous chapter examined two immediate metabolites of PLZ metabolism by MAO-B, phenylethyldiazene (PEDz) and phenylethylidenehydrazine (PEH), and the sequence in which they are formed. The data presented support the stepwise mechanism, whereby PEDz is the sole metabolite after an N(5) attack by the flavin cofactor breaks a C<sub>α</sub>-H bond on PLZ. After formation, PEDz is released from the active site and can undergo intramolecular rearrangement in bulk solvent

to form PEH. This chapter explores the other fate of PEDz, irreversible inhibition of MAO-B by covalent modification of FAD, and the role of oxygen therein.

### 3.1.2. Hypotheses

- A critical role of O<sub>2</sub> in the irreversible inhibition of MAO-B by PLZ is to re-oxidize the flavin, and not solely to radicalize PEDz as hypothesized in the forked mechanism.
- PEDz (or the phenylethyl radical derived therefrom) interacts covalently with oxidized FAD, but not with reduced FAD; consequently, following oxidation of PLZ to generate PEDz, re-oxidation of FAD is necessary before enzyme inhibition through PEDz can occur.

### 3.1.3. Specific Aims

- Determine the influence of DCPIP on the inhibition of MAO-B by PLZ in anaerobic conditions. DCPIP is a redox dye capable of re-oxidizing FAD cofactors, but not radicalizing PEDz. Therefore, addition of DCPIP to an anaerobic incubation of MAO-B and PLZ could lead to one of two outcomes: (a) anaerobic inactivation of MAO-B, which would indicate that the only role played by oxygen is flavin re-oxidation; or (b) no inactivation of MAO-B, but rapid inactivation on reintroducing oxygen, which would confirm that oxygen is necessary to radicalize PEDz, but which would offer little insight into oxygen's role in re-oxidizing flavin.

## 3.2. Materials and Methods

### 3.2.1. Materials

All water used in the experiments was filtered through a Millipore Milli-Q filtration system. BZ hydrochloride, PLZ sulfate, DCPIP sodium salt, and horseradish peroxidase (Type II) were purchased from Sigma-Aldrich. Amplex Red reagent (N-acetyl-3,7-dihydroxyphenoxazine) was purchased from Invitrogen. Monobasic and dibasic potassium phosphate and hydrochloric acid were obtained from Fisher Scientific. For spectrophotometric experiments, 96-well microplates were obtained from Greiner Bio-One. Argon was obtained from Praxair. Assay constituents, including substrates and inhibitors, were prepared only in colourless disposable virgin polypropylene plasticware manufactured by Eppendorf AG in order to avoid interferences from leachates (McDonald et al., 2008).

Full length hMAO-B was expressed in *Pichia pastoris* yeast and was either purified partially by ion exchange chromatography, generating a soluble enzyme that was approximately 50% pure, or was isolated in a membrane-bound form from yeast mitochondria, in our laboratory. PEH was synthesized from phenylacetaldehyde and hydrazine monohydrate in the laboratories of Dr. Velázquez-Martínez in the Faculty of Pharmacy and Pharmaceutical Sciences, University of Alberta. MAO-B activities in purified preparations or in membrane fractions were measured continuously with BZ as substrate in 96-well plates or quartz cuvettes. All assays were carried out at 37°C under atmospheric oxygen, unless otherwise indicated.

### 3.2.2. Anaerobic Experiments

Solutions of MAO-B, PLZ, BZ, and DCPIP were made anaerobic by flushing samples with argon (99.998%) which had first been passed through a Matheson Tri-gas oxygen purifier to remove any remaining traces of oxygen, at a pressure of 1 m of water, followed by degassing

samples under vacuum for approximately 30 seconds. After repeating this process three times, reagents were left under a positive pressure of argon (1 m of water) for 16 hours, at which point they were degassed and flushed with argon three further times. A quartz cuvette, modified to incorporate a septum, was flushed with argon that had been bubbled through water to saturate the gas before addition of incubation components. Stainless steel, gas-tight, glass syringes (Hamilton, Oregon) with beveled needles were then used in delivery of reagents from the gas train apparatus to the cuvette with the aim of minimizing exposure of anaerobic reagents to O<sub>2</sub>.

### 3.2.3. MAO-B Incubation

In all relevant incubations, DCPIP was added to MAO-B and allowed to equilibrate for at least 5 minutes before addition of BZ as substrate. Inhibition reactions were initiated by addition of a small volume of concentrated PLZ after equilibration of all other reactants for 5 minutes.

### 3.2.4. Benzaldehyde Assay

For measurement of MAO-B activity in some experiments, a spectrophotometric assay for measurement of benzaldehyde production was used. Metabolism of BZ by MAO-B produces benzylimine, which quickly hydrolyzes to benzaldehyde after formation such that enzymatic turnover of one molecule of BZ generates one benzaldehyde molecule. Benzaldehyde has a characteristic absorbance at a wavelength of 254 nm ( $\epsilon \approx 12,500 \text{ M}^{-1}\text{cm}^{-1}$ ), the change in which is measured through a continuous kinetic assay during incubation of MAO-B and BZ,  $\pm$  drugs, in physiological buffer.

### 3.2.5. Analysis and Statistics

Substrate metabolism by MAO-B was graphed as absorbance versus time for each incubation, with the slope of the initial pseudo-linear portion of the resulting curve representing the initial rate of MAO-B activity (mOD/min). For the FlexStation data, initial rates of product

formation over time were determined by linear regression (SoftMax Pro v. 4.8) and were fitted to the equations indicated with the nonlinear regression facility of GraphPad Prism v. 7.0 for Mac OS X (GraphPad Software Inc., San Diego, CA), global fit  $\pm$  SEM. Data from the Cary 60 spectrophotometer were exported to Prism for analysis as described above.

### 3.3. Results and Discussion

#### 3.3.1. Spectral Properties of DCPIP

The molar absorption coefficient of DCPIP in KP buffer (0.1 M, pH 7.4) was determined at 604 nm (Figure 3.1a). A spectral scan of 50  $\mu$ M DCPIP in H<sub>2</sub>O then revealed a peak at 270 nm which was nearly as intense as that at 604 nm, as well as a shoulder peak at 309 nm. Reduction of DCPIP to DCPIPH<sub>2</sub> by excess HCl (200  $\mu$ M) produced a spectrum in which the peak at 604 nm disappeared completely and the UV-range peak/shoulder couple at 270 and 309 nm shifted left to 247 and 280 nm, respectively (Figure 3.1b).

Due to the fact that the benzaldehyde assay measures MAO-B activity as an increase in absorbance at 254 nm, the molar absorption coefficients for DCPIP and DCPIPH<sub>2</sub> were then determined, in H<sub>2</sub>O, at both 604 and 250 nm (Figure 3.1c). For both wavelengths, the molar absorption coefficient for DCPIP was subtracted from that of DCPIPH<sub>2</sub>, in order to calculate the contribution of DCPIP reduction to the increase in absorbance at 254 nm in the benzaldehyde assay. From oxidized DCPIP to reduced DCPIPH<sub>2</sub>, the molar absorption coefficient at 250 nm increases from 9,300 M<sup>-1</sup>cm<sup>-1</sup> to 15,000 M<sup>-1</sup>cm<sup>-1</sup>, while at 604 nm the coefficient decreases from 18,000 M<sup>-1</sup>cm<sup>-1</sup> to 900 M<sup>-1</sup>cm<sup>-1</sup>. Therefore, in assaying the activity of MAO-B by spectrophotometric measurement of the production of benzaldehyde at 254 nm in the presence of DCPIP, the reduction of DCPIP will contribute to the measured increase in absorbance and will

cause an over-estimation of the rate of benzaldehyde production.

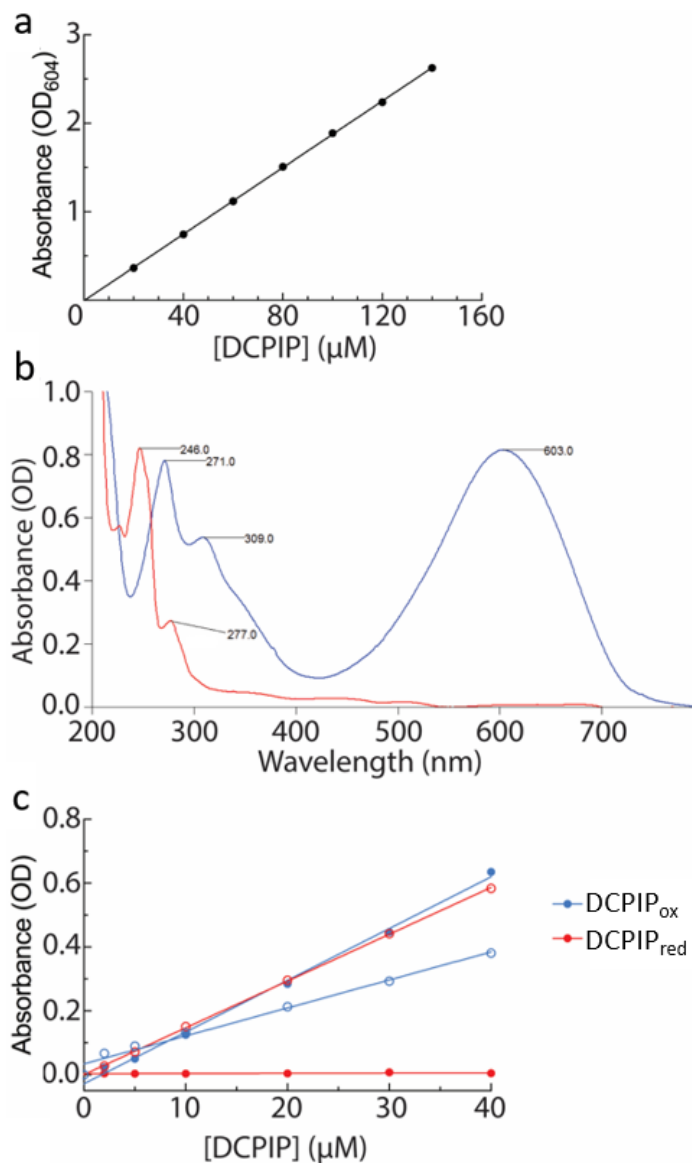


Figure 3.1 Spectral characteristics of DCPIP.

(a) Standard curve of DCPIP absorbance at 604 nm in 0.1 M KP buffer, pH 7.4. The slope of the linear regression ( $r^2 = 0.9999$ ) of absorbance (OD) versus DCPIP concentration corresponds to a molar absorption coefficient of  $\epsilon_{604} = 19,000 \text{ M}^{-1}\text{cm}^{-1}$ . (b) Spectral scan of oxidized 50 μM DCPIP (blue line) in H<sub>2</sub>O. Addition of 200 μM HCl reduces DCPIP (red line), removing the peak at 604 nm and shifting the peaks in the UV range to the left. (c) Standard curve of DCPIP absorbance at 250 and 604 nm, in H<sub>2</sub>O, in the presence or absence of HCl. Open circles = Abs<sub>250</sub>; closed circles = Abs<sub>604</sub>. Reduction of DCPIP results in a decrease in absorbance at 604 nm and an increase at 250 nm. Oxidized:  $\epsilon_{604} = 18,000 \text{ M}^{-1}\text{cm}^{-1}$  ( $r^2 = 0.9960$ ) and  $\epsilon_{250} = 9,300 \text{ M}^{-1}\text{cm}^{-1}$  ( $r^2 = 0.9845$ ). Reduced:  $\epsilon_{604} = 900 \text{ M}^{-1}\text{cm}^{-1}$  ( $r^2 = 0.3069$ ) and  $\epsilon_{250} = 15,000 \text{ M}^{-1}\text{cm}^{-1}$  ( $r^2 = 0.9999$ ).  $\epsilon_{\Delta 604} = 17,000 \text{ M}^{-1}\text{cm}^{-1}$  and  $\epsilon_{\Delta 250} = 5,900 \text{ M}^{-1}\text{cm}^{-1}$ .

### 3.3.2. Interactions

In order to account for all potential sources of spectral interference, DCPIP was incubated with various compounds that would be expected to be found in a typical incubation, including BZ and PLZ, as well as their respective metabolites, benzaldehyde and PEH; phenylacetaldehyde (PAcA) is a starting reagent in the synthesis of PEH, and is also a final product in the metabolism of PLZ by MAO-B, so it was tested as well.

Given that the assay for remaining activity has been a benzaldehyde assay, it was reasonable to test the potential interactions between ascorbate and benzaldehyde. Various concentrations of benzaldehyde (1 - 20  $\mu\text{M}$ ) in a UV  $\frac{1}{2}$  area plate were measured at 254 nm and the molar absorption coefficient ( $\epsilon$ ) calculated from the slope of the linear regression at both wavelengths (Figure 3.2).

The molar absorption coefficient for benzaldehyde absorbance at 254 nm was calculated to be  $3,984 \text{ M}^{-1}\text{cm}^{-1}$ , which is about a third of the literature value of  $12,500 \text{ M}^{-1}\text{cm}^{-1}$  (Suva & Abeles, 1978). The discrepancy in peak absorbance and  $\epsilon_{254}$  between these results and the literature values, as well as the observed increased viscosity of the reagent, suggests that the reagent compound had been exposed to air and had been converted to benzoic acid (Sankar et al., 2014), despite being flushed with and stored under argon.

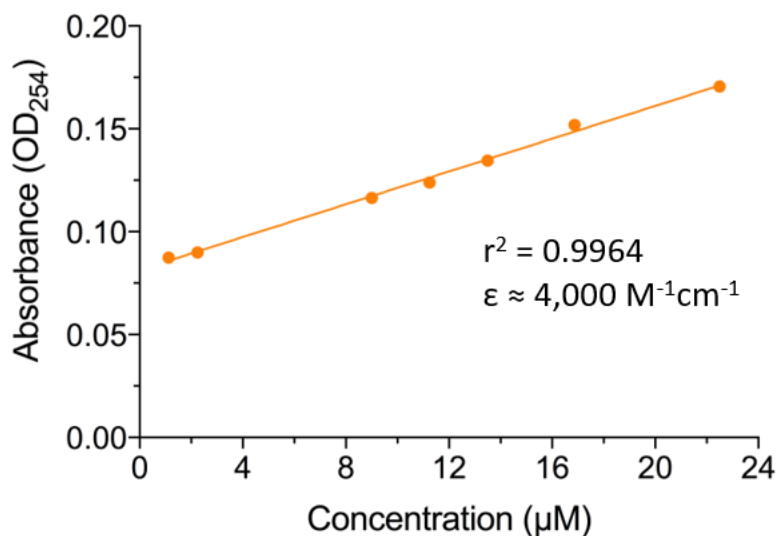


Figure 3.2 Calculation of molar absorption coefficient of benzaldehyde.

The molar absorption coefficient for the reagent benzaldehyde at 254 nm was calculated to be approximately  $4,000 \text{ M}^{-1}\text{cm}^{-1}$ . The large deviation from the literature molar absorption coefficient of  $12,500 \text{ M}^{-1}\text{cm}^{-1}$  (Suva & Abeles, 1978) suggests that the reagent benzaldehyde used in this experiment had possibly polymerized during storage. Therefore, the literature value was used in all calculations regarding benzaldehyde production.

Incubation of PLZ, PEH, or PAcA (1 mM) with DCPIP (50 µM) resulted in a decrease in absorbance at 604 nm and an increase at 254 nm (Figure 3.3), consistent with reduction of DCPIP to DCPIPH<sub>2</sub>. To expand on the PLZ data, a range of PLZ concentrations (0-50 µM) was incubated with DCPIP (50 µM) in a microplate for 4 hours and absorbance monitored at 604 nm. The interaction between DCPIP and PLZ seems to be concentration-dependent, with higher concentrations of PLZ interacting with DCPIP faster, resulting in an increased “rate” of reduction until a plateau is reached (Figure 3.4).

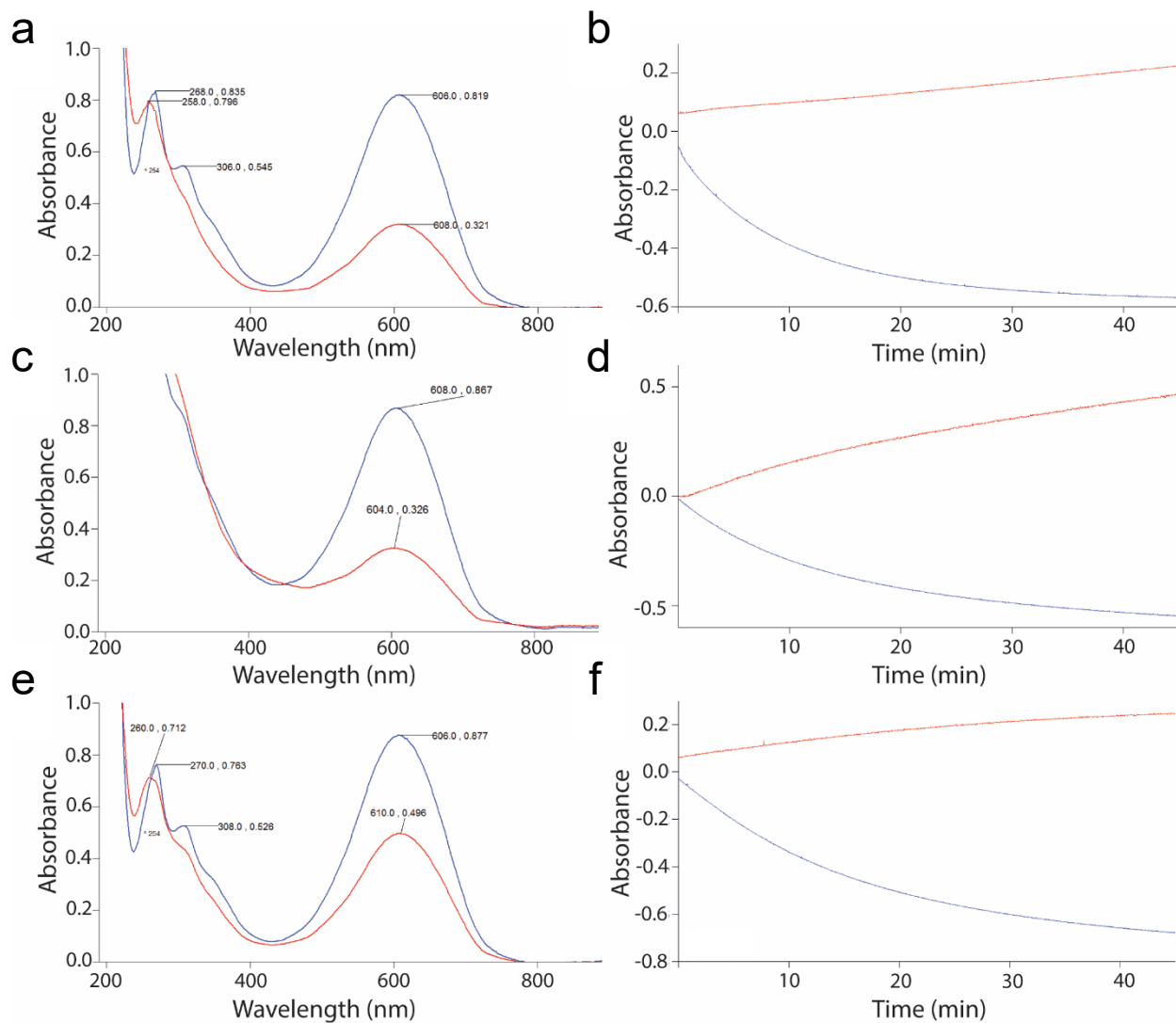


Figure 3.3 Spectral interaction between DCPIP and PLZ and its metabolites.

Absorbance of DCPIP (50  $\mu\text{M}$ ) from 190-900 nm before (blue trace) and 30 minutes after (red trace) addition of 1 mM (a) PLZ, (c) PEH, or (e) PACa. Interaction between DCPIP and 1 mM (b) PLZ, (d) PEH, or (f) PACa over the course of a 45-minute incubation at 250 nm (red trace) and 604 nm (blue trace). Both groups were incubated in pH 7.4 NaP (0.05 M) at 37°C in a quartz cuvette. At 604 nm, PLZ reduced 29.6  $\mu\text{M}$  DCPIP (499 mOD), PEH reduced 32.4  $\mu\text{M}$  DCPIP (545 mOD), and PACa reduced 22.4  $\mu\text{M}$  DCPIP (377 mOD) over 40 minutes (panels a, c, and e, respectively) ( $\epsilon_{\Delta 604} = 17,000 \text{ M}^{-1}\text{cm}^{-1}$ ; Figure 3.1).

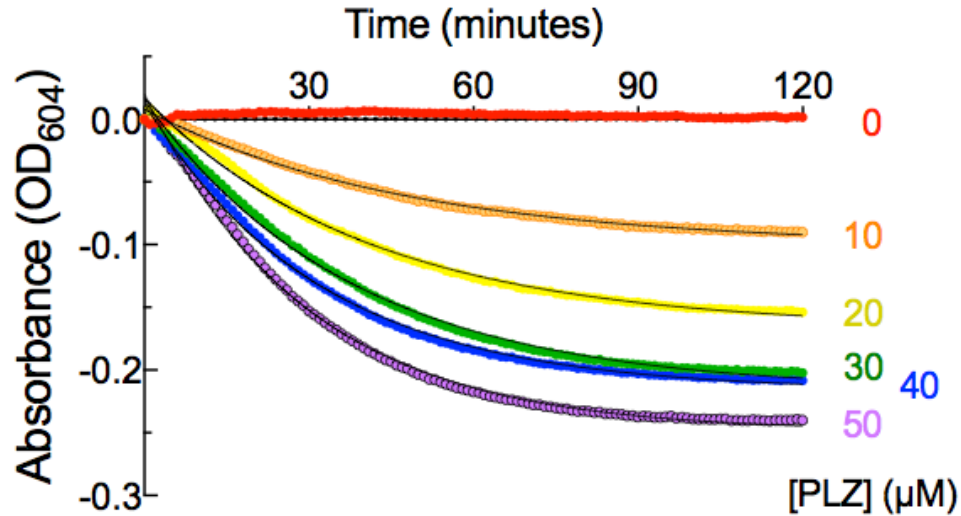


Figure 3.4 Interaction between 50  $\mu\text{M}$  DCPIP and PLZ in 0.1 M KP buffer at 30°C. Control = red (no PLZ), 10  $\mu\text{M}$  = orange ( $r^2 = 0.9781$ ), 20  $\mu\text{M}$  = yellow ( $r^2 = 0.9878$ ), 30  $\mu\text{M}$  = green ( $r^2 = 0.9724$ ), 40  $\mu\text{M}$  = blue ( $r^2 = 0.7232$ ), 50  $\mu\text{M}$  = purple ( $r^2 = 0.7852$ ). At higher concentrations of PLZ, sufficient DCPIP was reduced to facilitate re-oxidation by air that was evident after 2 hours, resulting in an increase in absorbance after the plateau was reached. Therefore, only data from the first two hours were fitted to a one-phase exponential decay equation, except for control (red), by nonlinear regression (Prism7). Using  $\epsilon_{\Delta 604} = 17,000 \text{ M}^{-1}\text{cm}^{-1}$  (Figure 3.1) and the plateaus obtained from nonlinear regression, it was calculated that 10  $\mu\text{M}$  PLZ would reduce 6.0  $\mu\text{M}$  DCPIP, 20  $\mu\text{M}$  PLZ would reduce 10  $\mu\text{M}$  DCPIP, 30 and 40  $\mu\text{M}$  PLZ would each reduce 13  $\mu\text{M}$  DCPIP, and 50  $\mu\text{M}$  PLZ would reduce 15  $\mu\text{M}$  DCPIP.

DCPIP and MAO-B aerobically incubated with PLZ resulted in an increase in absorbance at 250 nm and a decrease at 604 nm over time (Figure 3.5). Given that neither MAO-B nor PLZ absorb at these wavelengths, these changes are assumed to be largely due to DCPIP reduction by enzyme re-oxidation or interaction with PLZ, although interactions with PEH and/or PAcA may contribute to a smaller degree, as evidenced in Figure 3.3.

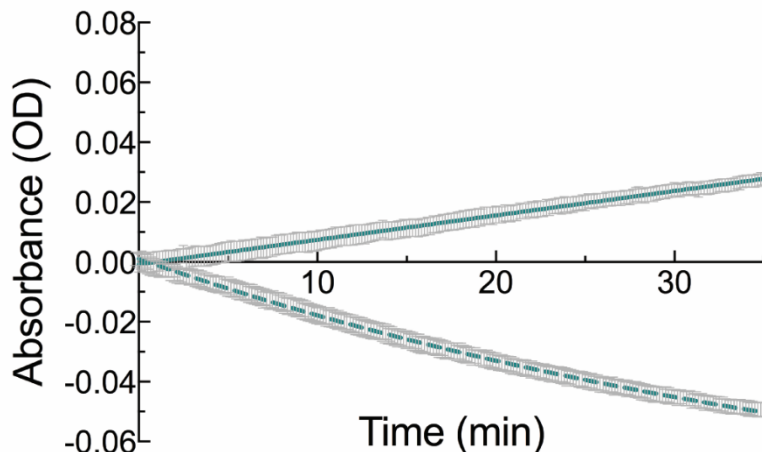


Figure 3.5 Re-oxidation of MAO-B by DCPIP during incubation with PLZ. 2.8 nM MAO-B + 80  $\mu$ M PLZ + 50  $\mu$ M DCPIP incubated 45 minutes at 37°C. Absorbance changes at 254 (solid line) and 604 nm (dashed line) were monitored; error bars (grey) are  $\pm$  SEM of 8 replicates.

### 3.3.3. Aerobic MAO-B Incubation

Assays were performed in the microplate reader using the Flex addition feature. This feature allows for the timed addition of an aliquot, by the internal multichannel pipette system, from a prepared compound plate to the microplate being read, while performing a kinetic analysis of the reaction before and after the addition. After 5 minutes of equilibration to establish a baseline, BZ or PLZ was added to the microplate and the reaction read for a further 40 minutes at 37° C.

The measured rate of change in absorbance at 254 nm due to metabolism of BZ (800  $\mu$ M) by pure MAO-B (2.8 nM) was 2.7 mOD/min (Figure 3.6a). Competition between PLZ (40 or 80  $\mu$ M) and BZ (800  $\mu$ M) for binding to the MAO-B active site resulted in an initial rate of about 1.8 mOD/min, equal to 67% of that in controls (Figure 3.6b). While the presence of DCPIP (40  $\mu$ M) did not seem to influence absorbance at 250 nm, at 604 nm the presence of PLZ resulted in a larger decrease in absorbance than the increase at 250 nm. However, as seen in Figure 3.4, this is likely

due to the interaction between DCPIP and PLZ rather than the influence of DCPIP on the reaction between MAO-B and PLZ.

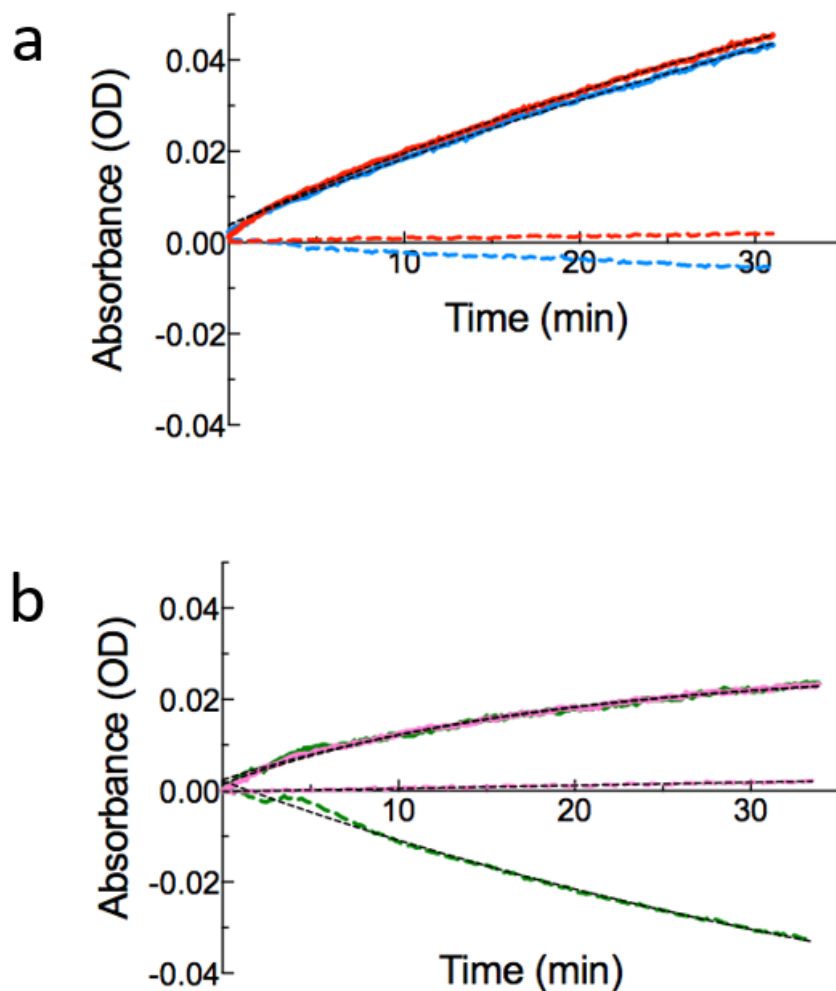


Figure 3.6 Aerobic incubation of 2.8 nM MAO-B and PLZ with or without DCPIP. MAO-B (2.8 nM) incubated aerobically in BZ (800  $\mu$ M) at 37°C in UV  $\frac{1}{2}$ -area plate (40 min). Dotted black lines are non-linear regression best fit lines (one-phase exponential association) for each trace; solid traces are absorbance changes at 254 nm and dashed traces are absorbance changes at 604 nm. (a) MAO-B in BZ alone (red;  $r^2 = 0.5444$ ) and +DCPIP (40  $\mu$ M, blue;  $r^2 = 0.8032$ ). (b) MAO-B incubated with PLZ (40  $\mu$ M) in BZ alone (pink;  $r^2 = 0.7677$ ) and +DCPIP (green;  $r^2 = 0.8422$ ). At these reagent concentrations, there was no measured difference in incubation of MAO-B with DCPIP, with or without PLZ.

Given the previous results, the experiment was repeated with alterations to reagent concentrations. The concentrations of MAO-B and BZ were increased (to 6 nM and 1 mM, respectively) in order to increase activity in controls, while the concentration of PLZ was decreased (12  $\mu$ M) in order to reduce possible competition between DCPIP and PLZ for binding to the active site, as well as to reduce interactions between these compounds, as shown in Figure 3.4. The results are shown in Figure 3.7. At 254 nm (solid lines; Figure 3.7a), DCPIP in the absence of PLZ (blue line) appeared to slightly inhibit MAO-B, reaching a plateau sooner than MAO-B alone (red line). The improved ratio between MAO-B and PLZ (Figure 3.7b) made for much more pronounced inhibition which was visibly different between incubations with (green line) and without (pink line) DCPIP.

The absorbance at 604 nm did not change over the course of the incubation unless DCPIP is included; therefore, changes at this wavelength were attributed to changes in the redox state of DCPIP. In the absence of PLZ (Figure 3.7a, dashed lines), DCPIP absorbance at 604 nm increased over time, plateauing at around 0.05 OD by 30 minutes (blue line). The presence of PLZ ameliorated this increase by about 50% (Figure 3.7b, green line), likely a result of the small interaction between DCPIP and PLZ as evidenced by the decrease in absorbance at about 24 minutes.

Ultimately, spectral interferences complicated analysis and prevented the drawing of firm conclusions. It was clear that there would have to be a sequence of additions, all monitored, to allow for parsing out specific influences on absorbance changes. However, these reagent concentrations and assay conditions served as the basis for the following anaerobic analysis, due to the amount of activity and degree of inhibition seen here.

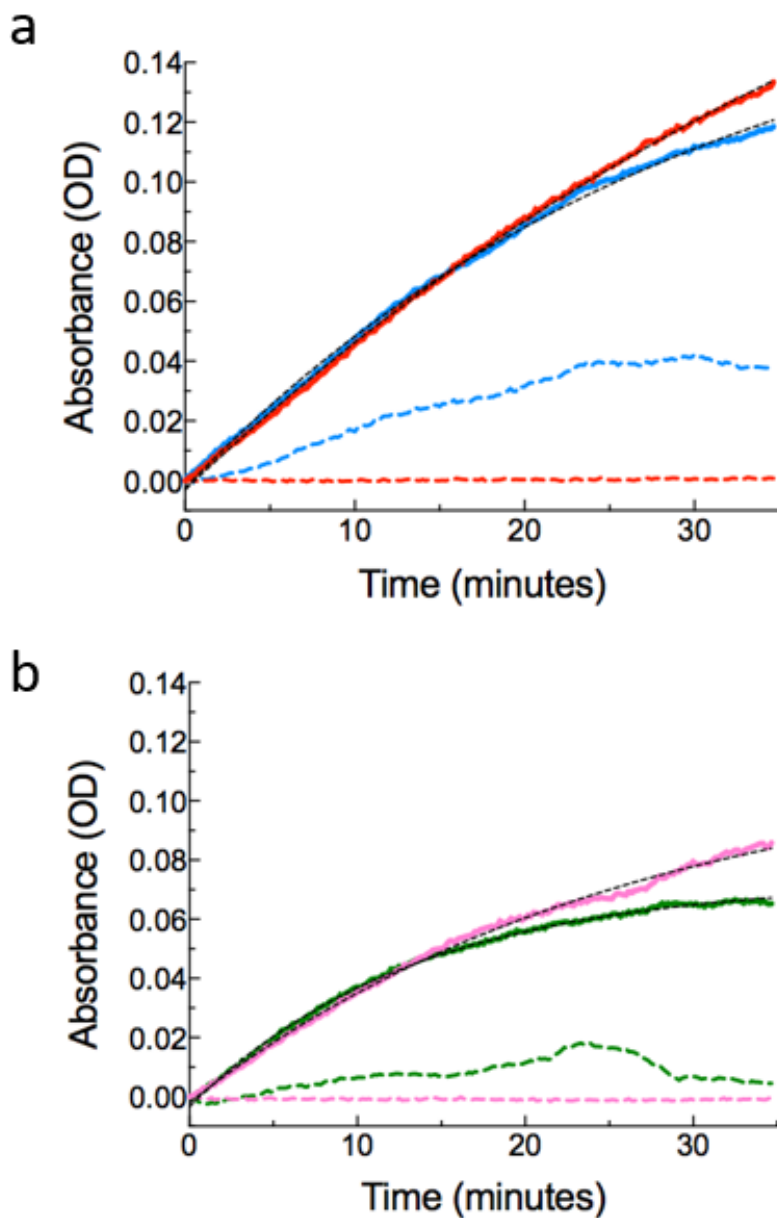


Figure 3.7 Aerobic incubation of 6 nM MAO-B and PLZ with or without DCPIP. MAO-B (6 nM) incubated aerobically in BZ (1 mM) at 37°C in UV  $\frac{1}{2}$ -area plate (40 min). Solid lines are non-linear regression best fit lines (one-phase exponential association) for the change in absorbance at 254 nm, while dashed lines are absorbance changes at 604 nm. **(a)** MAO-B in BZ alone (red;  $r^2 = 0.9950$ ) and with DCPIP (40  $\mu$ M, blue;  $r^2 = 0.9873$ ) did not differ in initial rate (4.6 and 4.7 mOD/min, respectively). **(b)** MAO-B incubated with PLZ (12  $\mu$ M) in BZ alone (pink;  $r^2 = 0.7213$ ) and +DCPIP (green;  $r^2 = 0.7358$ ) also did not differ in initial rate (3.5 mOD/min each), but did differ in  $t_{1/2}$ , from 18.4 min to 9.3 min, when DCPIP was included.

#### 3.3.4. Anaerobic MAO-B Incubation

DCPIP (50  $\mu$ M), BZ (1 mM), MAO-B (6 nM), PLZ (12  $\mu$ M), and H<sub>2</sub>O were made anaerobic overnight, as described above. For each reaction (Table 3.1), a 90-minute pre-incubation of MAO-B at 37°C ensured that any differences in enzyme activity would be the result of the reactants and not due to differences in enzyme incubation across reactions. This was followed by simultaneous injection of BZ (3 mM) and O<sub>2</sub> (200 cc, 95%) into the reaction vessel. The changes in absorbance at 250 and 604 nm were monitored for 40 minutes at 37°C (Figure 3.8). Anaerobic pre-incubations were monitored for absorbance changes over the course of the pre-incubation and the aerobic reaction. Incubations varied by inclusion of DCPIP and PLZ, and by the chronology of their addition to the cuvette.

In otherwise-matched anaerobic pre-incubations of MAO-B and PLZ, the initial rate of remaining enzyme activity ( $v$  (mOD/min)), measured as the increase in absorbance at 254 nm, after introduction of O<sub>2</sub> and BZ to the cuvette, should be lower for the reaction which contained DCPIP than that which did not. This would reflect enzyme inhibition in the absence of O<sub>2</sub> due to the re-oxidation of MAO-B by DCPIP. As well, it is possible that inhibition of the remaining MAO-B after re-introduction of O<sub>2</sub> would occur faster in the presence of DCPIP due to a build up of the inhibitory diazene in solution. If DCPIP is not an efficient flavin oxidizer compared to oxygen, PEDz released from the active site after formation may remain stable in the absence of a stronger oxidizer, resulting in rapid irreversible inhibition of the remaining MAO-B after oxygen is re-introduced.

For controls, MAO-B was pre-incubated aerobically, alone (Reaction 1, Table 3.1) or with PLZ (Reaction 4), and then the solution was injected with O<sub>2</sub> and BZ simultaneously. Untreated MAO-B produced an initial rate of increase in absorbance of 10.6 mOD/min ( $\Delta$ Abs = 480 mOD;

$r^2 = 0.9976$ ; Figure 3.8a), while pre-incubation with PLZ resulted in almost complete loss of activity, with a measured increase in absorbance of only 6 mOD over the 45-minute incubation, or 1.2% of untreated activity (Figure 3.8d). These controls served as positive and negative controls, representing 100% and 0% enzyme activity, respectively.

Addition of PLZ with BZ and O<sub>2</sub> to MAO-B after aerobic pre-incubation alone (Reaction 2) resulted in an initial rate of 8.1 mOD/min, which showed a downwards curvature consistent with time-dependent inhibition, such that the absorbance after 40 minutes was only about 31% of that in controls (Figure 3.8b). When DCPIP was added as well as PLZ, BZ, and O<sub>2</sub> (Reaction 3), the absorbance at both wavelengths increased over the incubation period (Figure 3.8c). The increase at 604 nm (black line; 95 mOD over 40 minutes) was likely due to re-oxidation of DCPIP by O<sub>2</sub> after its reintroduction during re-oxidation of MAO-B. The increase at 254 nm (125 mOD), however, was likely the additive effects of DCPIP reduction and benzaldehyde production.

After aerobic controls were performed, MAO-B and PLZ were anaerobically pre-incubated, with DCPIP (Reaction 6) or without (Reaction 5), and changes in absorbance measured. In the absence of DCPIP (Figure 3.8e), there was a negligible increase in absorbance at 254 nm; after addition of oxygen and BZ (arrow), however, the absorbance change had an initial rate (1 mOD/min) which did not plateau within the incubation time frame. The presence of DCPIP in the anaerobic pre-incubation (Figure 3.8f) resulted in a change in absorbance at 604 nm, consistent with interaction with PLZ and reduction to DCPIPH<sub>2</sub>. Introduction of oxygen (arrow) led to an increase in absorbance at both wavelengths, at a rate of 1 mOD/min each. This increase did not plateau by the end of the incubation period.

Table 3.1

Reaction (Figure)	Condition	Pre-incubation (90 min, 37°C)	Incubation (45 min, 37°C)
1 (Figure 3.8a)	Aerobic	MAO-B	BZ + O <sub>2</sub>
2 (Figure 3.8b)	Aerobic	MAO-B	PLZ + BZ + O <sub>2</sub>
3 (Figure 3.8c)	Aerobic	MAO-B	PLZ + DCPIP + BZ + O <sub>2</sub>
4 (Figure 3.8d)	Aerobic	MAO-B + PLZ	BZ + O <sub>2</sub>
5 (Figure 3.8e)	Anaerobic	MAO-B + PLZ	BZ + O <sub>2</sub>
6 (Figure 3.8f)	Anaerobic	MAO-B + PLZ + DCPIP	BZ + O <sub>2</sub>

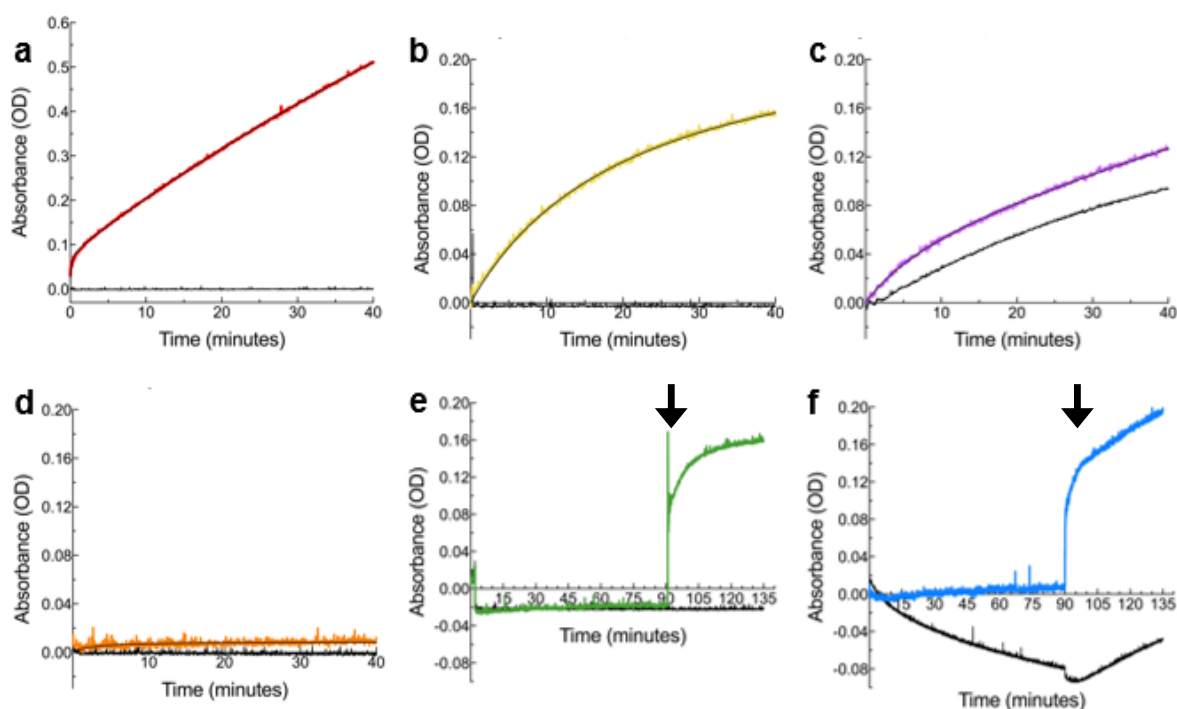


Figure 3.8 Influence of DCPIP on inhibition of MAO-B by PLZ with or without O<sub>2</sub> present. MAO-B (12 nM) pre-incubated at 37°C (90 minutes) before addition of BZ (1 mM) and O<sub>2</sub> (200 cc, 95%). Change in absorbance was measured at 254 nm (colored lines) and 604 nm (black traces) via continuous kinetic assay at 37°C (40 minutes). Curves fitted to one-site (a) or two-site (b, c, d) exponential equations. (a) Aerobic pre-incubation of MAO-B resulted in an initial rate of 10 mOD/min ( $r^2 = 0.9996$ ), serving as control enzyme activity. (b) MAO-B pre-incubated aerobically, followed by simultaneous addition of PLZ+BZ+O<sub>2</sub>. Inhibition by PLZ was monitored over the course of the incubation ( $r^2 = 0.9979$ ). (c) A repeat of (b) in which DCPIP was added to the reaction with PLZ+O<sub>2</sub>+BZ ( $r^2 = 0.9984$ ). (d) Aerobic pre-incubation of MAO-B with PLZ (12  $\mu$ M) resulted in a rate approaching zero, which indicated that the concentrations did result in virtually complete inhibition of MAO-B within the allotted time frame ( $r^2 = 0.1162$ ). (e) Anaerobic pre-incubation of MAO-B and PLZ without DCPIP produced little change in absorbance at either wavelength (0-90 min), and addition of O<sub>2</sub>+BZ at 90 minutes (arrow) gave a curve which plateaued much sooner than (c). (f) Anaerobic pre-incubation of MAO-B with PLZ and DCPIP (50  $\mu$ M) resulted in a decrease in absorbance at 604 nm and a concomitant increase at 254 nm (0-90 min). Introduction of O<sub>2</sub>+BZ at 90 min (arrow) resulted in an increase at both 604 and 254 nm.

In order to quantify the change in absorbance at 254 nm that is due to benzaldehyde production, spectrophotometric data were fitted to an equation for one-phase exponential association via non-linear regression analysis (Prism 7). Re-introduction of oxygen to the incubations which included DCPIP resulted in a background rate of increase in absorbance at 250 nm at just over 10 minutes into the read (Figures 3.9b and 3.9d, arrows). This was likely attributable to DCPIP reduction (see Figure 3.1). Baseline removal of this linear increase from the entire trace revealed, in both cases, a curve which plateaued after roughly 10 minutes (Figures 3.9b, d). In the case of the anaerobic incubations, inhibition of MAO-B by PLZ occurred more rapidly when DCPIP was included (Figure 3.9d) than not (Figure 3.9c).

Given the semi-quantitative nature of these observations, a different method for parsing out spectral influences in a reaction was investigated. Stopped-flow, or pre-steady-state, spectrophotometry is a technique that can provide extensive spectral data of the first few milliseconds of a reaction, before any equilibrium has been established. While the rapid scanning capabilities of the instrument would not be required in this study, the software used to analyse stopped-flow data is capable of isolating changes in concentrations of individual species within a complex spectrum, given information about spectra of the various species participating in the reaction, and this capability may facilitate isolation of spectral changes due solely to anaerobic reduction of DCPIP. However, preliminary experiments revealed that intense radiation in the far-UV range generated by the mercury lamp resulted in photochemical changes (perhaps related to the presence of  $\beta$ -octyl glucopyranoside and/or glycerol in the solubilized enzyme solution) and a large accompanying increase in absorbance at 267 nm that masked enzyme-mediated spectral signals. As a result, this approach was not pursued.

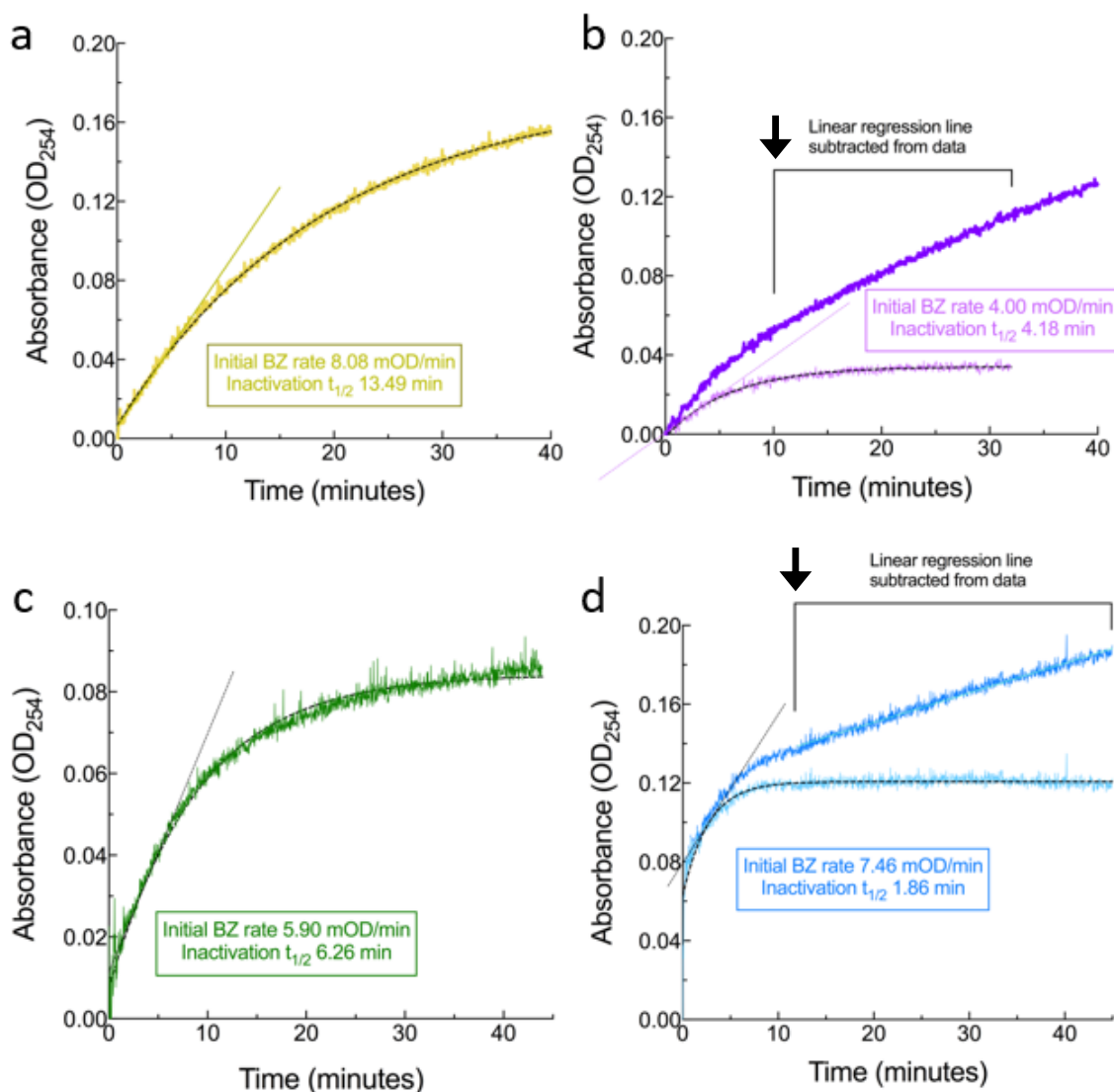


Figure 3.9 Comparisons between  $\pm$  DCPIP for aerobic and anaerobic reactions.

Comparisons between aerobic reactions 2 (a) and 3 (b) from Table 3.1, as well as between anaerobic reactions 5 (c) and 6 (d), reaction pairs which differ by the presence of DCPIP. Incubations with DCPIP (b and d) were baseline corrected for the increase in absorbance at 250 nm due to DCPIPH<sub>2</sub> formation (bracketed section), revealing a plateau of enzyme activity reached very rapidly (at arrows), compared with equivalent reactions done in the absence of DCPIP (a and c, respectively). Inclusion of DCPIP in the anaerobic incubation of MAO-B and PLZ resulted in a much faster  $t_{1/2}$  (1.86 min) compared to without (6.26 min) and compared to the aerobic incubation of MAO-B with PLZ and DCPIP (4.18 min), despite a lower initial rate of activity after pre-incubation (7.46 mOD/min versus 5.90 mOD/min and 4.00 mOD/min, respectively), for an overall faster inactivation of MAO-B. Curved fitted by non-linear regression to one-phase exponential association curves ( $r^2 = 0.9981, 0.9733, 0.9032, \text{ and } 0.9937$ , respectively; Prism7).

### 3.4. Conclusion

DCPIP as a replacement for oxygen in the redox cycle of FAD yielded some promising results. It was clear from these experiments that DCPIP could re-oxidize MAO-B, as incubating MAO-B and DCPIP together resulted in changes in absorbance that were consistent with DCPIP reduction to DCPIPH<sub>2</sub> (Figures 3.5 and 3.6). This reduction of DCPIP to DCPIPH<sub>2</sub> results in a decrease in absorbance at 604 nm, but also an increase at 254 nm (Figure 3.1c), necessitating the removal of this contribution from the resulting kinetic reads, as seen in Figures 3.9b and d. Interactions between DCPIP and PLZ (Figure 3.4), as well as between DCPIP and PEH and PAcA (Figure 3.3), also have to be accounted for in analyzing results.

Figures 3.9c and d provide the best approximation for the influence of DCPIP on the inhibition of MAO-B by PLZ in anaerobic conditions. While the initial rate of activity remaining after re-introduction of oxygen was not lower in pre-incubations of MAO-B and PLZ in the presence of DCPIP (7.5 mOD/min +DCPIP (Figure 3.9d) vs 5.9 mOD/min -DCPIP (Figure 3.9c)), the half-life of inactivation was greatly reduced (1.86 min +DCPIP vs 6.26 min -DCPIP). The decrease in absorbance at 604 nm during the anaerobic pre-incubation of MAO-B and PLZ in the presence of DCPIP (Figure 3.8f, black trace) indicates reduction of DCPIP, which is mirrored in the increase in absorbance at 250 nm (blue line) over the same period of time. In contrast, anaerobic pre-incubation without DCPIP (Figure 3.8e) saw no change in absorbance until the introduction of O<sub>2</sub>, after which point enzyme activity was comparable to control (Figure 3.8a, red line) as well as the aerobic version of this reaction (Reaction 2, Figure 3.9a). This suggests that MAO-B was not inhibited during anaerobic pre-incubation, despite clear indication that MAO-B was being re-oxidized by DCPIP (Figure 3.5).

However, the fact that the half-life was less than a third that of the -DCPIP reaction indicated that there had been an accumulation of PEDz in bulk solvent during anaerobic pre-incubation which, after re-introduction of O<sub>2</sub>, rapidly inhibited MAO-B. This accumulation could be explained by increased stability of the diazene in anaerobic conditions, as shown by Battioni et al. (1983).

The capacity of DCPIP to re-oxidize MAO-B in place of oxygen allowed for accumulation of PEDz in solution under anaerobic conditions, which would only occur if PEDz was formed and released from the active site preceding re-oxidation of FAD, which must occur before PEDz can irreversibly inactivate MAO-B. That MAO-B was not able to be irreversibly inhibited anaerobically, despite the capacity to be re-oxidized by DCPIP, suggests a role of O<sub>2</sub> in not only re-oxidizing FAD, but in radicalizing PEDz as well, after release from the active site.

Future directions for this technique are exciting; these include measuring remaining enzyme activity using radioactive BZ and measuring radioactive benzaldehyde production in order to circumvent spectral interferences between reaction components and the mechanism by which turnover is quantified. Given that these interferences were the largest hurdle in this study, accounting for, or circumventing them would go a long way in confirming these initial results.

## Chapter Four

### Evidence for the Dissociation of PEDz From the Active Site of Reduced MAO-B

#### 4.1. Introduction

Ascorbate has been shown to act as a scavenger of reactive compounds, such as diazenes, and that is the capacity in which ascorbate is used in this line of experiments. Ascorbic acid (vitamin C) is an important antioxidant with many biological roles. The fully reduced ascorbic acid (AA;  $pK_a = 4.2$ ) can oxidize once to form an ascorbate anion ( $A^-$ ;  $pK_a = 11.6$ ), which can then donate a second  $H^+$  as well as two electrons to form the fully oxidized dehydroascorbic acid (DHA; Figure 4.1). These three compounds are able to be reduced and/or oxidized repeatedly in the absence of enzymatic DHA degradation (Buettner, 1990). The majority of ascorbate at physiological pH (pH 7.4) is  $A^-$ , which can donate or accept an electron.

Ascorbate autoxidizes in the presence of adventitious transition metals like iron and copper. These metals are common contaminants in phosphate buffers, which contain 0.001-0.008% iron, enough that a 20 mM solution can contain between 0.2 and 1.6  $\mu M$  iron, resulting in a 5-11% loss of a 0.1 M solution of ascorbate (11.67  $\mu M$ ) at pH 7.4 (Buettner, 1988). Metal contaminants such as iron ( $Fe^{2+/3+}$ ) and copper ( $Cu^{2+}$ ) in buffers have long been known to alter the dynamics of redox reactions, due to the ability of these metals to easily accept or donate electrons to other species. Chelators such as diethylenetriaminepentaacetic acid (DTPA) and ethylenediaminetetraacetic acid (EDTA) chelate iron and copper readily (Buettner & Czapski, 1986). EDTA, however, forms an EDTA- $Fe^{3+}$  complex with increased capacity to oxidize ascorbate through the Haber-Weiss driven Fenton reaction, which can result in 30% loss of ascorbate (0.1 mM, pH 7.0) over 15 minutes (Buettner & Czapski, 1986). DTPA is an aminopolycarboxylic acid chelating agent which does

not form pro-oxidant species with the transition metals in question (Halliwell, 1978).

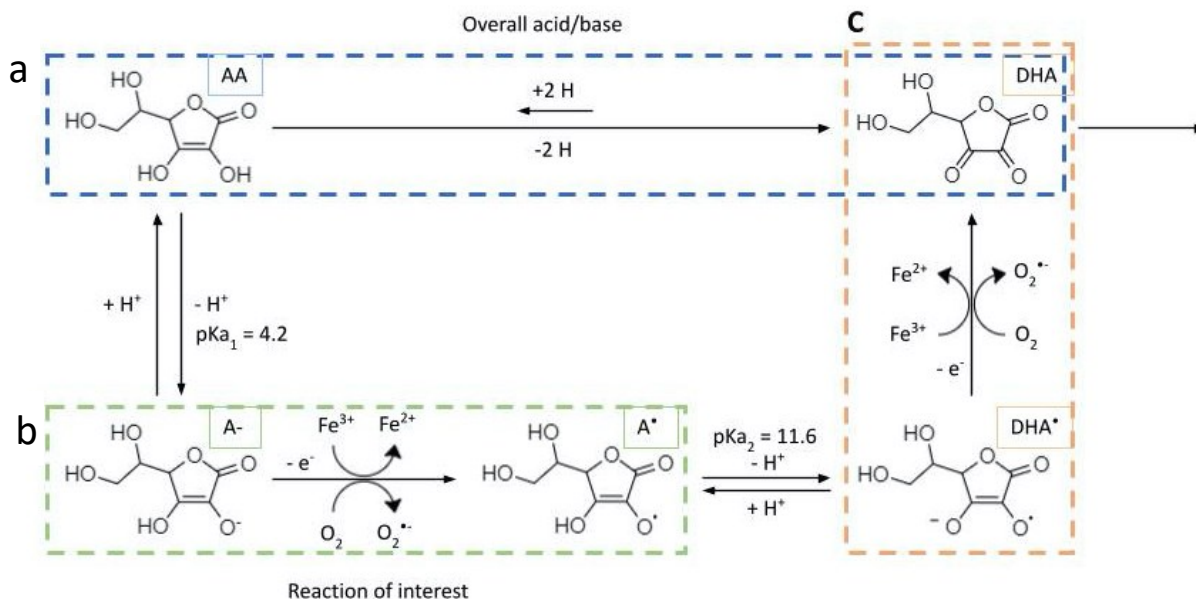


Figure 4.1 Reaction mechanism for ascorbate.

(a) Acid/base reaction in which ascorbic acid (AA) loses two hydrogens overall to become dehydroascorbate (DHA; blue dashed box). (b) AA can lose one hydrogen to form an ascorbate anion (A<sup>-</sup>; pK<sub>a1</sub> = 4.2), which autoxidizes in the presence of Fe<sup>3+</sup> and O<sub>2</sub> to an ascorbate radical (A<sup>•</sup>; green dashed box). (c) At high pH, A<sup>•</sup> loses another hydrogen (pK<sub>a2</sub> = 11.6) to form DHA radical (DHA<sup>•</sup>), which again is oxidized by Fe<sup>3+</sup> and O<sub>2</sub> to form DHA (orange box). DHA is then broken down to ketones, removing it from the cycle. Removing as much iron as possible will reduce the loss of ascorbate to autoxidation (figure adapted from Figueroa-Méndez & Rivas-Arancibia, 2015).

Chapter 2 of this thesis looked at how the metabolites PEDz and PEH may be formed, providing evidence for the stepwise mechanism. According to the hypothesized mechanism, MAO-B oxidizes PLZ to PEDz, which undergoes intramolecular rearrangement in bulk solvent to form PEH. Chapter 3 explored the role of O<sub>2</sub> in the inhibition of MAO-B by PLZ, providing evidence for movement of PEDz from the active site into bulk solvent, and thus the potential for obligate re-oxidation of the FAD before covalent modification by PEDz. Here, the reductive ability of ascorbate was examined with respect to re-oxidizing PEDz to PLZ. If ascorbate could convert

PEDz back to PLZ before forming PEH or inactivating the enzyme, it would likely do so outside of the active site. Scavenging the diazene intermediate was suggested by Silverman (1995a) as a method of investigating the dissociation of PEDz from the active site, and had been attempted previously in this lab with other free radical scavengers, specifically glutathione (GSH) and N-acetylcysteine (NACys) (unpublished work); these were also revisited, briefly, in this chapter.

Initially, inhibition of soluble MAO-B by PLZ in the presence of ascorbate was monitored spectrophotometrically, although interferences necessitated a different approach using membrane particles. The use of membrane particles (membrane-bound human MAO-B in a homogenate of mitochondrial membranes isolated from *Pichia pastoris* yeast) allowed for spectral analysis of pre-treated enzyme without the problem of overlapping, interfering spectral changes between reactants. By centrifuging and resuspending the membrane particles in fresh physiological buffer after incubation, the remaining activity could be measured in an Amplex Red assay.

#### 4.1.1. Hypotheses

- PEDz formed from the oxidation of PLZ by MAO-B dissociates from the reduced enzyme before covalent modification of the re-oxidized FAD cofactor.
- Ascorbate, as a free radical scavenger, will reduce PEDz back to PLZ, preventing inhibition of MAO-B.

#### 4.1.2. Specific Aims

- Test ascorbate autoxidation and DTPA chelation of metal ion contaminants in sodium phosphate (NaP) buffer at pH 7.4.
- Test the influence of ascorbate on inhibition of MAO-B by PLZ. A reduction in the extent of MAO-B inhibition by PLZ in the presence of ascorbate will support the hypothesis that PEDz leaves the active site after formation.

## 4.2. Materials and Methods

### 4.2.1. Materials

All water used in the experiments was filtered through a Millipore Milli-Q filtration system. Benzylamine (BZ) hydrochloride, HRP (Type II), catalase, iron sulfate heptahydrate, H<sub>2</sub>O<sub>2</sub>, PLZ sulfate, sodium ascorbate, DTPA, and EDTA were purchased from Sigma-Aldrich. Amplex Red reagent (N-acetyl-3,7-dihydroxyphenoxazine) was purchased from Invitrogen. Methanol, mono-basic and di-basic sodium phosphate, and mono-basic and di-basic potassium phosphate were obtained from Fisher Scientific. For spectrophotometric experiments, 96-well microplates were obtained from Greiner Bio-One. All plasticware was purchased from Eppendorf. Full length hMAO-B was expressed in *Pichia pastoris* yeast and purified in our laboratory in two forms, soluble enzyme and mitochondrial membrane-bound enzyme. PEH was synthesized from phenylacetaldehyde and hydrazine monohydrate in the laboratories of Dr. Velázquez-Martínez in the Faculty of Pharmacy and Pharmaceutical Sciences, University of Alberta.

Phosphate buffers were prepared as described in Chapter 1; mono-basic and di-basic sodium or potassium phosphate solutions were made up in H<sub>2</sub>O (0.2 M each), and di-basic was added to mono-basic solution until the desired pH of 7.4 was reached. Pure enzyme was incubated in 0.05 M NaP buffer and membrane particle-bound enzyme was incubated in 0.1 M potassium phosphate (KP) buffer. Ascorbate, PLZ, BZ, EDTA, and DTPA were dissolved in H<sub>2</sub>O. PEH has low solubility in water, and therefore was prepared in methanol before being diluted 10-fold in H<sub>2</sub>O as needed, such that the final methanol content is 0.1% in the spectrophotometric assay. PLZ, PEH, BZ, Amplex Red, and ascorbate were made fresh for each experiment.

#### 4.2.2. MAO-B Incubation

All MAO-B incubations were performed at 30°C. The stock concentration of MAO-B was determined as described previously ( $[\text{MAO-B}]_{\text{stock}} = 0.56 \mu\text{M}$ ; Chapter 2, section 2.3.1). MAO-B was pre-incubated in the absence or presence of drugs for a range of times such that the longest incubation was started first and the “0” time incubation occurred just before the reaction was stopped in all samples at once, allowing for better control of the incubation time. To prevent further inhibition of MAO-B after pre-incubation, a saturating concentration of substrate was added so as to outcompete inhibitor binding, or the reaction vessel was chilled rapidly to around 0°C to greatly reduce further enzyme-mediated PLZ turnover. The latter method was used with membrane particle incubations before centrifugation removed the majority of ligands. In this way, the reaction was essentially paused until the remaining enzyme activity could be assayed, minimizing further loss of activity.

#### 4.2.3. Spectrophotometry

Experiments were performed in a Cary 60 spectrophotometer, with cuvette temperature controlled by a water-cooled Peltier thermoelectric device and with sample mixing achieved with an incorporated magnetic stirrer. Some assays were done in quartz cuvettes (1 or 3 mL) to allow for measuring absorbance at wavelengths below 340 nm, when required. Others were performed in a FlexStation microplate reader. Microplates (96-well) were obtained from Greiner Bio-One; assays performed in the UV range were read in UV plates (cyclic olefin copolymer; COC); otherwise, the plates were polystyrene.

#### 4.2.4. Benzaldehyde Assay

For measurement of MAO-B activity in some experiments, a spectrophotometric assay for measurement of benzaldehyde production was used. Metabolism of BZ by MAO-B produces benzylimine, which quickly hydrolyzes to benzaldehyde after formation such that enzymatic turnover of one molecule of BZ generates one benzaldehyde molecule. Benzaldehyde has a characteristic absorbance at a wavelength of 254 nm ( $\epsilon \approx 12,500 \text{ M}^{-1}\text{cm}^{-1}$ ), the change in which is measured through a continuous kinetic assay during incubation of MAO-B and BZ,  $\pm$  drugs, in physiological buffer.

#### 4.2.5. Amplex Red Peroxidase Assay

A more sensitive assay for the remaining MAO-B activity is the Amplex Red peroxidase (AR/P) assay, in which the change in absorbance at 571 nm is coupled to the metabolism of substrate by MAO-B. Amplex Red is a chromogenic compound which is near-colourless. Horseradish peroxidase (HRP) utilizes  $\text{H}_2\text{O}_2$ , a by-product of the MAO-B oxidative half-reaction, to convert Amplex Red to resorufin, a bright pink compound which absorbs strongly at 571 nm ( $\epsilon \approx 70,600 \text{ M}^{-1}\text{cm}^{-1}$ ) in a stoichiometric relationship such that one enzyme turnover results in one molecule of resorufin being produced. Therefore, the rate of increase in absorbance at 571 nm is an indirect measure of enzyme activity.

A solution of BZ (3 mM, final), Amplex Red (20  $\mu\text{M}$ , final), and HRP (5  $\mu\text{g}/\text{ml}$ , final) in KP buffer (0.1 M) was added to an aliquot of enzyme and immediately read in a continuous kinetic assay at 25°C. Initial rate of activity at each time point of incubation was graphed in Prism7.

#### 4.2.6. Ascorbate Oxidation

The rate of autoxidation was defined as change in absorbance at 266 nm over time (mOD/min). The final concentration of ascorbate in pre-incubations was 50  $\mu\text{M}$  unless otherwise stated. Oxidants were  $\text{Fe}^{2+}$  (10  $\mu\text{M}$ , final) and  $\text{H}_2\text{O}_2$  (200  $\mu\text{M}$ , final); iron sulphate heptahydrate ( $\text{FeSO}_4 \cdot 7\text{H}_2\text{O}$ ) supplied  $\text{Fe}^{2+}$  ions. For each incubation, all reactants except ascorbate were allowed to equilibrate for 5 minutes in the cuvette, with the addition of a small volume of concentrated ascorbate starting the reaction. Initial absorbance of ascorbate was determined as the first stable portion of the readout after addition to the cuvette. The plateau was considered to be the point at which no further oxidation of ascorbate occurred.

#### 4.2.7. Membrane Particle Preparations

The concentration of MAO-B in the membrane particle stock was 2.87  $\mu\text{M}$ . The tube containing aliquots of membrane particles was removed from  $-20^\circ\text{C}$  storage and thawed on ice, vortexing occasionally until all visible clumps had dissipated and the solution appeared well-mixed. Membrane particles were added to a 1.5 mL Eppendorf tube containing a minimal volume of buffer (15  $\mu\text{L}$  0.1 M KP buffer), such that the total volume for homogenizing did not exceed 50  $\mu\text{L}$ , and homogenized with a pellet pestle on ice until the contents were frothy. Larger volumes of enzyme mixture were homogenized as described in batches ( $\leq 50 \mu\text{L}$ ) and combined in the final container. The pestle was then rinsed in the buffer that was added to the tube in order to dilute to the target concentration, such that the final concentration of MAO-B in the membrane particle preparation was 10.8 nM in pre-incubations and 5.38 nM in the spectrophotometric assay.

The pre-incubation temperature was maintained at  $30^\circ\text{C}$  in a water bath. The reaction was slowed rapidly by submersion of tubes into a salted ice water bath ( $-4^\circ\text{C}$  -  $0^\circ\text{C}$ ); this chilled temperature was maintained throughout the rest of the preparation, until analysis, by returning

tubes to the salted ice water bath between processing steps.

The tubes were then centrifuged twice at 14,000 rpm (20,817 g) for 15 minutes at 0°C, retaining the pellet; the aspirated supernatant was either discarded or collected in a clean tube and kept chilled prior to analysis. After the first centrifugation, fresh ice-cold KP buffer was added to the pellet, the tubes briefly vortexed (5 seconds), and centrifuged again. After the second centrifugation, the pellet was resuspended as previously described and kept chilled in a salted ice water bath until analysis.

#### 4.2.8. Analysis and Statistics

Substrate metabolism by MAO-B was graphed as absorbance versus time for each incubation, with the slope of the initial pseudo-linear portion of the resulting progress curve representing the initial rate of MAO-B activity (mOD/time). FlexStation data were exported to GraphPad Prism 7 to reproduce progress curves. Initial rates of product formation over time were determined by linear regression (SoftMax Pro v. 4.8) and were fitted to the equations indicated with the nonlinear regression facility of GraphPad Prism v. 7.0 for Mac OS X (GraphPad Software Inc., San Diego, CA), global fit  $\pm$  SEM. Groups were compared by one-way ANOVA followed by Sidak's multiple comparisons test, and significance was set at  $p < 0.05$ . For the FlexStation data,

### 4.3. Results and Discussion

#### 4.3.1. Ascorbate Redox Profile

In order to determine the amount of ascorbate that is oxidized in the presence of oxidants, the change in absorbance of different concentrations of ascorbate (20, 40, and 60  $\mu\text{M}$ ) was measured over time in unchelated buffer (Figure 4.2; red line). From the slope of a replot of peak absorbance values, an estimate of  $14,800 \text{ M}^{-1}\text{cm}^{-1}$  was obtained for the molar absorption coefficient of ascorbate, which agrees well with a literature value of  $14,500 \text{ M}^{-1}\text{cm}^{-1}$  at pH 7.7 and 265 nm (Karayannis et al., 1977). Overloading the unchelated buffer with  $\text{Fe}^{2+}$  and  $\text{H}_2\text{O}_2$  resulted in 96-99% autoxidation of ascorbate (blue line). This highlighted the need for chelation of the buffer in order to minimize ascorbate autoxidation.

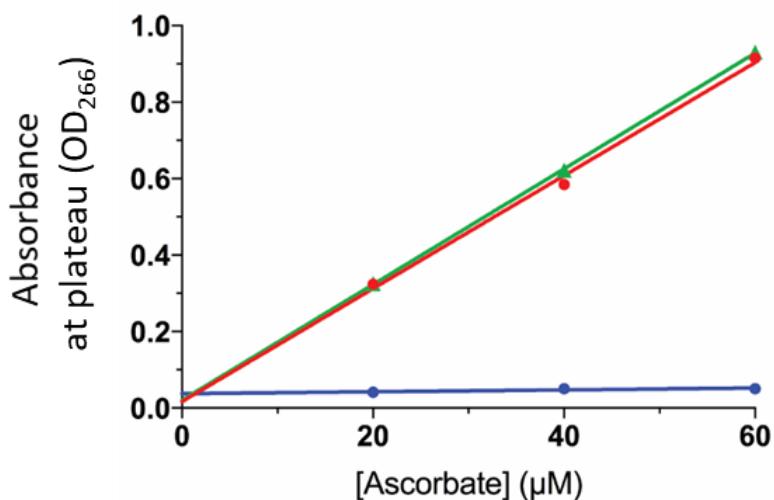


Figure 4.2 Absorbance of ascorbate in presence or absence of excess antioxidants.

Absorbance in KP buffer (266 nm, 0.1 M, pH 7.4) was measured (room temperature), once the trace stabilized, after addition of ascorbate (20, 40, or 60  $\mu\text{M}$ ; red line), immediately after addition of excess antioxidants (10  $\mu\text{M}$   $\text{Fe}^{2+}$  and 200  $\mu\text{M}$   $\text{H}_2\text{O}_2$ ; green line) to the ascorbate, and after trace plateau (at least 100 minutes; blue). From the slope of the replot of ascorbate absorbance (red), an estimated molar absorption coefficient of  $14,800 \text{ M}^{-1}\text{cm}^{-1}$  was determined for ascorbate. There was little difference between absorbances in control (red) and immediately after oxidant addition (green). However, the absorbance at plateau for each ascorbate concentration incubated with autoxidants was indistinguishable from zero (blue).

#### 4.3.2. Chelating Iron Contaminants in Buffer

Ascorbate autoxidation in buffer which had been chelated with either EDTA or DTPA was measured via a continuous kinetic read for 20 minutes at room temperature (Figure 4.3a). Without chelation, 0.05 M NaP contains sufficient contaminants to oxidize about 26% of the ascorbate over 20 minutes (grey bar). With EDTA, that value falls only to 23% (green bar). This is likely due to the formation of EDTA-Fe complexes, which remain capable of catalyzing ascorbate autoxidation (Buettner & Czapski, 1986). With DTPA, autoxidation of ascorbate was reduced by 99.5% (blue bar), which is the lower limit of metal chelation before the environment becomes the limiting factor (Buettner, 1988). DTPA does not form pro-oxidant complexes with metal ions, including  $\text{Fe}^{2+}$ , therefore ascorbate autoxidation in DTPA-chelated buffer is reduced virtually to zero.

#### 4.3.3. Interactions with PEH or PLZ

As the goal was to measure the impact of ascorbate on the inhibition of MAO-B by PLZ, through a redox reaction between ascorbate and PEDz, interactions between reaction components and ascorbate needed to be accounted for. Therefore, the influence of PLZ and PEH on ascorbate oxidation was measured in both unchelated (NaP) and DTPA-chelated buffer ( $\text{NaP}_{\text{DTPA}}$ ; Figure 4.3b).

In NaP, PEH (red) and PLZ (yellow) both resulted in nearly the same rate of ascorbate autoxidation as control (25% and 26% versus 26%, respectively). When added to NaP that had been chelated with DTPA, ascorbate autoxidation rates decreased to those seen with  $\text{NaP}_{\text{DTPA}}$  alone (0.95% each). This indicated that there was no interaction between ascorbate and PLZ or PEH, and further solidified the decision to include DTPA in future incubations in which iron contamination may pose an issue, especially in light of the underwhelming results for EDTA.

#### 4.3.4. MAO-B Test

Preliminary experiments were run in order to gauge viability of the experimental approach. In a 1.5 mL tube, pure MAO-B (20 nM) was incubated with PLZ (20  $\mu$ M) in the presence and absence of ascorbate (50  $\mu$ M) in NaP<sub>DTPA</sub> (0.05 M pH 7.4 NaP and 100  $\mu$ M DTPA) and catalase for 60 minutes at room temperature; MAO-B incubated alone served as control. Catalase (1  $\mu$ g/mL, 10 IU/mL) was included in the incubation in order to break down any H<sub>2</sub>O<sub>2</sub> produced from MAO-B activity, minimizing ascorbate autoxidation as well as oxidation of enzyme residues, such as sulfhydryl groups on cysteines. Over the course of an hour, at each of 14 time points, an aliquot was removed from the reaction tube and added to a UV microplate well containing cold BZ (1 mM). The microplate was kept on ice to prevent excess enzyme turnover in pre-incubated aliquots as the time course progressed. The plate was then warmed in the FlexStation spectrophotometer (37°C) for 3 minutes and benzaldehyde production was read via a continuous kinetic assay for 1 hour, at 17 second intervals. Data were imported into and analyzed in Prism7 (Figure 4.4).

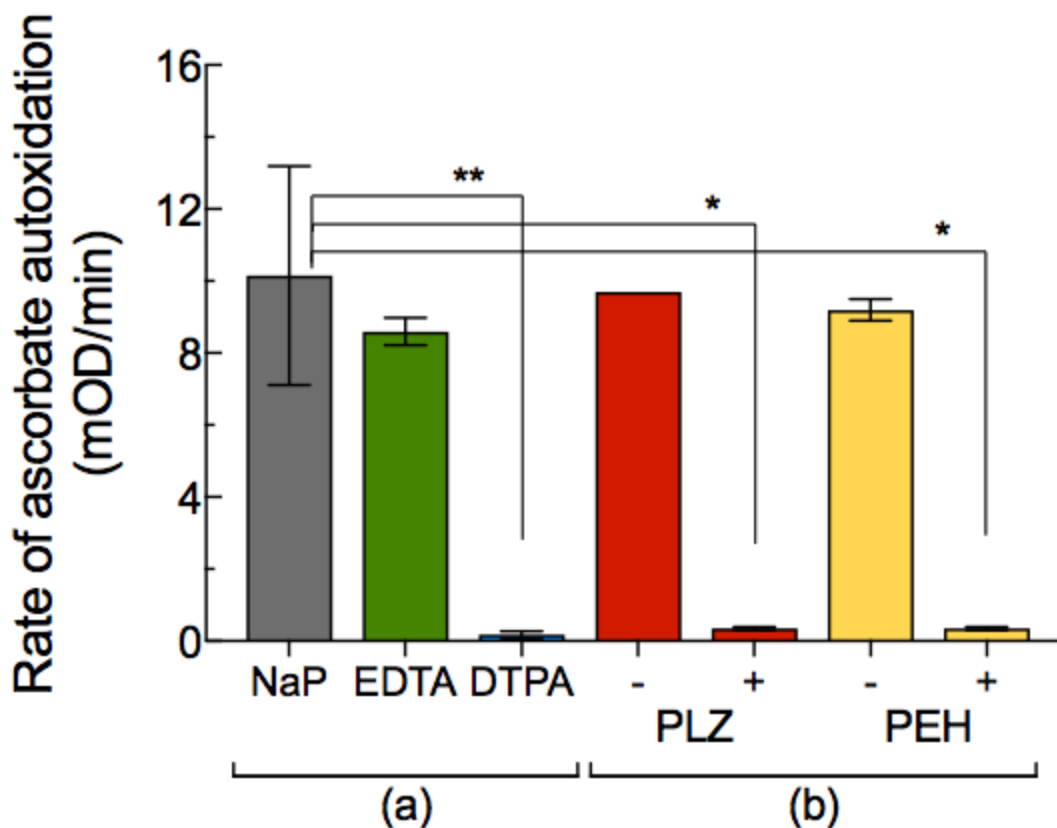


Figure 4.3 Ascorbate autoxidation in NaP buffer ± chelator.

(a) The rate of ascorbate autoxidation (mOD/min) in unchelated NaP buffer (pH 7.4 0.05 M; grey bar (n=4)) compared to buffer that had been chelated with 100  $\mu$ M EDTA (green bar (n=3)) or 100  $\mu$ M DTPA (blue bar (n=4)). Autoxidation in unchelated buffer ( $10.2 \pm 3.0$  mOD/min) was not statistically different from that of EDTA-chelated buffer ( $8.6 \pm 0.38$  mOD/min;  $p = 0.9707$ ), but was statistically different from DTPA-chelated buffer ( $0.18 \pm 0.10$  mOD/min;  $**p = 0.0031$ ). (b) The influence of 10  $\mu$ M PLZ (red bars) or 10  $\mu$ M PEH (yellow bars) on ascorbate autoxidation in unchelated (-) and in DTPA-chelated (+) buffer (n=2, each). The difference in autoxidation rate between unchelated and DTPA-chelated buffer carried over to incubations with PEH and PLZ. Ultimately, PLZ and PEH did not influence ascorbate autoxidation, whether in the presence ( $0.35 \pm 0.05$  mOD/min for both,  $*p = 0.0152$ ) or absence ( $9.7 \pm 0.0$  mOD/min,  $p = 0.9998$ ; and  $9.2 \pm 0.3$  mOD/min,  $p = 0.9982$ ; respectively) of DTPA. One-way ANOVA was performed for n replicate measurements and multiple comparisons performed for each group; error bars are mean  $\pm$  SEM.

Unfortunately, in these preliminary experiments, the low sample size and large scatter of points along the line of best fit for initial rates of activity at different time points failed to conclusively demonstrate an effect by ascorbate on inhibition of MAO-B by PLZ. Control rates appeared to increase with preincubation time, and it seems reasonable to assume that this may also have occurred in reactions containing PLZ and PLZ+ascorbate, to a similar degree (Figure 4.4a). To normalize for this effect, the rate of enzyme activity was expressed as % control activity at each time point (Figure 4.4b), revealing no discernible difference in MAO-B inhibition by PLZ in the presence of ascorbate. Alternative approaches were then considered that might either confirm or refute this initial observation.

#### 4.3.5. Diazene Sequestering Agents

Inhibitor plots for ascorbate, GSH, and NAcCys against MAO-B (2 nM) were generated using the benzaldehyde assay to determine if these sequestering agents were inhibitory towards MAO-B (Figure 4.5a). GSH (green line) and NAcCys (blue line) showed no evidence of inhibition, nor did ascorbate (yellow line), despite the large drop in rate at concentrations above 30  $\mu$ M; this drop in rate can be explained by the decrease in absorbance at 266 nm due to ascorbate oxidation interfering with absorbance at 254 nm, as demonstrated previously. It was clear that monitoring MAO-B activity in incubations which included ascorbate was not feasible via the benzaldehyde assay.

An attempt to assay enzyme activity by an AR/P assay revealed interactions between these free radical scavengers that were in line with documented interactions in the literature (Votyakova & Reynolds, 2004). Resorufin production due to ascorbate (Figure 4.5b) and GSH (Figure 4.5c) was very evident at low micromolar concentrations. NAcCys was not tested for this interaction as

its interaction with Amplex Red has been documented previously (Votyakova & Reynolds, 2004). Therefore, an AR/P assay was unlikely to be feasible, as was the case with the benzaldehyde assay.

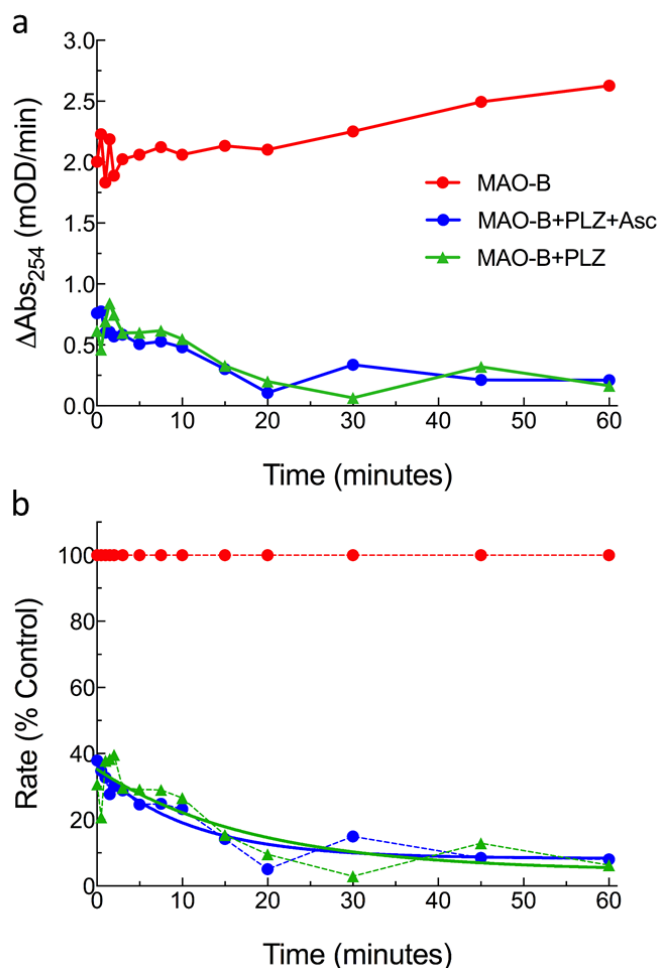


Figure 4.4 Soluble MAO-B inhibition by PLZ in the presence of ascorbate. Initial rate of change in absorbance at 254 nm (mOD/min) in BZ (1 mM) after incubation of MAO-B (20 nM) alone (red line), with PLZ (20  $\mu\text{M}$ ; green line), and with PLZ and ascorbate (50  $\mu\text{M}$ ; blue line) at room temp for up to one hour, plotted against incubation time (min). (a) Given the increase in control activity (red) over the incubation period, it is reasonable to assume a similar discrepancy occurred for the inhibition reactions (green and blue). (b) By comparing rates as a percent of the control activity at each time point, the influence of increasing rate is accounted for. One-site exponential decay equations were fitted to the inhibition curves by non-linear regression (Prism7). In the absence of ascorbate (green), the half-life of inactivation ( $t_{1/2}$ ) was 12.53 min ( $\text{CI}_{95} = 4.91\text{-}154.7$  min) and activity plateaued at about 4.4% control or 95.6% inhibition ( $r^2 = 0.7553$ ), while the presence of ascorbate decreased  $t_{1/2}$  to 7.53 min and plateaued at about 8.3% control activity ( $r^2 = 0.9090$ ).

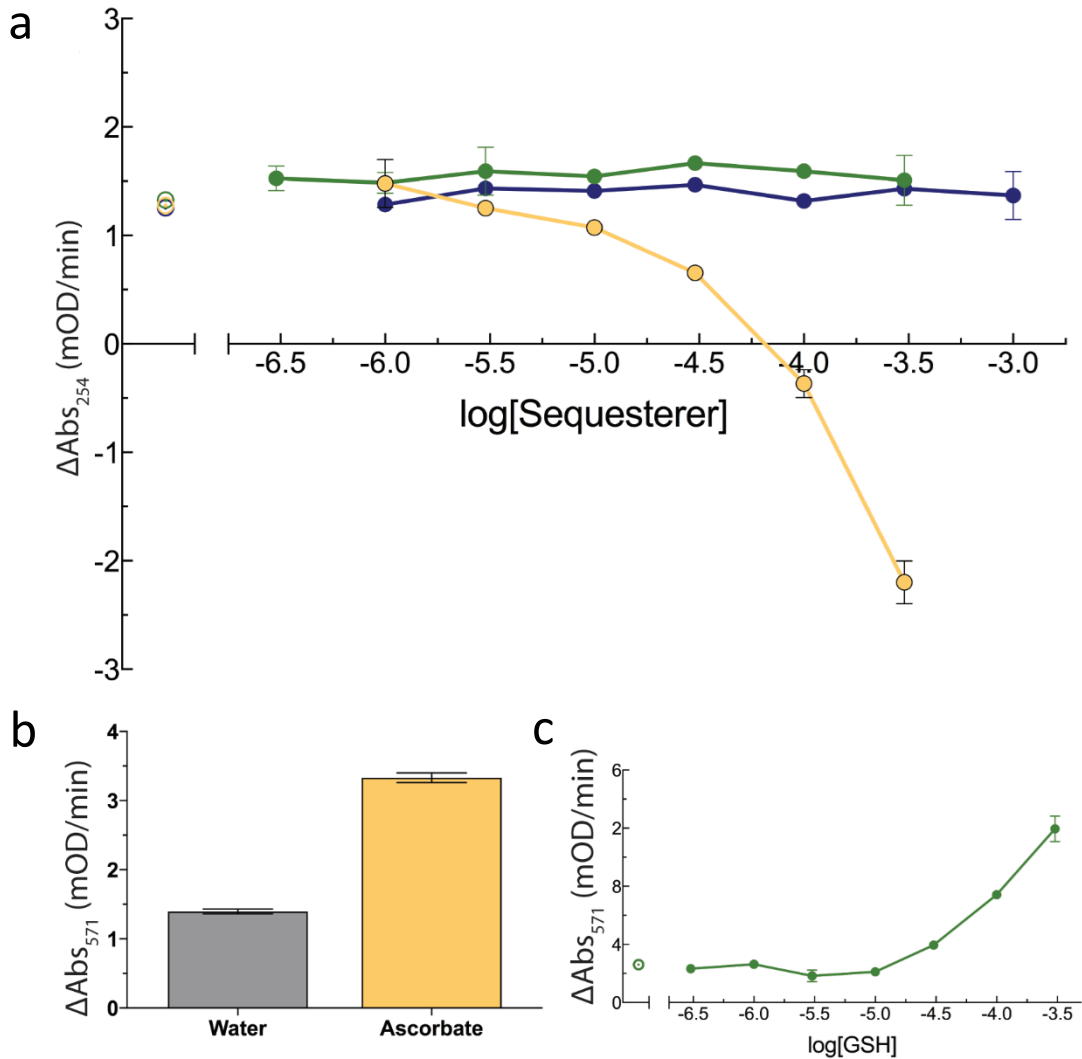


Figure 4.5 Interaction between ascorbate and free radical scavengers.

(a) Inhibition plots for ascorbate (yellow), GSH (green), and NAcCys (blue). MAO-B (2 nM) assessed using the benzaldehyde assay (500  $\mu$ M BZ). Initial rates of change in absorbance at 254 nm (mOD/min) were plotted against the log of the relevant concentration. (b) Rate of resorufin production (mOD/min) from Amplex Red (20  $\mu$ M) in H<sub>2</sub>O compared to ascorbate (50  $\mu$ M). (c) Rate of resorufin production from Amplex Red plotted against the log of incubated GSH concentrations. In all cases, interaction between Amplex Red and free radical scavenger prevented meaningful analysis of the data.

#### 4.3.6. Membrane Particles

Interference in assays of MAO-B activity by sequestering agents required that these reagents be separated from the enzyme after incubation with PLZ and prior to addition of substrate. However, the soluble, purified enzyme has been shown previously in our laboratory to lose activity when applied to a desalting column or a centrifugal concentrator device, and separation by centrifugation to create a protein pellet would require an ultracentrifugation apparatus not available to us. An alternative separation strategy was therefore sought. In the process of isolating and purifying the overexpressed MAO-B from *P. pastoris*, the outer mitochondrial membrane fraction can be retained and frozen at -80° C for several years without appreciable loss in enzyme activity. These membrane particles contain MAO-B with greater activity at similar concentrations compared to the soluble, pure MAO-B, as the membrane environment may facilitate a more efficient handling of amine substrates (see Cruz & Edmondson, 2007 for review). The membrane particles can be centrifuged at relatively low speeds, forming a pellet from which nearly all unbound ligands are removed. In this way, interactions between pre-incubation reagents and those in the activity assay are avoided, allowing for an AR/P assay of remaining activity.

Membrane particle-bound MAO-B was prepared as described above and incubated ± ascorbate for 25 minutes at 30°C. At various time points in the incubation, PLZ was added to + and - ascorbate tubes. The last addition of PLZ, the “0” time incubation, was made immediately prior to rapidly chilling all tubes in a salted ice water bath and centrifuging twice for 15 minutes at 0°C and 14,000 rpm (20,817 x g) in an Eppendorf 5810 R centrifuge; addition of water instead of PLZ into + and - ascorbate tubes at time “0” served as controls. In order to determine the extent to which ascorbate was actually removed in the ascorbate group by each centrifugation, both supernatants were retained from each time point of that group. The resuspended samples and

retained supernatants were plated on a 96-well microplate and an AR/P assay performed. Initial rates were obtained and graphed in Prism as described.

The supernatants collected after the first centrifugation had initial rates of absorbance change at 571 nm of about 6.3 mOD/min (Figure 4.6a, teal line), likely due to the noted interaction between Amplex Red and ascorbate (Figure 4.5), as opposed to loss of MAO-B due to centrifugation (see Chapter 5). After the second centrifugation, that rate had dropped dramatically to 0.076 mOD/min (orange line), indicating that the majority of the ascorbate had been removed from the pellet after the first centrifugation. As for the degree of inhibition of MAO-B, the result was an impressive reduction in the half-life of inactivation ( $t_{1/2}$ ) of MAO-B by PLZ in the presence of ascorbate (Figure 4.6b, from 12.9 minutes without ascorbate (red line;  $CI_{95} = 8.6-23.5$  minutes;  $r^2 = 0.9746$ ) to 1.74 minutes with ascorbate present (green line;  $CI_{95} = 1.6-1.9$  minutes;  $r^2 = 0.9968$ )); this was the opposite result than had initially been hypothesized, indicating an important role for ascorbate in the action of PLZ on MAO-B. However, it does not tell us much about the underlying mechanism of ascorbate's role.

This initial experiment was done in unchelated KP buffer and was therefore repeated in its entirety in DTPA-chelated KP buffer ( $KP_{DTPA}$ ) in order to rule out an involvement of ascorbate autoxidation in the previous results (Figure 4.6b). There was no real difference in inhibition  $\pm$  ascorbate when DTPA was included, each experiment having a  $t_{1/2}$  of roughly 4 minutes (+ ascorbate: blue line,  $CI_{95} = 3.0-4.2$  minutes,  $r^2 = 0.9965$ ; - ascorbate: purple line,  $CI_{95} = 3.8-4.5$  minutes,  $r^2 = 0.9850$ ). It seems that as long as either ascorbate or DTPA are present, MAO-B inhibition by PLZ occurs more rapidly than in their absence, but their combination is neither synergistic nor additive.

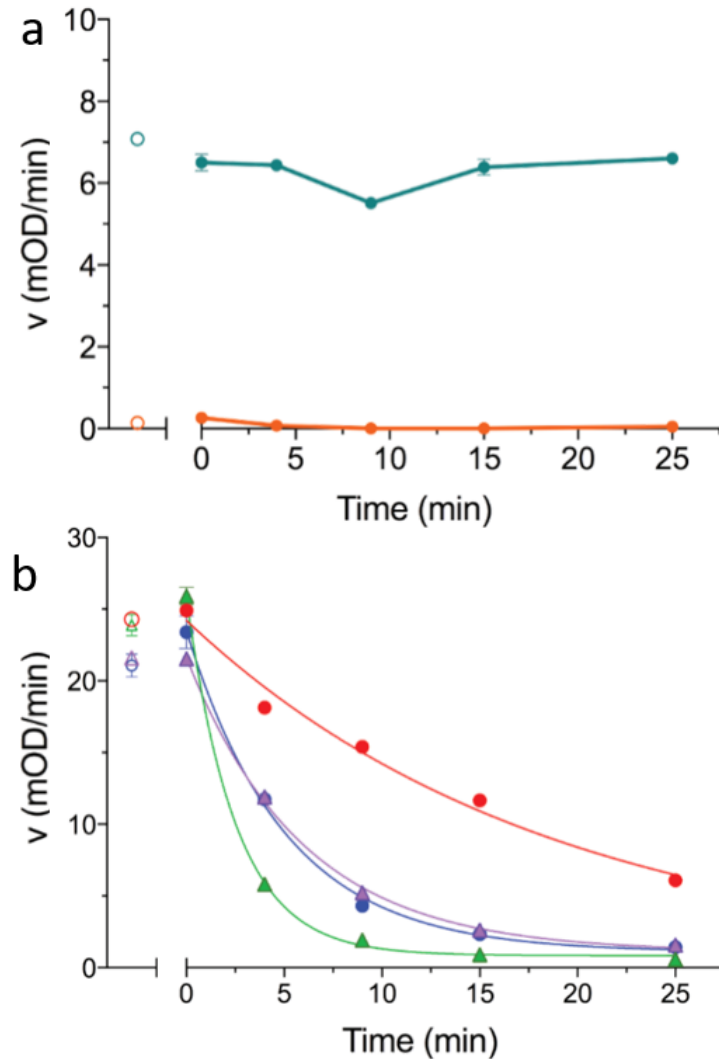


Figure 4.6 Influence of ascorbate on inhibition of MAO-B by PLZ.

(a) Initial rate of increase in absorbance (at 571 nm) of supernatants from the first and second centrifugations of the incubation of MAO-B, PLZ, and ascorbate. The first supernatant (teal) contained a lot of ascorbate; the consistency of the rate across time points indicates that the rate is not solely due to MAO-B-mediated production of resorufin, but instead the result of other interfering components that were washed from the enzyme. The second supernatant (orange) caused a negligible absorbance change, again consistent across all time points of incubation, indicating that virtually all interfering components were removed from the pellet in the first centrifugation step. (b) Inhibition of MAO-B (16.1 nM) by PLZ (20  $\mu$ M) alone (red circles), with ascorbate (50  $\mu$ M; green triangles), with DTPA (100  $\mu$ M; purple triangles), and with ascorbate and DTPA (blue circles) for up to 25 minutes (30°C). Initial rate (mOD/min; n=4) plotted against time incubated (min) and data fitted to a one-phase exponential decay equation by nonlinear regression (Prism7). Half-life of inactivation decreased from 12.9 minutes (red line;  $r^2 = 0.9746$ ) to 1.74 minutes ( $r^2 = 0.9968$ ) when ascorbate was included (green line), and to roughly 4 minutes when DTPA was included, regardless of the presence of ascorbate ( $r^2 = 0.9965$  with ascorbate (blue line),  $r^2 = 0.9850$  without (purple line)).

#### 4.3.7. Influence of DTPA and Ascorbate Together on Inhibition

The degree of influence that ascorbate and DTPA each have on the inhibition of MAO-B by PLZ was tested by changing the redox environment and assessing how each component is affected. Iron ions autoxidize ascorbate (Figure 4.1) but are chelated by DTPA (Figure 4.3); catalase metabolizes H<sub>2</sub>O<sub>2</sub> produced from enzymatic turnover, minimizing protein oxidation and ascorbate autoxidation. The contribution that ascorbate and/or DTPA provides to PLZ-mediated inhibition of MAO-B can be investigated by altering the redox environment of Fe<sup>3+/2+</sup> ions and H<sub>2</sub>O<sub>2</sub> in solution and comparing the resulting degrees of inhibition.

MAO-B (10.8 nM) was incubated with PLZ (20 μM), in the presence and absence of ascorbate (50 μM), DTPA (100 μM), Fe<sup>2+/3+</sup> (10 μM), and catalase (0.5 μg/mL, 5 IU/mL) for 10 minutes at 30°C; MAO-B incubated alone served as control (100%) and brought the total number of incubations to 17. The remaining activity was measured (n=5) via the benzaldehyde assay (250 nm, 25°C) against BZ (1 mM) and the initial rates (mOD/min) were compared (data not shown). Altering ascorbate autoxidation by elevating ferric iron concentrations, or mopping up H<sub>2</sub>O<sub>2</sub> with catalase, did not seem to influence remaining enzyme activity compared to incubations in which iron or catalase were not included. In otherwise-matched pre-incubations, only ± ascorbate and ± DTPA showed significant differences. Therefore, iron and catalase were not considered further as potential confounding variables, and the reactions were regrouped according to the presence of ascorbate and DTPA only (n=20; Figure 4.7a).

This experiment was repeated, in the absence of additional iron and catalase, with a 25-minute pre-incubation at 30°C. Remaining activity was assayed in BZ (3 mM) via the benzaldehyde assay (250 nm, 25°C) and initial rates for 5 replicate measures averaged and plotted as % control (Figure 4.7b, grey bar).

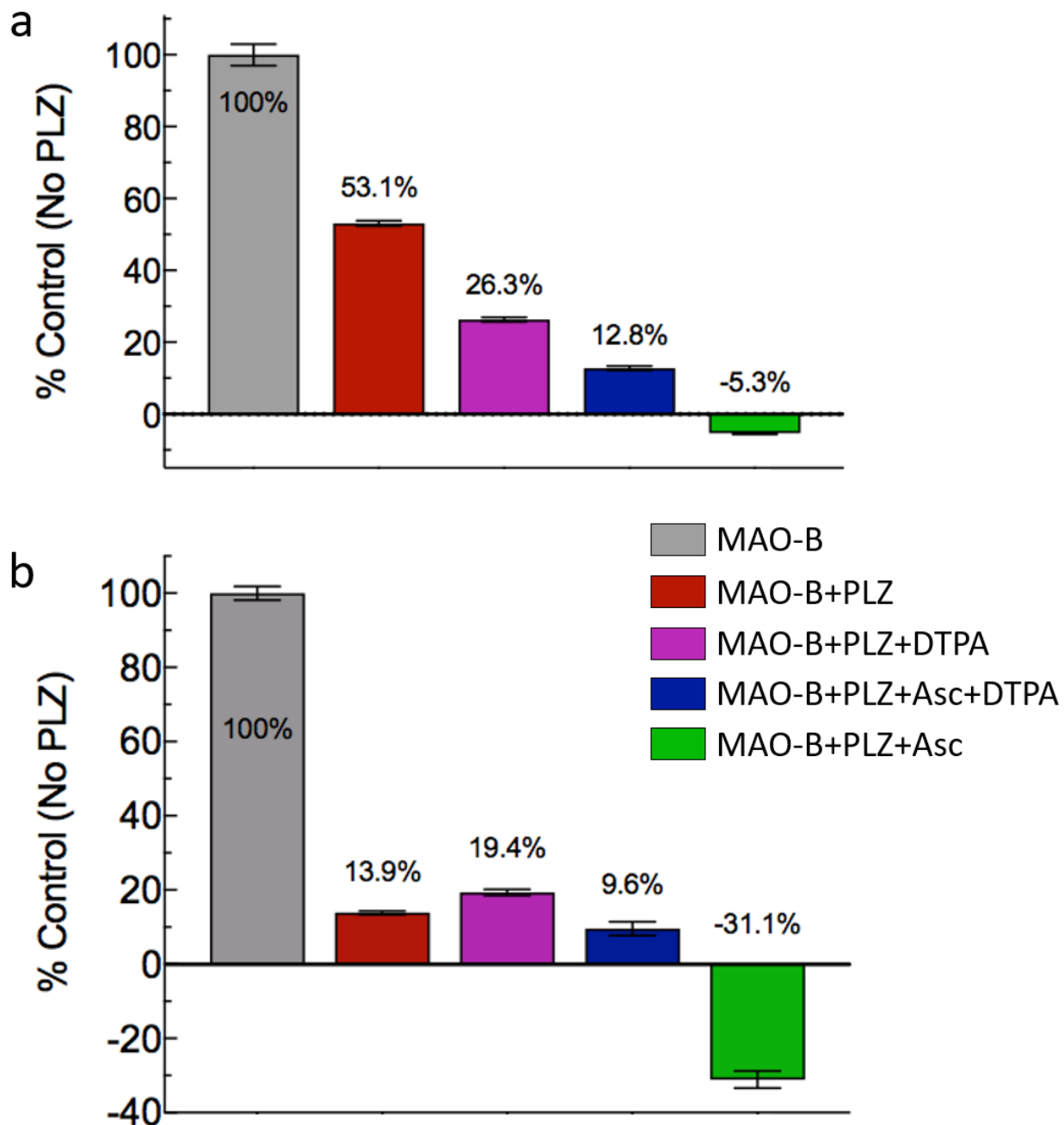


Figure 4.7 Influence of ascorbate and DTPA on inhibition of MAO-B by PLZ. MAO-B (10.8 nM) was incubated with PLZ (20  $\mu$ M),  $\pm$  ascorbate (50  $\mu$ M) and DTPA (100  $\mu$ M), for (a) 10 minutes (n=20) and (b) 25 minutes (n=5) at 30°C. The remaining activity in 5.38 nM MAO-B was assayed in 1 or 3 mM BZ (a and b, respectively) via the benzaldehyde assay (250 nm; 25°C) and inhibition compared as a percent of the control activity (MAO-B alone, grey bar).

Incubation of MAO-B and PLZ for 10 minutes at 30°C (Figure 4.7a; red bar) resulted in nearly 47% inhibition compared to control (grey bar). In DTPA-chelated buffer, the remaining activity (purple bar) was further reduced to 26.3% of control. The addition of ascorbate (blue bar) resulted in 87.2% inhibition after incubating for just 10 minutes. In the absence of DTPA, ascorbate incubation with MAO-B and PLZ (green bar) produced a negative rate due to spectral interference as ascorbate is autoxidized by metal contaminants in the buffer (see Figure 4.2).

The degree of inhibition of MAO-B by PLZ in DTPA-chelated buffer after 25 minutes at 30°C (Figure 4.7b; purple bar) was similar to that after 10 minutes (19.4% remaining activity compared to 26.3%), as was the case for incubations which contained both ascorbate and DTPA (Figure 4.7a and b, blue bar; 9.6% compared to 12.8%), indicating that the majority of the reaction was complete after 10 minutes. This was consistent with earlier results, shown in Figure 4.6, in which the half-life of inactivation of MAO-B by PLZ decreased from 12.9 to 3.5 minutes in the presence of DTPA and ascorbate. Inhibition by PLZ alone (red bar) was greater after 25 minutes than after 10 minutes, as expected.

Because these reactions were not centrifuged to remove excess ligands prior to addition of BZ substrate, the impact of ascorbate on the inhibition of MAO-B by PLZ (green bars) was not discernable. The negative rate of absorbance change at 254 nm that increased between 10- and 25-minutes pre-incubation was consistent with the autoxidation of ascorbate in unchelated buffer, resulting in a loss of absorbance at ascorbate's peak (266 nm) which concomitantly reduces absorbance at 250 nm.

#### 4.3.8. Is Ascorbate Reducing PEH to PEDz, Thereby Increasing the Rate of Inhibition by PLZ?

To investigate the influence of ascorbate on inhibition, the possibility of ascorbate interacting with PEH to form PEDz again was tested. In a similar manner to the original hypothesis, if PEH was being converted back to PEDz by ascorbate, it could explain why the half-life of inactivation in the presence of ascorbate is so short. Rather than (or perhaps, in addition to) ascorbate reducing PEDz back to PLZ and preventing inhibition, perhaps ascorbate reduces PEH back to PEDz, thereby increasing the concentration of PEDz and increasing the likelihood of an inhibition event occurring.

MAO-B (10.8 nM) was incubated with PEH (20  $\mu$ M),  $\pm$  ascorbate (50  $\mu$ M) and  $\pm$  DTPA (100  $\mu$ M), in KP buffer (0.1 M, pH 7.4) for 20 minutes at 30°C. Centrifugation and resuspension of the pellet in fresh buffer was followed by an AR/P assay of remaining enzyme activity in 3 mM BZ. Initial rates (mOD/min; mean of  $n=5 \pm$  SEM) were plotted for each group and a one-way ANOVA with multiple comparisons was performed (Figure 4.8).

In the absence of DTPA, ascorbate (green bar) had no effect on rate compared to control (red bar;  $p = 0.7451$ ), as was the case when DTPA was included without ascorbate (purple;  $p = 0.2168$  vs control). Ascorbate and DTPA together with MAO-B and PEH resulted in the only statistically significant, but small, decrease in activity versus control (blue bar;  $p = 0.0224$ ), which was 3.8 mOD/min less than the activity with DTPA alone ( $p = 0.0004$ ). Overall, PEH does not seem to be converting back to PEDz in the presence of ascorbate or DTPA, at least not to an extent which would explain the dramatic reduction in half-life of inactivation seen in the presence of ascorbate and/or DTPA.

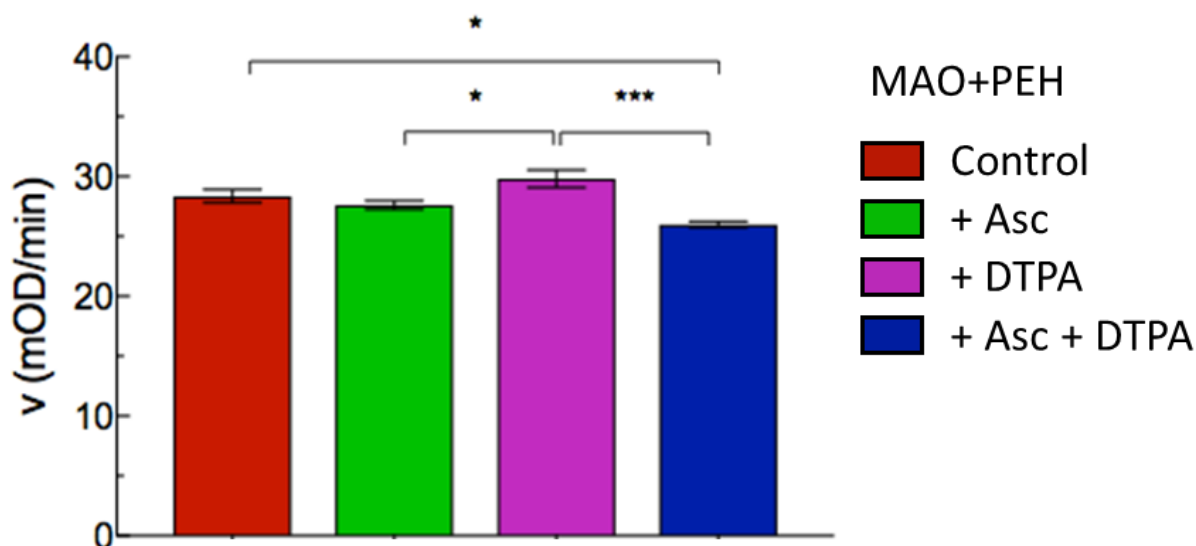


Figure 4.8 Inhibition of MAO-B by PEH in the presence of ascorbate and/or DTPA.

Initial rate of absorbance change (mOD/min; 571 nm) due to oxidation of 3 mM BZ by 5.4 nM MAO-B, measured in an AR/P assay, after incubation of MAO-B (10.8 nM) with PEH (20  $\mu$ M) in the presence of one or both of ascorbate (50  $\mu$ M) and DTPA (100  $\mu$ M) for 20 min (30°C; in 0.1 M KP). MAO-B incubated alone with PEH served as control (red bar; 28.4  $\pm$  0.55 mOD/min). With ascorbate, the rate was 27.6  $\pm$  0.36 mOD/min (green bar;  $p$  = 0.7451 vs control). DTPA without ascorbate resulted in a rate of 29.8  $\pm$  0.74 mOD/min (purple bar;  $p$  = 0.2168 vs control), which was 3.8 mOD/min higher than the rate of 26.0  $\pm$  0.25 mOD/min when incubated with DTPA and ascorbate (blue bar;  $p$  = 0.0004 (vs purple) and 0.0224 (vs control)). PEH likely is not converted by ascorbate to PEDz.

#### 4.3.9. Ascorbate Concentration Response

MAO-B (10.8 nM) was incubated with a range of ascorbate concentrations, from 100 nM to 3.2 mM, in KP<sub>DTPA</sub> (0.1 M) for 10 minutes in a 30°C water bath, followed by centrifugation and resuspension. In quadruplicate, a benzaldehyde assay (250 nm) was performed (1 mM BZ) at 25°C to measure remaining activity. Initial rate of activity (% control; mean of  $n=4$  replicate measures  $\pm$  SEM) was plotted for each ascorbate concentration on semi-logarithmic axes (Figure 4.9a) and the data fitted to a sigmoid by nonlinear regression (Prism7).

Interestingly, MAO-B was almost completely inhibited by ascorbate at mM concentrations, with an IC<sub>50</sub> for inhibition of 500  $\mu$ M. Interaction between MAO-B and ascorbate had been cited

in the literature previously when Galzigna et al. (1971) noted that substrate amine metabolism by MAO-B increased with the addition of ascorbate. This experiment was repeated with the addition of PLZ (20  $\mu\text{M}$ ) to the pre-incubation, and remaining activity (mOD/min; n=4) was measured in 3 mM BZ. In this experiment, the “IC<sub>50</sub>” (the point at which inhibition is enhanced by ascorbate by 50%) was slightly higher at 877  $\mu\text{M}$  (Figure 4.9b), suggestive of competition between ascorbate and PLZ (or PEDz) for binding to whatever site ascorbate interacts with to inhibit MAO-B, as seen in Figure 4.9a.

Finally, MAO-B and PLZ were incubated with a range of ascorbate (1 nM to 100  $\mu\text{M}$ ) in the absence of DTPA. This resulted in a leftward shift on the semi-log plot of remaining activity (mOD/min; n=4) versus log[ascorbate], with an “IC<sub>50</sub>” of 2.04  $\mu\text{M}$  (Figure 4.9c). The fact that the enzyme was washed of unbound ligands and other pre-incubation constituents before its activity was measured means this is an effect ascorbate is having on MAO-B, which is influenced by the presence of DTPA. This means that whatever DTPA and/or ascorbate are doing to influence inhibition, it is more than the effect of chelation or autoxidation alone.

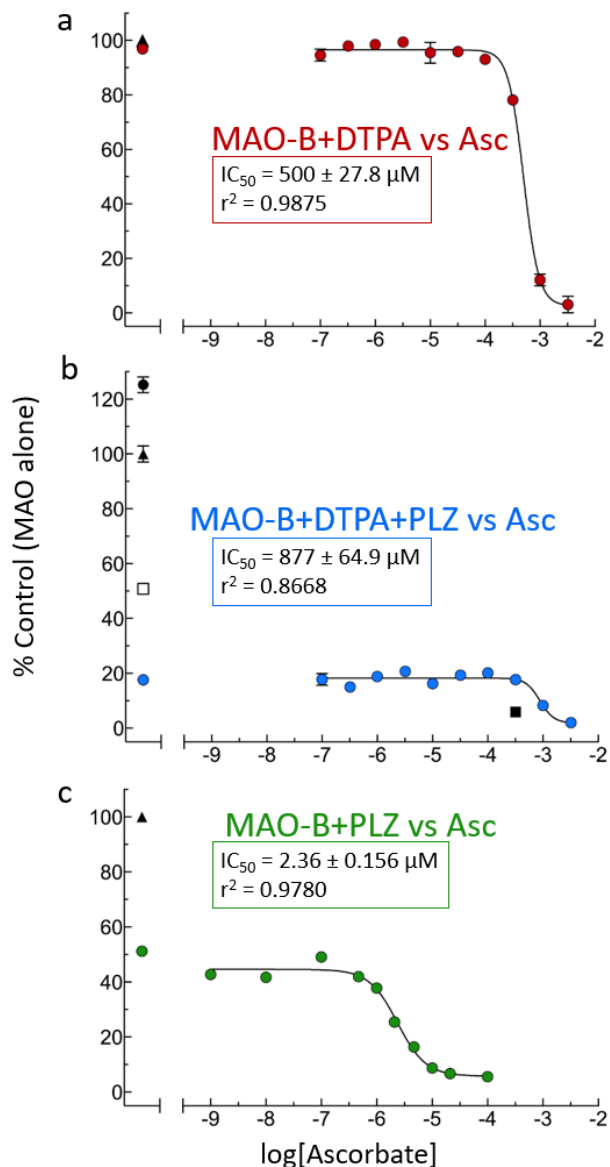


Figure 4.9 Inhibitor plots for inhibition of MAO-B by ascorbate,  $\pm$  PLZ,  $\pm$  DTPA.

MAO-B (10.8 nM) incubated with various concentrations of ascorbate, in the presence of one or both of PLZ (20  $\mu\text{M}$ ) and DTPA (100  $\mu\text{M}$ ). After pre-incubation for 10 min (30°C, in 0.1 M pH 7.4 KP buffer), samples were centrifuged and the enzyme pellet resuspended, and remaining enzyme activity (5.4 nM) in saturating BZ was assayed via a benzaldehyde assay (250 nm). Initial rates plotted as % control (black triangles, 100%) versus log[ascorbate]. **(a)** In DTPA-chelated buffer, ascorbate inhibited MAO-B with an  $IC_{50}$  of  $500 \pm 27.8 \mu\text{M}$  ( $r^2 = 0.9875$ ). **(b)** MAO-B incubated with PLZ in the presence of DTPA had the lowest activity remaining, even in the absence of ascorbate (open square), with a slightly higher  $IC_{50}$  of  $877 \pm 64.9 \mu\text{M}$  ( $r^2 = 0.8668$ ). Incubations of MAO-B and DTPA alone (closed black circle) demonstrated a 22% increased activity compared to MAO-B alone. **(c)** When MAO-B was incubated with PLZ in unchelated buffer, the  $IC_{50}$  dropped to  $2.36 \pm 0.156 \mu\text{M}$  ( $r^2 = 0.9780$ ), 2.5-3 orders of magnitude lower than in the presence of DTPA.

#### 4.3.10. DTPA Concentration Response

The impact of DTPA on MAO-B inhibition by PLZ proved more difficult to assess. A range of DTPA concentrations, from 0.01 nM to 3 mM, was incubated with MAO-B (10.8 nM) and PLZ (20  $\mu$ M) for 10 minutes at 30°C before centrifugation and resuspension of MAO-B. In quadruplicate, remaining activity was measured by the AR/P assay (3 mM BZ at 25°C). The initial rate (mOD/min) was plotted on a semilog scale against the log of DTPA concentrations (Figure 4.10). The IC<sub>50</sub> for DTPA in the presence of PLZ, or the concentration range at which PLZ inhibition of MAO-B was enhanced by 50%, was 12.7  $\mu$ M. Given that iron contamination in a 20 mM phosphate buffer solution can be 0.2-1.6  $\mu$ M, and that these experiments taking place in 0.1 M phosphate buffer, this low  $\mu$ M result lines up well with the estimation of 1-8  $\mu$ M iron contamination in the incubation. However, more experiments testing a larger range of DTPA concentrations would serve to improve confidence in these results.

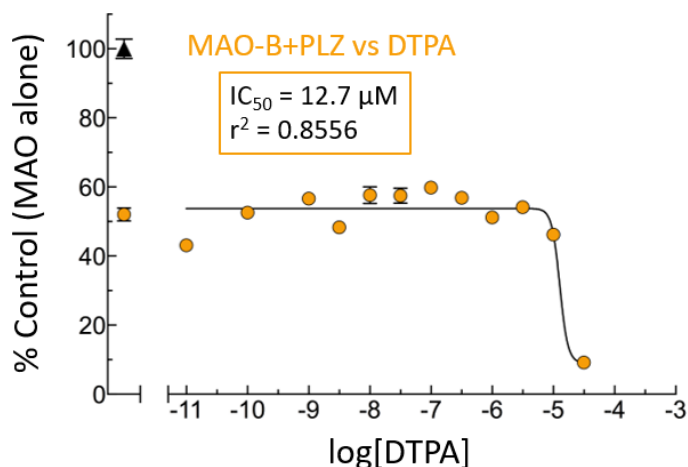


Figure 4.10 Inhibitor plot for MAO-B and PLZ incubated in a range of DTPA concentrations. 10.8 nM MAO-B incubated with 20  $\mu$ M PLZ for 10 min at 30°C (0.1 M KP). Remaining activity of 5.4 nM MAO-B after centrifugation and resuspension in fresh buffer was assayed by the AR/P assay (3 mM BZ, 25°C, 571 nm). Initial rate (% control, black triangles; mean of  $n=4 \pm$  SEM) was plotted against the log of DTPA concentration and data fitted to a sigmoid by nonlinear regression (Prism7). In the absence of DTPA, PLZ inhibited about 52% of the MAO-B activity, a degree of inhibition which was maintained in the presence of up to 3  $\mu$ M DTPA, after which point inhibition of MAO-B increased to about 91% of control. The IC<sub>50</sub> for DTPA in the presence of PLZ was calculated to be 12.7  $\mu$ M ( $r^2 = 0.8556$ ).

## 4.5. Conclusion

Initially, it was hypothesized that the inclusion of ascorbate would prevent PLZ-mediated inhibition of MAO-B by reducing PEDz back to PLZ before covalently modifying the FAD. Surprisingly, results shown here directly reject that hypothesis. When MAO-B was incubated with PLZ in the presence of ascorbate, the half-life of inactivation decreased over 6-fold, from 12.9 minutes to 1.7 minutes (Figure 4.6b). This was in contrast to incubations conducted in DTPA-chelated buffer, in which  $t_{1/2}$  was roughly 4 minutes,  $\pm$  ascorbate.

In order to ascertain whether ascorbate and/or DTPA bind to and inhibit MAO-B, inhibitor plots for each in the presence of PLZ were generated (Figures 4.9 and 4.10). The  $IC_{50}$  for ascorbate in the presence of DTPA was 500  $\mu$ M (Figure 4.9a), which increased to 877  $\mu$ M when PLZ was included as well (Figure 4.9b), consistent with competition between ascorbate and PLZ for binding to the same site. The sigmoidal nature of the inhibitor plots may suggest a possible binding interaction between MAO-B and ascorbate, as well as between MAO-B and DTPA. However, the steepness of the curves argues against a binding interaction, and in favour of a chemical interaction with one or more species that influences either MAO-B activity or PLZ potency.

When ascorbate and PLZ were incubated together in the absence of DTPA, the  $IC_{50}$  dropped to 2.04  $\mu$ M (Figure 4.9c) and the  $t_{1/2}$  was under 2 minutes (Figure 4.6b). That, in the absence of chelation, inactivation of MAO-B by PLZ was enhanced suggests interaction between ascorbate and whatever was being chelated by DTPA, here  $Fe^{3+}$ . As shown in Figure 4.1, ascorbate exists predominantly in its anionic form ( $A^-$ ) at physiological pH, which readily reacts with  $Fe^{3+}$  to form an ascorbate radical ( $A^{\cdot}$ ) and reduced  $Fe^{2+}$ . Figure 4.2 illustrates the impact of iron contamination on ascorbate absorbance at 266 nm, likely the result of loss of ascorbate anion to radical formation.

$\text{Fe}^{3+}$  is a pro-oxidant which could degrade any PEDz (Mahy et al., 1994) which may leave the active site of MAO-B after formation, preventing rebinding of the diazene to oxidized enzyme and thereby protecting MAO-B from inhibition by PLZ. Reduction of  $\text{Fe}^{3+}$  to  $\text{Fe}^{2+}$  by  $\text{A}^-$  would preserve the released PEDz long enough to inactivate the enzyme with fewer turnovers of PLZ and therefore a shorter  $t_{1/2}$  compared to incubations without ascorbate. That  $\text{Fe}^{3+/2+}$  addition did not influence these effects (Figure 4.7a) is likely indicative of the hypothesized catalytic capacity of the metal ions, that is, the catalytic species is not depleted in forming the radical, therefore any amount of metal ions in the solution will amount to a similar impact on inhibition. This is opposed to the hypothesized redox action of ascorbate, in which both ascorbate and  $\text{Fe}^{3+}$  are consumed in the ensuing reaction (Shen et al., 2021), which would produce more of a concentration-dependent response to varying concentrations of iron contamination. This line of reasoning lines up with the purpose for including DTPA in this study, which was to remove adventitious metal ion contaminants in the phosphate buffer which may interact with components of the incubation.

Overall, it appears that inhibition of MAO-B by PLZ depends greatly on the presence of iron in solution, here as high as 8  $\mu\text{M}$ . If  $\text{Fe}^{3+}$  degrades PEDz, it is unlikely that a triply-charged ion would be allowed access to the active site of MAO-B, therefore it is maintained that PEDz is released from the active site after formation from PLZ. Chelation of  $\text{Fe}^{3+}$  or reduction to  $\text{Fe}^{2+}$  may preserve PEDz which has been released from the active site after formation long enough to bind to and irreversibly inactivate MAO-B.

## Chapter Five

### **Unexpected Mechanistic Insights From a Study of the Concentration-Dependence of MAO-B Inhibition by PLZ**

#### **5.1. Introduction**

Many of the irreversible MAOIs used today are mechanism-based inhibitors, compounds which require activation by the enzyme to form the inhibitory species, such as mofegiline and pargyline (Silverman, 1995b). Initial activation of the drug by the enzyme follows reversible binding to the active site, with the proportion of active sites occupied determined by the compound's concentration and its dissociation constant ( $K_D$ ). In the presence of substrate, the drug competes for binding; a saturating concentration of substrate can outcompete inhibitor binding (substrate protection), while saturating inhibitor concentrations maximize the rate of inactivation, with the fraction of enzyme inactivated in unit time defined as  $k_{inact}$  (Patek & Hellerman, 1974). After formation of the inhibitory species, MAO is irreversibly inactivated, generally by covalent modification of the N(5)-C(4a) loci of FAD in a first-order reaction. The requirement for activation of the inhibitor gives this two-step inhibition a time-dependence in onset of irreversible inhibition which depends upon both the  $K_D$  and  $k_{inact}$  (Holt, 2018).

In order to determine whether or not an inhibitor is mechanism-based in its actions, several criteria must be met, such as stoichiometry of inactivation, catalytic activation of the parent compound, and irreversible inactivation of the enzyme before release of the active species from the binding site, as well as the above-mentioned time dependence of inactivation, substrate protection, and saturation kinetics. This chapter will detail evidence that PLZ is not a mechanism-based inhibitor by comparing its inhibitor profile to that of well-understood mechanism-based inhibitors mofegiline and pargyline. Mofegiline is a stoichiometric inhibitor in which binding of

the inhibitor results in covalent modification of the FAD in a near 1:1 ratio (Milczek et al., 2008). Pargyline is also an irreversible inhibitor, but is metabolized to either an inhibitory species, which binds to the active site much like mofegiline, or to form a non-inhibitory species, which dissociates from the enzyme (Ramsay et al., 2020). The rate of formation of the latter versus the former, termed the partition ratio, is more or less constant (Silverman, 1995b).

This is the suggested mechanism for PLZ as well, according to the forked mechanism. One estimation of the partition ratio for PLZ metabolism by MAO-B is 36-40 (Binda et al., 2008); i.e., for every 36-40 molecules of PLZ metabolized by MAO-B, only one becomes PEDz, which inactivates the enzyme *in situ*. However, evidence provided thus far in this thesis point to inactivation of MAO-B by PEDz after release from the reduced enzyme and re-binding to the re-oxidized active site. It is this that disqualifies PLZ from being a mechanism-based inhibitor, as the final criterion for classification of an irreversible inhibitor as mechanism-based is *in situ* inactivation by the inhibitory species after formation (Silverman, 1995b).

#### 5.1.1. Hypotheses

- If PEDz must dissociate and then reassociate with the enzyme, at any given PLZ concentration, a higher concentration of MAO will oxidize PLZ and generate PEDz in solution more rapidly than will a lower concentration of the enzyme, resulting in more rapid inactivation of the enzyme and a shorter half-life for inactivation.
- In order to return to the active site, PEDz will compete for binding with PLZ and PEH.

### 5.1.2. Specific Aims

- To establish an optimized separation protocol that uses hMAO-B present in mitochondrial membrane particles of *P. pastoris* that facilitates removal of unbound inhibitors and other reactants that might interfere with assays of remaining enzyme activity, prior to assay.
- To compare inhibition profiles of PLZ with those of the established mechanism-based inhibitors mofegiline and pargyline in order to obtain evidence for a unique mechanism.

## **5.2. Materials and Methods**

### 5.2.1. Materials

All water used in the experiments was filtered through a Millipore Milli-Q filtration system. BZ hydrochloride, PLZ sulfate, pargyline hydrochloride, and HRP (Type II) were purchased from Sigma-Aldrich. Mofegiline hydrochloride was a generous gift from Dr. David Smith (BioTie Therapies, Turku, Finland). Amplex Red reagent (N-acetyl-3,7-dihydroxyphenoxazine) was purchased from Invitrogen. Monobasic and dibasic potassium phosphate were obtained from Fisher Scientific. For spectrophotometric experiments, 96-well microplates were obtained from Greiner Bio-One. Full length hMAO-B was expressed in *P. pastoris* yeast and was either purified partially by ion exchange chromatography, generating a soluble enzyme that was approximately 50% pure, or was isolated in a membrane-bound form from yeast mitochondria, in our laboratory. PEH was synthesized from phenylacetaldehyde and hydrazine monohydrate in the laboratories of Dr. Velázquez-Martínez in the Faculty of Pharmacy and Pharmaceutical Sciences, University of Alberta.

Assay constituents, including substrates and inhibitors, were prepared only in colourless disposable virgin polypropylene plasticware manufactured by Eppendorf AG in order to avoid

interferences from leachates (McDonald et al., 2008). Phosphate buffers were prepared as described in Chapter 1; mono-basic and di-basic potassium phosphate (KP) solutions were made up in H<sub>2</sub>O (0.2 M each), and di-basic was added to mono-basic solution until the desired pH of 7.4 was reached. PLZ and BZ were prepared in H<sub>2</sub>O before each experiment.

### 5.2.2. MAO-B Incubation

The concentration of stock MAO-B was determined by mofegiline titration as described previously (Chapter 2); the soluble enzyme used here was the same as used in Chapter 2 ([MAO-B]<sub>stock</sub> = 0.56 μM; section 2.3.1). MAO-B was pre-incubated with or without drugs for a range of time such that the longest incubation was started first and the “0” time incubation occurred just before the reaction was stopped in all samples at once, allowing for better control of the incubation time. In order to prevent further inhibition of MAO-B after pre-incubation, a saturating concentration of substrate was added to outcompete inhibitor binding, and/or by rapidly chilling the reaction vessel to around 0°C to greatly reduce enzyme activity. The latter method was used with membrane particle incubations before centrifugation to remove unbound ligands. In this way, the reaction was essentially paused until the remaining enzyme activity could be assayed without further unintended loss of activity.

MAO-B activities in purified preparations or in membrane fractions from *P. pastoris* yeast were measured continuously with BZ as substrate in 96-well plates or quartz cuvettes, depending on the experiment. Mofegiline titration of remaining active sites after pre-incubation of MAO-B with PLZ was performed by incubating samples at 30°C with mofegiline for 30 minutes to 2 hours, depending on the experiment, as indicated in the results section. All assays were carried out at 25°C under atmospheric oxygen, unless otherwise indicated.

### 5.2.3. Membrane Particle Preparation

Membrane particles were removed from  $-80^{\circ}\text{C}$  storage and thawed on ice, vortexing occasionally until all visible clumps were gone and the solution appeared well-mixed. Membrane particles were added to a 1.5 mL Eppendorf tube containing a minimal volume of buffer (15  $\mu\text{L}$  0.1 M KP buffer), such that the total volume for homogenizing did not exceed 50 $\mu\text{L}$ , and were homogenized with a pellet pestle on ice until the contents were frothy. Larger volumes of enzyme mixture were prepared by homogenizing as described in small batches ( $\leq 50 \mu\text{L}$ ) and combining homogenates. The pestle was then rinsed in the buffer that was added to the tube in order to dilute to the target concentration, such that the final concentration of membrane particles was 16 nM in pre-incubations and 8 nM in the spectrophotometric assay.

Pre-incubations of membrane particles and PLZ were initiated by the addition of PLZ to reaction vessels and the temperature was maintained at  $30^{\circ}\text{C}$  in a water bath. After pre-incubation, the reaction was slowed rapidly by submersion of tubes into a salted ice water bath ( $-4^{\circ}\text{C} - 0^{\circ}\text{C}$ ); this chilled temperature was maintained throughout the rest of the preparation, until analysis, by returning tubes to the salted ice water bath between processing steps.

The tubes were then centrifuged twice at 14,000 rpm ( $20,817 \times g$ ) for 15 minutes at  $0^{\circ}\text{C}$ , retaining the pellet; the aspirated supernatant was either discarded or collected in a clean tube and kept chilled until analysis. After the first centrifugation, fresh ice-cold KP buffer was added to the pellet, the tubes vortexed briefly (5 seconds), and centrifuged again. After the second centrifugation, the pellet was resuspended as described previously and kept chilled in a salted ice water bath until analysis.

#### 5.2.4. Benzaldehyde Assay

For measurement of MAO-B activity in some experiments, a spectrophotometric assay for measurement of benzaldehyde production was used. Metabolism of BZ by MAO-B produces benzylimine, which quickly hydrolyzes to benzaldehyde after formation such that enzymatic turnover of one molecule of BZ generates one benzaldehyde molecule. Benzaldehyde has a characteristic absorbance at a wavelength of 254 nm ( $\epsilon \approx 12,500 \text{ M}^{-1}\text{cm}^{-1}$ ), the change in which is measured through a continuous kinetic assay during incubation of MAO-B and BZ,  $\pm$  drugs, in physiological buffer (0.1 M KP). Here, this assay was performed in a Molecular Devices FlexStation 3 microplate reader at 25°C, unless otherwise indicated.

#### 5.2.5. Amplex Red Assay

A more sensitive assay for the remaining MAO-B activity is the Amplex Red peroxidase (AR/P) assay, in which the change in absorbance at 571 nm is coupled to the metabolism of substrate by MAO-B. Amplex Red is a chromogenic compound which is near-colourless. Horseradish peroxidase (HRP) utilizes  $\text{H}_2\text{O}_2$ , a by-product of the MAO-B oxidative half-reaction, to convert Amplex Red to resorufin, a bright pink compound which absorbs strongly at 571 nm ( $\epsilon \approx 70,600 \text{ M}^{-1}\text{cm}^{-1}$ ) in a stoichiometric relationship such that one enzyme turnover results in one molecule of resorufin being produced. Therefore, the rate of increase in absorbance at 571 nm is an indirect measure of enzyme activity.

A solution of BZ (3 mM, final), Amplex Red (20  $\mu\text{M}$ , final), and HRP (5  $\mu\text{g}/\text{ml}$ , final) in KP buffer (0.1 M) was added to an aliquot of enzyme in a microplate and immediately read in a continuous kinetic assay at 571 nm (25°C).

### 5.2.6. Analysis and Statistics

Substrate metabolism by MAO-B was graphed as absorbance (mOD) versus time (min) for each incubation, with the slope of the initial pseudo-linear portion of the resulting progress curve representing the initial rate of MAO-B activity (mOD/min). FlexStation data were exported to GraphPad Prism v. 7.0 for Mac OS X (GraphPad Software Inc., San Diego, CA) to reproduce the progress curves. These curves were fitted via linear or non-linear regression and kinetic constants obtained, global fit  $\pm$  SEM. Groups were compared by one-way ANOVA followed by Sidak's multiple comparisons test, and significance was set at  $p < 0.05$ .

## **5.3. Results**

### 5.3.1. Effects of MAO-B Concentration on Rate of Inactivation by PLZ

Multiple MAO-B concentrations (0.54-4.3 nM in 0.1 M pH 7.4 KP buffer) were incubated with PLZ (20  $\mu$ M) and BZ (600  $\mu$ M) in a microplate (30°C) and enzyme activity was measured by an AR/P assay (571 nm) over the course of four hours (Figure 5.1a). FlexStation data were fit to two-phase exponential binding equations by non-linear regression, due to the contribution of the inactivation of MAO-B on the activity remaining as well as the interaction between PLZ and Amplex Red (see results) on the overall change in absorbance. The calculated half-life of inactivation ( $t_{1/2}$ ; min; Figure 5.1b) and rate constant ( $k_{\text{inact}}$  ( $\text{min}^{-1}$ ); Figure 5.1c) for each enzyme concentration were then compared (blue lines); this procedure was also repeated in its entirety in 200  $\mu$ M and 2 mM BZ (red lines and purple lines, respectively).

As show in Figure 5.1b and c, regardless of the concentration of BZ included in the incubation, the  $t_{1/2}$  decreased (and the rate constant for inactivation increased) with increasing concentrations of MAO-B. At the lowest MAO-B concentration, competition between BZ, PLZ,

and PEDz resulted in the greatest difference in  $t_{1/2}$  across the concentrations of BZ tested, from 17.5 minutes at 200  $\mu\text{M}$  BZ (Figure 5.1b, red line) to 26.2 minutes at 2 mM BZ (purple line). Consistent with this trend was the decreased impact that competition had on  $t_{1/2}$  for incubations with higher concentrations of MAO-B, which led to more rapid production of PEDz to compete for binding. These data were consistent with increased competition for binding to the active site at higher BZ concentrations. Modeling of the kinetic data obtained in this experiment using the free webtool Enzo (Bevc et al., 2011) (A. Holt, unpublished observations) also supported competition as the driving force for increased  $t_{1/2}$  at lower MAO-B concentrations and higher BZ concentrations, as well as the plateau of remaining activity being above zero, as evidenced here.

This directly contradicts the forked mechanism, whereby irreversible inactivation by PEDz occurs *in situ*. If PEDz did not leave the active site after formation and before inhibition, the concentration of MAO-B would be irrelevant in determining the rate at which that happens. Instead, these data support the hypothesis that PEDz once formed leaves the active site; increasing the concentration of active sites that can bind the released PEDz increases the likelihood of PEDz binding to and inactivating MAO-B. However, by increasing the concentration of BZ, competition for active site binding increases, and the rate of inhibition decreases.

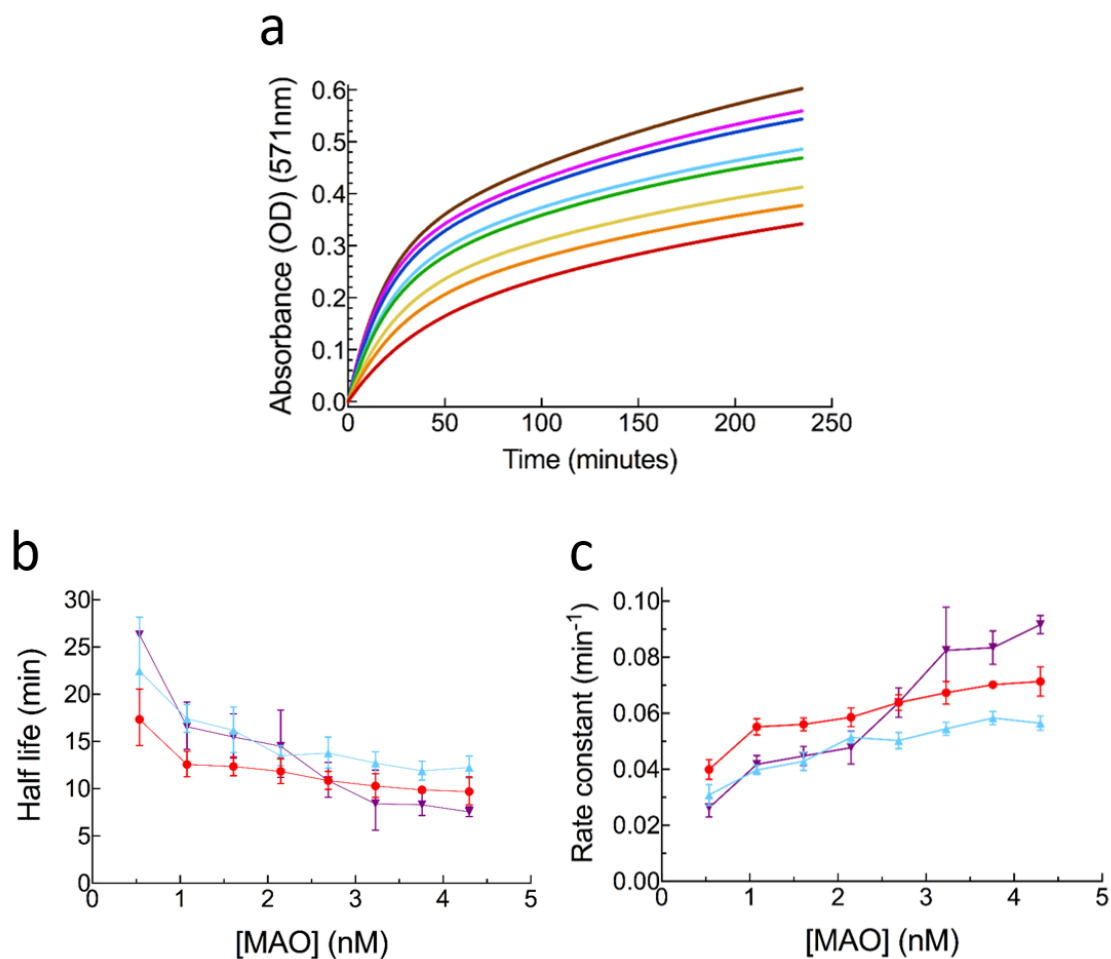


Figure 5.1 Impact of MAO-B concentration on inhibition by PLZ.

(a) Inhibition of a range of MAO-B concentrations (0.54 (red) - 4.3 nM (brown)) by 20  $\mu\text{M}$  PLZ over the course of 4 hours (30°C). Enzyme activity measured via AR/P assay (571 nm) against 600  $\mu\text{M}$  BZ, and data ( $n=4$ ) were fit to two-site exponential binding equations by nonlinear regression;  $r^2 = 0.9696$  (red); 0.9869 (orange); 0.9446 (yellow); 0.9612 (green); 0.9633 (light blue); 0.9691 (dark blue); 0.9770 (purple); and 0.9632 (brown). Plots of the (b) half-life of inactivation ( $t_{1/2}$ ) and (c) rate constant ( $K_D$ , turnovers per minute;  $\text{min}^{-1}$ ) calculated for all [MAO-B] in 200  $\mu\text{M}$  (red), 600  $\mu\text{M}$  (blue), and 2 mM BZ (purple); error bars are mean  $\pm$  SEM of 4 replicate measures.

### 5.3.2. Inhibitor Plots for Mofegiline, Pargyline, and Phenelzine

The previous results were inconsistent with PLZ having a fixed partition ratio, as seen with pargyline; the half-life of inactivation of the population of MAO-B would be consistent at different MAO-B concentrations in the presence of any given concentration of PLZ. To understand how these differences translate, multiple MAO-B concentrations were inhibited with a range of mofegiline, pargyline, and PLZ concentrations and the remaining activity measured in a microplate via the AR/P assay (571 nm, 37°C). Because mofegiline is stoichiometric in its inhibition, the range of concentrations used to generate an inhibitor plot encompasses the concentration range of MAO-B used (3-30 nM). As well, interaction between MAO-B and mofegiline occurs very quickly (Milczek et al., 2008), so MAO-B was incubated with mofegiline for one hour (37°C) to ensure the reaction had gone to completion. Pargyline has a partition ratio of about six (A. Holt, unpublished results), meaning for every seven molecules metabolized by MAO-B only one will inactivate the enzyme. As a result, the range of pargyline concentrations tested spanned 4 orders of magnitude for the same MAO-B concentrations and inhibition was assessed over a 24-hour incubation period; the incubation was also performed at 9°C rather than 37°C to reduce natural enzyme inactivation over time.

Mofegiline and pargyline had inhibitor plots which were consistent with the literature (Milczek et al., 2008). Slopes of the mofegiline titration were parallel to each other, meaning that activity remaining after inhibition was proportional to the amount of mofegiline required to inhibit the enzyme (Figure 5.2a). Given that mofegiline is a stoichiometric inhibitor of MAO-B, this is unsurprising. In fact, MAO-B concentration is often determined by titrating its activity with mofegiline, with the x-intercept of a linear regression of the steep portion of the inhibitor plot

approximately equal to the concentration of enzyme present; this value is simply multiplied by its dilution factor in the assay to give the stock concentration.

Inhibition of MAO-B by pargyline was graphed on a semilog plot of remaining activity ( $v$ ; mOD/min) versus  $\log[\text{pargyline}]$ , in order to visualize inhibition across the range of inhibitor concentrations used. This produced a sigmoidal curve for each concentration of MAO-B (Figure 5.2b). From this sigmoid, the  $IC_{50}$ , or the concentration of pargyline at which 50% of MAO-B inhibition had occurred, was obtained. Because pargyline is an inhibitor with a fixed partition ratio, the  $IC_{50}$  is influenced by both the concentration of MAO-B and that of pargyline. Here, the  $IC_{50}$  does change in proportion to the MAO-B concentration.

PLZ was tested in much the same way as pargyline, with PLZ concentrations spanning 3.5 orders of magnitude and reactions incubated at 9°C. However, a larger range of MAO-B concentrations (3 to 60 nM) was tested and inhibition was assessed after a 48 hour pre-incubation period. As with pargyline, initial rates of activity were plotted against  $\log[\text{PLZ}]$  for each concentration of MAO-B, again generating sigmoidal curves (Figure 5.2c) that showed increasing  $IC_{50}$  increasing concentrations of MAO-B. In fact, both pargyline and PLZ showed a linear relationship between the  $IC_{50}$  and the concentration of MAO-B (Figures 5.2b and c, inset). However, while the linear regression line for pargyline intersected at the origin ( $CI_{95} = -19.6$  to 3.8), the same was not true for PLZ ( $CI_{95} = 1.3$  to 3.7).

This could be explained through the lens of competition: as the concentration of MAO-B increased, PLZ metabolism, and therefore PEDz production, occurred faster, but the amount of PEDz needed to inactivate the enzyme was increased. At the other end of the scale, at extremely low concentrations of MAO-B, PLZ turnover and PEDz generation slowly occurred, with most PEDz converted to PEH before binding and inhibiting an enzyme. Therefore, a plot of  $IC_{50}$  versus

MAO-B concentration would be visually flatter near the origin, before increasing reasonably linearly. Indeed, this does appear to be the case for PLZ.

Of course, some limitations must be considered such as the interaction between PLZ and Amplex Red, in which high concentrations of PLZ convert Amplex Red to resorufin, thereby artificially increasing the recorded initial rate. Fitting data to a two-phase exponential equation, with one phase accounting for the concentration-dependent interaction between PLZ and resorufin, should minimize the impact of this confounding factor. In fact, the highest PLZ concentration tested here was chosen in an attempt to minimize the extent of the interaction, a limit which prevented resolution of the bottom of the sigmoidal curves in Figure 5.2c.

Despite attempts to account for this interference through use of biphasic exponential fitting, it remained unclear as to why 60 nM MAO-B did not appear to have been inhibited completely by over 300  $\mu$ M PLZ after 48 hours, despite the fact that the literature  $K_I$  for PLZ is 15  $\mu$ M (Binda et al., 2008). This prompted further investigation of MAO-B inhibition by very high concentrations of PLZ.

Unfortunately, the soluble MAO-B-based paradigm used here would not suffice moving forward; the AR/P assay is a more sensitive measure of MAO-B activity compared to the benzaldehyde assay, but the interaction of Amplex Red with PLZ prevents a fully-quantitative analysis of enzyme in the presence of PLZ concentrations greater than 10  $\mu$ M (A. Holt, unpublished observations). To facilitate examination of the effects of higher PLZ concentrations, the unbound PLZ needed to be removed before remaining enzyme activity was measured.

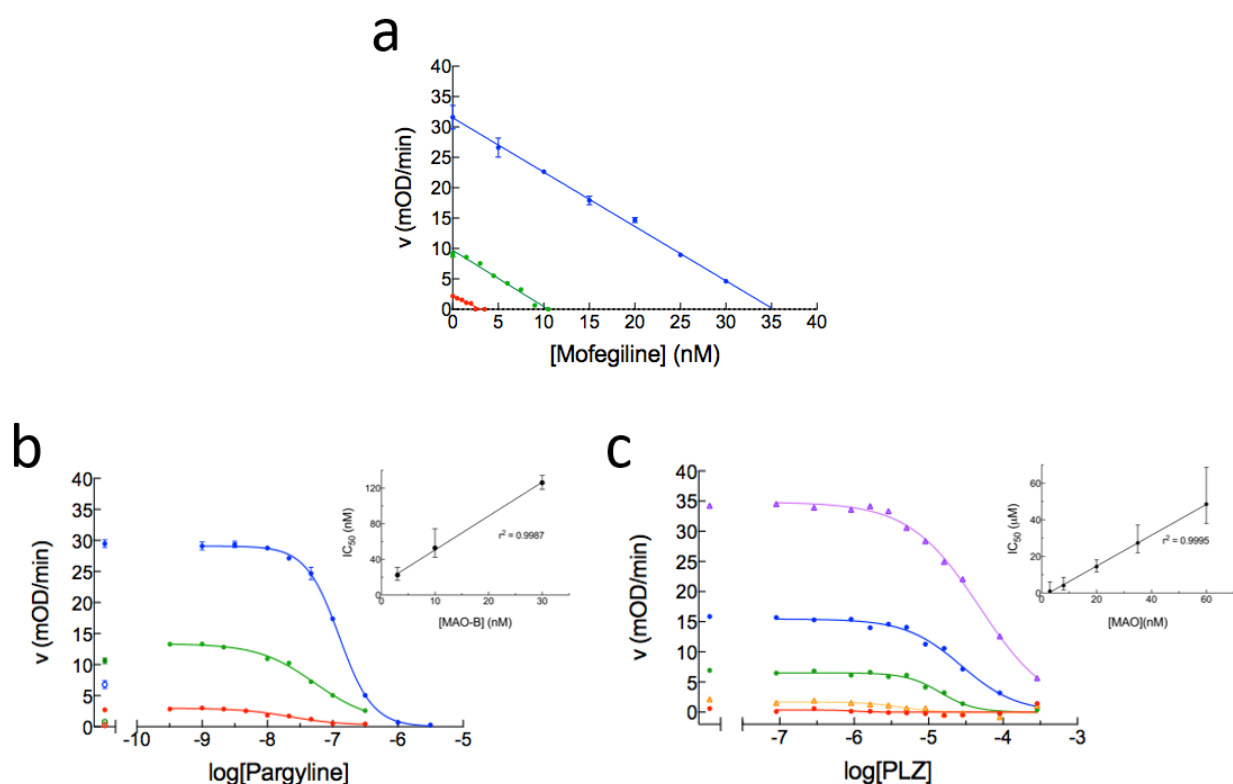


Figure 5.2 Inhibitor plots for the inhibition of a range of MAO-B concentrations by mofegiline, pargyline, and phenelzine.

After pre-incubation with inhibitors, enzyme was centrifuged and resuspended, and, in triplicate, the enzyme activity remaining (mOD/min) was measured against BZ (3 mM) via the AR/P assay (571 nm; 37°C). (a) Initial rate, after pre-incubation of 3, 10, or 30 nM MAO-B with 0-35 nM mofegiline for 1 hour at 37°C, plotted against mofegiline concentration. Mofegiline completely inhibited MAO-B stoichiometrically, such that the x-intercept of the linear regression (Prism7) for each incubation was equivalent to the initial concentration of MAO-B in the assay: 3.1 (red line, nominally 3 nM,  $CI_{95} = 2.72-3.64$ ;  $r^2 = 0.9422$ ), 10.5 (green line, nominally 10 nM,  $CI_{95} = 9.68-11.55$ ;  $r^2 = 0.9789$ ), and 35.25 (blue line, nominally 30 nM,  $CI_{95} = 34.42-36.15$ ;  $r^2 = 0.9983$ ). (b) Initial rate, after pre-incubation of 3 (red), 10 (green), or 30 nM (blue) MAO-B with 0-3.16  $\mu$ M pargyline for 24 hours at 9°C, plotted against log[pargyline]. The  $IC_{50}$  for pargyline increased with MAO-B concentration, at 22.4 nM with 3 nM MAO-B ( $r^2 = 0.9584$ ), 52.7 nM with 10 nM MAO-B ( $r^2 = 0.9820$ ); and 126.1 nM with 30 nM MAO-B ( $r^2 = 0.9982$ ). (c) Initial rate, after pre-incubation of 3 (red), 8 (orange), 20 (green), 35 (blue), and 60 nM MAO-B (purple) with 0-316  $\mu$ M PLZ for 48 hours at 9°C, plotted against log[PLZ].  $IC_{50} = 1.0 \mu$ M (3 nM;  $r^2 = 0.06858$ ), 4.1  $\mu$ M (8 nM;  $r^2 = 0.6635$ ), 14.5  $\mu$ M (20 nM;  $r^2 = 0.9468$ ), 27.4  $\mu$ M (35 nM;  $r^2 = 0.9815$ ), and 48.5  $\mu$ M (60 nM;  $r^2 = 0.9926$ ). Insets: Plots of  $IC_{50}$  versus MAO-B concentration for pargyline (b;  $r^2 = 0.9987$ , x-intercept  $CI_{95} = -19.6$  to 3.8) and PLZ (c;  $r^2 = 0.9995$ , x-intercept  $CI_{95} = 1.3$  to 3.7).

### 5.3.3. Membrane Particle Protocol Development

During the process of harvesting hMAO-B from *P. pastoris*, the outer mitochondrial membrane can be isolated as a pellet. Membranes can be stored at  $-80^{\circ}\text{C}$  indefinitely with little loss in activity, and loss of activity is modest even with multiple freeze/thaw cycles at  $-20^{\circ}\text{C}$ . The membrane particle fraction contains the overexpressed hMAO-B still anchored, via its N-terminal, to the mitochondrial membrane, and the proximity of the membrane to the active site entrance channel is thought to mimic the *in vivo* situation, impacting substrate and inhibitor interactions of hMAO-B (Cruz & Edmondson, 2007). The size and density of the particles allow for low-speed centrifugation and separation of the enzyme from the incubation environment as a pellet. The concentration of MAO-B can then be determined by mofegiline titration of an aliquot of thawed membrane particles which had been thoroughly homogenized and diluted in pH 7.4 KP buffer (0.1 M), as previously described (Figure 5.3).

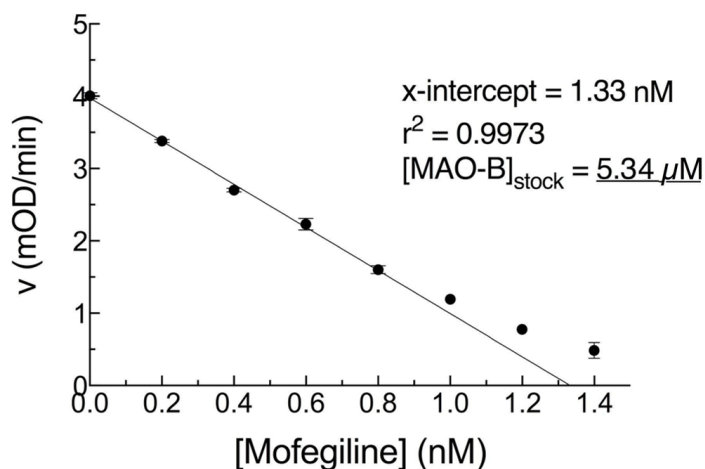


Figure 5.3 Mofegiline titration of MAO-B activity to determine stock concentration.

In quadruplicate, a known volume of MAO-B (in 0.1 M pH 7.4 KP buffer) was incubated in a microplate with a range of mofegiline concentrations for 30 minutes at  $37^{\circ}\text{C}$ . After incubation, BZ (1 mM) and AR/P were added to the wells and absorbance (571 nm) was measured over 35 min at  $37^{\circ}\text{C}$ . Initial rate of change was plotted against [mofegiline] and analyzed by linear regression (Prism7). A concentration of 1.33 nM mofegiline was needed to completely inactivate the incubated enzyme. Taking into account the dilution factor of 4000, the stock MAO-B concentration was calculated as  $5.34\ \mu\text{M}$  (global  $r^2 = 0.9973$ ).

In order to ensure minimal enzyme loss to the supernatant during centrifugation, homogenized membrane particles (containing 16 nM MAO-B) were centrifuged in one of two rotors at one of two speeds for 15 minutes at 4°C (see Table 5.1 for rotor information); uncentrifuged MAO-B served as control. After centrifugation, the supernatant was aspirated and saved for analysis (1st supernatant). The pellet was resuspended in minimal chilled buffer, diluted to its original concentration, and half the volume was set aside (1st wash). The remaining incubation was then centrifuged and processed exactly as before. In quadruplicate, the samples were assayed for remaining activity via AR/P, with BZ as substrate (3 mM), in a microplate, at 30°C. Initial rates of change in absorbance (mOD/min; 571 nm) for each sample were plotted in Prism7 (Figure 5.4).

Centrifugation at 6,000 rpm (Table 5.1) for both rotors (1.5 mL tube rotor =  $9,257 \times g$  and 5 mL tube rotor =  $8,922 \times g$ ) resulted in the most activity in the supernatants (Figure 5.4, green and purple bars), and for all groups except the  $20,817 \times g$  group the activity in the second supernatant was less than the first, a trend mirrored in an increase in activity in the twice-centrifuged enzyme (blue bar) compared to the singly-centrifuged enzyme (red bar). Differences in enzyme retention observed between the rotors at each speed may have been due to the sizes of the tubes that were centrifuged since the g-force at each speed was very similar between rotors;  $9,257$  and  $8,922 \times g$  at 6,000 rpm, and  $18,514$  and  $20,817 \times g$  at max speed for 5 mL and 1.5 mL tube rotors, respectively. The larger the base of the tube, the less compact the pellet, and the harder it was to remove all of the supernatant without disturbing the pellet. This may have resulted in the loss of some enzyme to facilitate complete removal of unbound ligand by centrifugation. The rotor/speed combination which resulted in the most retained activity in the pellet relative to the supernatant was the FA-45-30-11 rotor for 1.5 mL tubes at its maximum force of  $20,817 \times g$ . This

influenced the scale of the remaining experiments, due to the volume limitations of only incubating in 1.5 or 2.0 mL tubes. It was decided to use only 1.5 mL tubes going forward as they were more conducive to collecting a compact pellet.

Table 5.1

Tube (mL) / Rotor type	Speed (rpm / x g)	Max Speed (rpm / x g)
5 / (F-34-6-38 rotor w/ 5804 777.000 adapter)	6,000 / 9,257	12,000 / 18,514
1.5 / (FA-45-30-11 rotor)	6,000 / 8,922	14,000 / 20,817

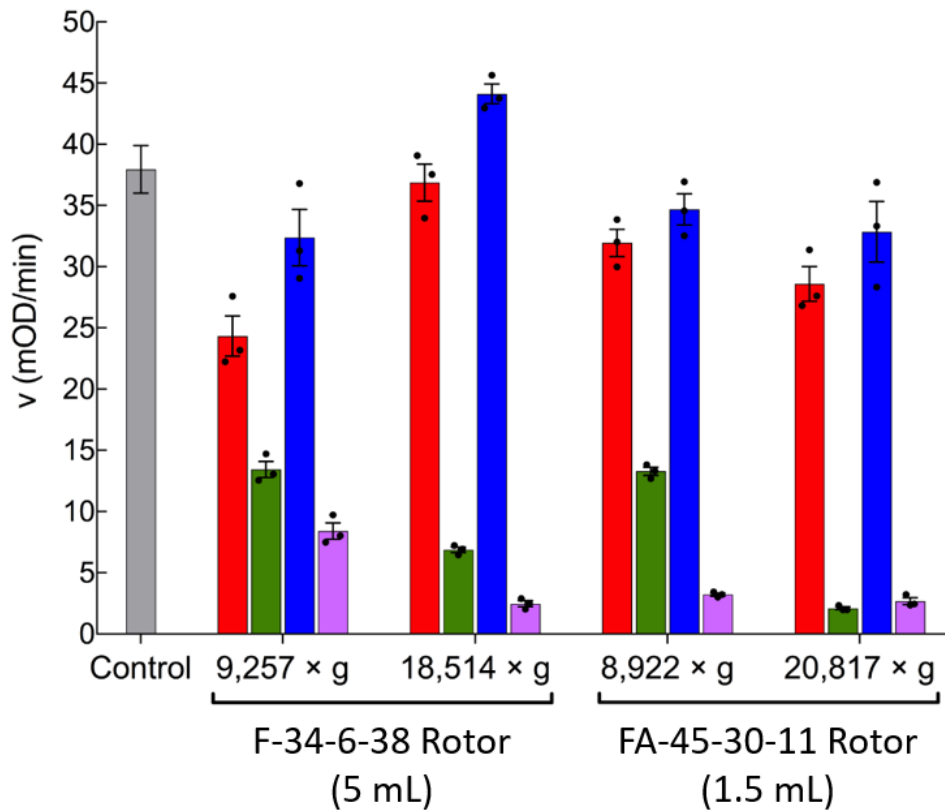


Figure 5.4 Influence of centrifuge rotor size and speed on PLZ removal from incubation. Initial rate of activity of 6.46 nM MAO-B in 3 mM BZ via the AR/P assay. Uncentrifuged control (grey bar; 1.5 mL tube) was compared to centrifuged and resuspended enzyme after one centrifugation (red bar) and two centrifugations (blue bar), as well as the supernatants from the first (green bar) and second (purple bar) centrifugations. The first two groups are 5 mL incubations and the second two are 1.5 mL incubations; an uncentrifuged control was made up in 1.5 mL tube as previously described.

Next, the ability of the centrifugation protocol to remove the majority of PLZ from the incubation in 1.5 mL tubes was tested. Ice-cold MAO-B (10.8 nM) and PLZ (25 mM) were mixed and immediately centrifuged (0°C) between one and four times as outlined in the previous experiment, retaining the pellet and discarding the supernatant; uncentrifuged MAO-B in the presence and absence of PLZ served as controls. To prevent as much enzyme inactivation as possible, samples were prepared and processed at 0°C until analysis to limit enzyme-mediated turnover. In quadruplicate, the initial rate of change in absorbance (571 nm) for each group was measured by the AR/P assay (30°C) and compared (Figure 5.5). The concentration of MAO-B in the well was 2.15 nM for groups 0 to 4 and 4.30 nM for control.

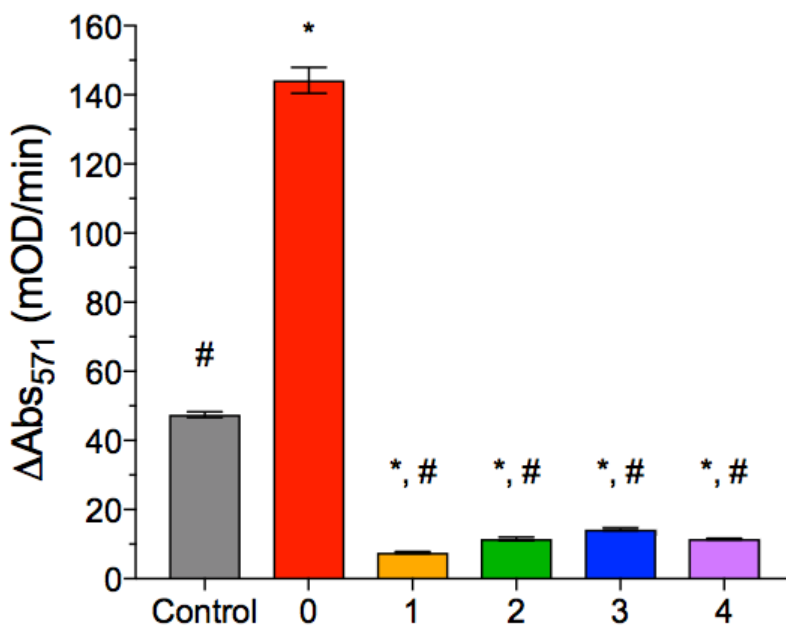


Figure 5.5 Extent of PLZ removal by centrifugation.

Initial rates of change in absorbance (571 nm) after mixing 10.8 nM MAO-B and 25 mM PLZ and centrifuging from zero to four times (14,000 rpm, 15 min, 0°C). Unincubated, uncentrifuged MAO-B (21.5 nM) served as control (grey bar). Change in absorbance was measured at 571 nm by the AR/P assay in 3 mM BZ for 4.30 nM MAO-B (control) and 2.15 nM MAO-B (0-4) at 30°C. (\*  $p < 0.0001$  vs control (grey), #  $p < 0.0001$  vs 0 group (red), multiple comparisons by one-way ANOVA and Tukey *post-hoc* test)

The initial rate of change in absorbance in the uncentrifuged sample ( $144 \pm 3.8$  mOD/min; red bar) was three times that of control ( $47.5 \pm 0.8$  mOD/min; grey bar) and plateaued after just two minutes. Considering that the concentration of PLZ in the 0 group was 12.5 mM in the well, this high rate is almost certainly unrelated to MAO-B activity, but rather is due to PLZ converting all of the Amplex Red in the well ( $20 \mu\text{M}$ ) to resorufin within the first two minutes. The centrifuged groups displayed much lower rates than the control (\*  $p < 0.0001$ ), even after considering the control group had twice the MAO-B concentration as the PLZ-incubated groups. An equivalent concentration of MAO-B in the control group would have had about half the measured rate, around 24 mOD/min, which still translates to a 50% decrease in activity in the centrifuged groups. Whether this decrease was due to inhibition of MAO-B by PLZ in the brief time they were incubated together or a result of centrifugation was unknown. There were no statistically significant differences between the centrifuged groups. Based on these data, the centrifugation protocol in further experiments was to centrifuge samples twice with a buffer change in between.

#### 5.3.4. Can We Reach Complete Inhibition of MAO-B by PLZ?

With an optimized protocol for the centrifugation of membrane particles, inhibition of MAO-B by very high PLZ concentrations could be measured. MAO-B (30 nM) was incubated alone or with PLZ (3  $\mu\text{M}$ , 300  $\mu\text{M}$ , or 30 mM) for up to four hours at  $10^\circ\text{C}$ . Tubes were then centrifuged twice (14,000 rpm, 15 minutes,  $0^\circ\text{C}$ ) with a buffer change in between; the supernatants from the first centrifugation were retained in new tubes and kept chilled. If enzyme inactivation is markedly slowed due to competition between PLZ and PEDz for binding to the active site, evidence of high PLZ turnover would be present in the supernatant after the first centrifugation. The number of turnovers which occurred during the incubation with PLZ was approximated by assessing the concentration of  $\text{H}_2\text{O}_2$ , released from the enzyme during the oxidative half-reaction,

in the supernatant. It was hypothesized that higher concentrations of PLZ would lead to a much greater increase in  $\text{H}_2\text{O}_2$  beyond that which would be predicted from exponential time course curves, as a result of competition between PEH, PEDz, and PLZ for binding to the active site, and the resulting decrease in the rate at which enzyme is inhibited.

Resuspended enzyme was assayed via AR/P in BZ (3 mM) and initial rate plotted as % control (0 PLZ = 100%; red line) against incubation time (Figure 5.6a). MAO-B incubated with 3  $\mu\text{M}$  PLZ had 56% remaining activity after 4 hours (green line), as did incubations with 300  $\mu\text{M}$  PLZ (blue line), although 3  $\mu\text{M}$  PLZ inhibited MAO-B slightly faster than 300  $\mu\text{M}$  PLZ, with a half-life of 52 minutes versus 66 minutes. Even with 30 mM PLZ, 2000 times the literature  $K_D$  of 15  $\mu\text{M}$  (Binda et al., 2008), there was still more than 20% enzyme activity remaining after 4 hours (purple line) and inactivation was the slowest, with a half-life of around 77 minutes. This is consistent with PEDz competing with PLZ and, to a smaller extent, PEH for binding to the enzyme, thereby increasing the half-life of inactivation and preventing complete inhibition.

Due to the sensitivity of the AR/P assay, the supernatant was diluted (1:150) in water before assaying (Figure 5.6b). The change in absorbance due to production of  $\text{H}_2\text{O}_2$  was taken as the first absorbance value after addition of AR/P to the supernatant in the plate, as at that point the interaction between Amplex Red and unreacted PLZ in the supernatant would be assumed to minimally influence the absorbance, given that the reaction which utilizes  $\text{H}_2\text{O}_2$  to produce resorufin occurs very rapidly. For all groups, absorbance did not increase with time incubated, as would be expected if  $\text{H}_2\text{O}_2$  was produced continuously over the course of the incubation. Instead, the measured absorbance was likely the result of interaction between the Amplex Red reagent and PLZ, which was negligible for 3 and 300  $\mu\text{M}$  PLZ incubations compared to control but was extensive for 30 mM PLZ.

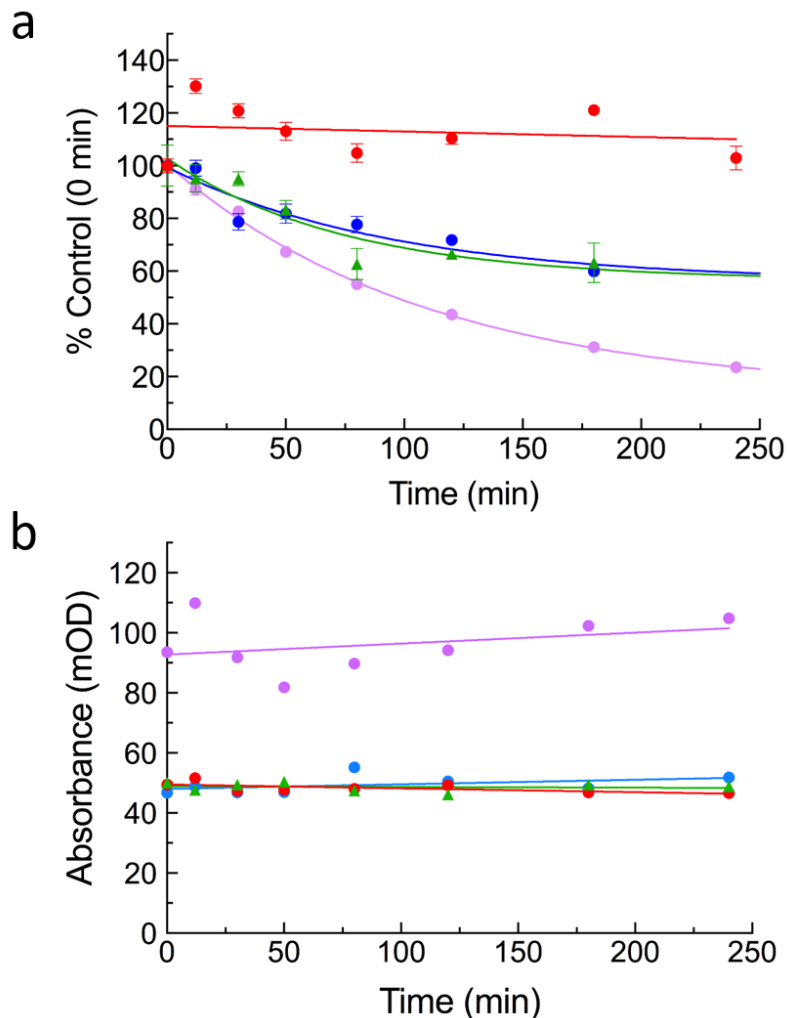


Figure 5.6 Inhibition of membrane particle-bound MAO-B by PLZ.

(a) Initial rate of activity of 15 nM MAO-B after incubation of 30 nM MAO-B with 0 (red), 3 μM (green triangles), 300 μM (blue), and 30 mM (purple) PLZ for up to four hours at 10°C. Resuspended enzyme assayed for remaining activity via AR/P assay in 3 mM BZ (30°C) and initial rate plotted as % control (0 PLZ) versus incubation time (minutes). Curves fitted by linear regression (control; red line) or one-phase exponential decay (Prism7, mean ± SEM, n=3). 3 and 300 μM PLZ inhibited the same amount of activity after four hours, about 44%, with  $t_{1/2}$  of 52 and 66 min, respectively. 30 mM PLZ inhibited the most activity at roughly 80% (purple line;  $r^2 = 0.9919$ ) but had the lowest  $t_{1/2}$  at 76.6 min. (b) Absorbance (mOD) of the supernatants from the first centrifugation. As the absorbance did not increase with incubation time, the presence of PLZ in supernatants, but not H<sub>2</sub>O<sub>2</sub> content, contributed to the amount of resorufin produced, especially for the 30 mM PLZ incubations.

### 5.3.5. Effects of High PLZ Concentrations on MAO-B Inactivation

To understand the effect of high PLZ concentrations on enzyme activity, pre-incubated enzyme which had been centrifuged and resuspended was titrated with mofegiline. Mofegiline titration allows for the determination of the concentration of enzyme active sites and is the standard in this laboratory for determining enzyme concentration, as demonstrated in previous sections of this thesis. MAO-B (30 nM) and PLZ (30 mM) were pre-incubated at 30°C for 3 hours; MAO-B pre-incubated alone served as a 0 PLZ control, and MAO-B which was unincubated and uncentrifuged served as a non-centrifuged control. The resuspended enzyme was then incubated with a range of mofegiline concentrations (0-30 nM; 30 minutes, 30°C) and remaining activity assayed by AR/P (3 mM BZ; 571 nm). Initial rates of activity ( $v$ ; mOD/min) at each time point of pre-incubation were plotted against mofegiline concentration (Figure 5.7) in all three groups, and the slopes (mOD/min/nM) compared.

Between the uncentrifuged (red line) and centrifuged (orange line) controls, there is a change in slope from -2.2 mOD/min/nM to -1.6 mOD/min/nM, which indicates that there is a loss of enzyme activity (y-axis) that is not reflected in an equivalent loss of active sites (x-axis). This result is also seen in the enzyme which had been pre-incubated with high PLZ (green line), where the slope is further reduced to -0.39 mOD/min/nM, nearly six times less active per nM enzyme than uncentrifuged control, and just over four times less than centrifuged control. Although the activity decreases by almost 30 mOD/min between control and 30 mM PLZ, the concentration of active sites only decreases by 6.3 nM. It appears that the enzyme is becoming less efficient after centrifugation or incubation, or both.

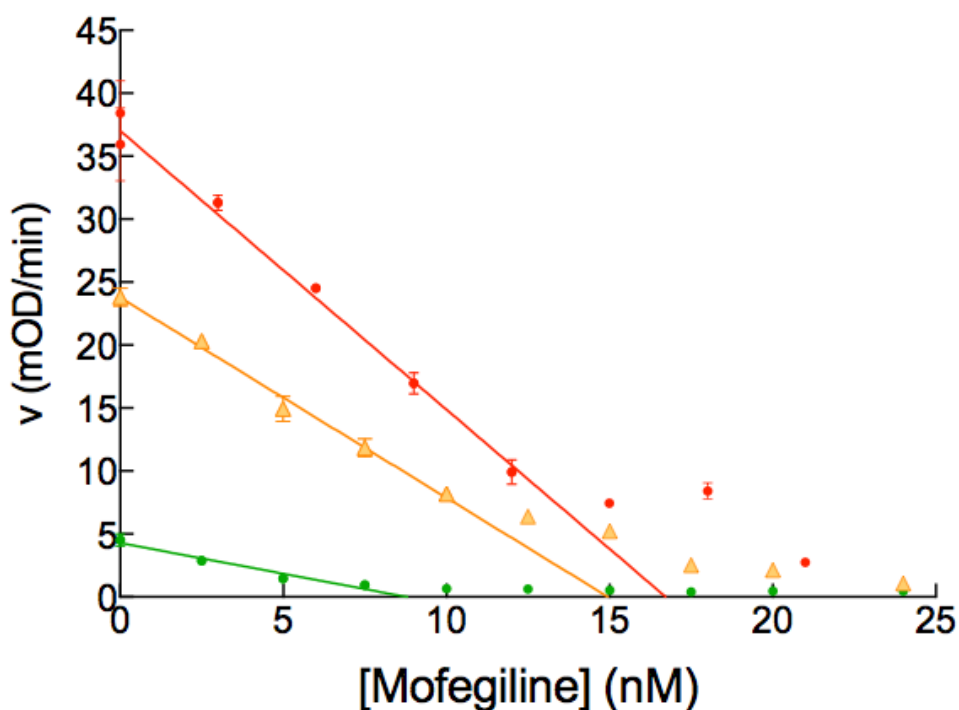


Figure 5.7 High [PLZ] inhibition of MAO-B followed by mofegiline titration.

Mofegiline titration of remaining enzyme (nominally 15 nM) after incubation of 30 nM MAO-B alone (orange) or with 30 mM PLZ (green) for 3 hours at 30°C. Samples were centrifuged to remove unbound ligand; uncentrifuged MAO-B served as control (red). In triplicate, samples were incubated with a range of mofegiline concentrations for 30 minutes at 30°C. Change in absorbance (571 nm) measured via AR/P and 3 mM BZ (30°C), and initial rate (mOD/min) plotted against mofegiline concentration (nM). Activity of uncentrifuged MAO-B was  $37 \pm 0.77$  mOD/min with an active site concentration of 16.7 nM, giving a slope of  $-2.2 \pm 0.11$  mOD/min/nM ( $r^2 = 0.9933$ ); centrifuged MAO-B alone had slightly lower activity at  $23.8 \pm 0.48$  mOD/min, but still retained 15.0 nM active sites, for a slope of  $-1.6 \pm 0.078$  mOD/min/nM ( $r^2 = 0.9928$ ); and MAO-B incubated with 30 mM PLZ had the shallowest slope of  $-0.39 \pm 0.072$  mOD/min/nM ( $r^2 = 0.9056$ ), despite having 10.4 nM mofegiline-titratable active sites present, due to the disproportionate decrease in activity to just  $4.04 \pm 0.44$  mOD/min. Results are expressed as mean  $\pm$  SEM of 3 replicate measures.

### 5.3.6. Effects of Low PLZ Concentrations on MAO-B Inactivation

MAO-B (16 nM) was incubated alone and with a range of PLZ concentrations from 158 nM to 50  $\mu$ M, encompassing the literature  $K_D$  for PLZ inhibition of MAO-B (15  $\mu$ M; Binda et al., 2008), for two hours at 30°C (in 0.1 M pH 7.4 KP). The incubations were then centrifuged and resuspended in fresh buffer and the remaining activity was assayed in saturating BZ (3 mM) via the AR/P assay (25°C). Initial rates (mOD/min) were plotted against log[PLZ] and the semilog plot fitted to a sigmoid (Figure 5.8). The  $IC_{50}$ , the concentration of PLZ which inhibits 50% of the enzyme, was 1.44  $\mu$ M.

An inhibition time course curve was then determined for MAO-B (16 nM) inhibited by 25  $\mu$ M PLZ over the course of 70 minutes at 30°C. Using the  $IC_{50}$  of 1.44  $\mu$ M determined just previously, this concentration should inhibit about 95% of the enzyme present in the pre-incubation. The AR/P assay of activity remaining in 3.2 nM of inhibited enzyme MAO-B revealed a mere 3% activity left (in 3 mM BZ) after just 35 minutes of incubation (Figure 5.9) and a half-life 6.2 minutes.

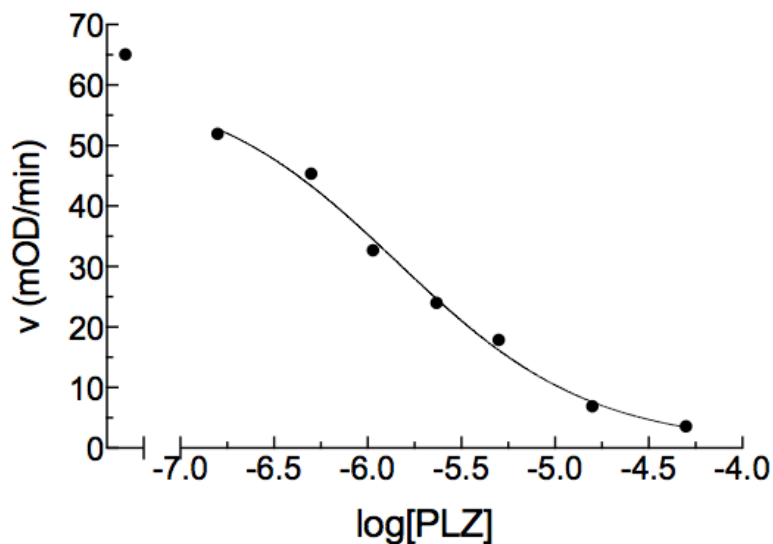


Figure 5.8 Initial rate of activity remaining in MAO-B plotted against log[PLZ]. MAO-B (16 nM) was pre-incubated with a range of PLZ concentrations for two hours at 30°C, the unbound PLZ was removed by centrifugation, and the enzyme (8.1 nM) was resuspended in fresh buffer for an AR/P assay (3 mM BZ, 571 nm, 30°C). Curve fit by nonlinear regression to a sigmoid (Prism7).  $IC_{50} = 1.44 \mu\text{M}$  ( $CI_{95} = 1.08\text{-}1.79 \mu\text{M}$ ,  $r^2 = 0.9918$ ).

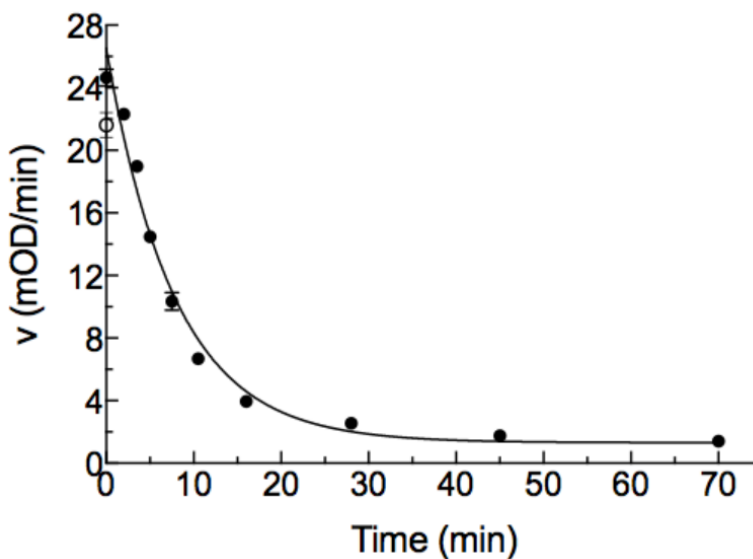


Figure 5.9 Initial rate of activity remaining in MAO-B versus incubation time. Open circle = -PLZ control. MAO-B (16 nM) was pre-incubated with 25  $\mu\text{M}$  PLZ for various times across two hours (30°C), the unbound PLZ was removed by centrifugation, and the enzyme was resuspended in fresh buffer (3.23 nM) for an AR/P assay (3 mM BZ, 571 nm, 30°C). Curve fit by nonlinear regression to a single exponential (Prism7),  $t_{1/2} = 6.2 \text{ min}$  ( $CI_{95} = 5.7\text{-}6.8 \text{ min}$ ).

### 5.3.7. Comparison of Inhibition of MAO-B by High and Low Concentrations of PLZ

With these parameters determined, incubation of MAO-B with PLZ for a range of time was performed, first with a low concentration of PLZ (25  $\mu$ M) and then with a high concentration (25 mM). Samples were centrifuged and resuspended as before, followed by a mofegiline titration of the remaining active enzyme (90 minutes incubation with mofegiline at 30°C). An AR/P assay (3 mM BZ) gave initial rates ( $v$ ; mOD/min) which were plotted against mofegiline concentration and fitted by linear regression (Figures 5.10a and 5.11a). From this linear regression, the slope of each line was plotted against time in order to assess whether or not the decrease in activity over time was accompanied by an equivalent decrease in mofegiline-titratable active sites (Figures 5.10b and 5.11b). The y-intercept was also plotted against time for each pre-incubation period and the curve fitted to a one-phase exponential decay equation to obtain a half-life for the loss of enzyme activity, as well as a plateau indicating maximum inhibition reached (Figures 5.10c and 5.11c). Finally, the remaining activity (y-intercept; mOD/min) was plotted against the concentration of active sites remaining (x-intercept; nM) for each preincubation time as a further approach to visualizing the relationship between loss of activity and loss of active sites (Figures 5.10d and 5.11d).

The linear relationship between the slope and incubation time (Figure 5.10b), as well as between the y-intercept and x-intercept (Figure 5.10d), indicate that MAO-B inhibition by low PLZ (25  $\mu$ M) resulted in a decrease in active sites which was proportional to the decrease in activity of the enzyme. For the association between the initial rate of activity and incubation time (Figure 5.10c), the “0 time” data point (closed circle) was not included, as the rate after 2 minutes of incubation was slightly higher than the activity of both “0 time” controls (closed circle = +PLZ, open circle = -PLZ); exclusion of this point improved the global fit of the regression line (from  $r^2$

= 0.9569 to 0.9952). The half life of inactivation of 16 nM MAO-B by 25  $\mu$ M PLZ was calculated to be 4.4 minutes.

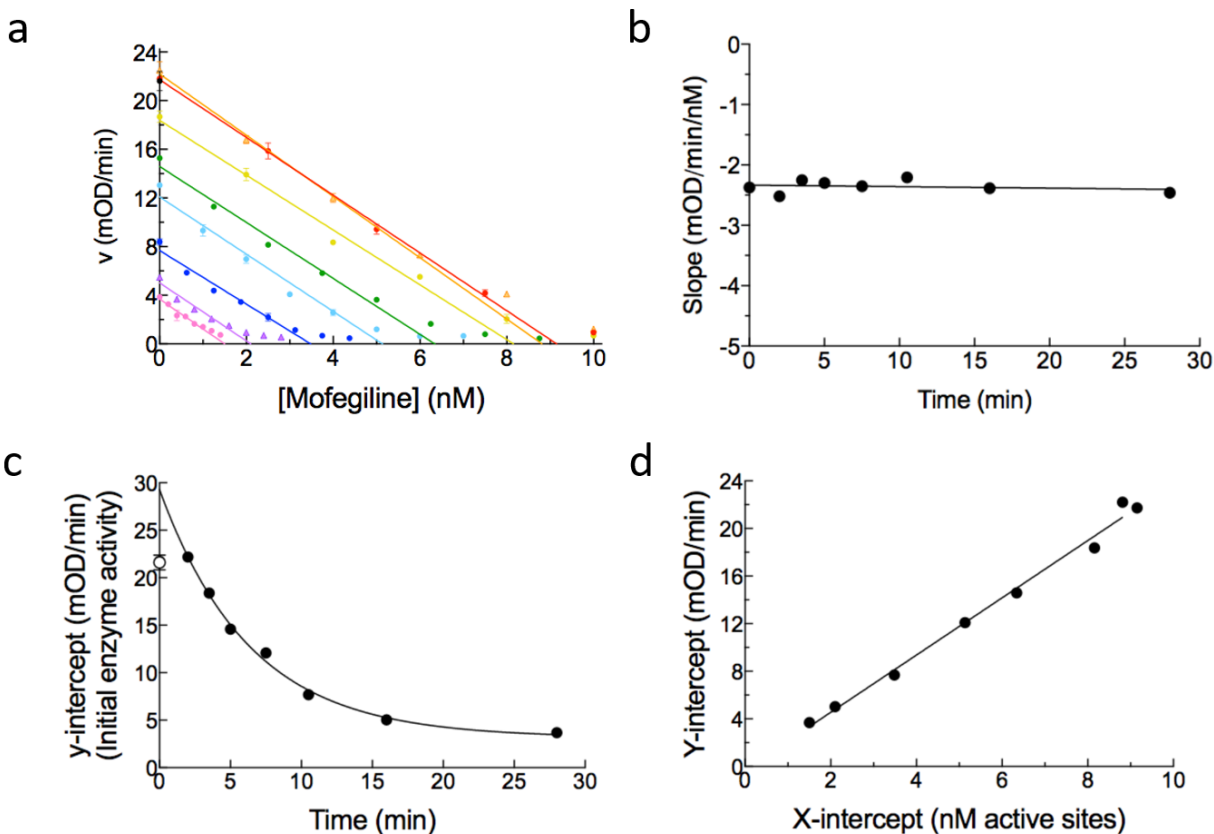


Figure 5.10 Inhibition of 16 nM MAO-B by low PLZ (25  $\mu$ M) over time. **(a)** Titration of active sites remaining in 8.1 nM MAO-B by mofegiline (90 min at 30°C) after pre-incubation and resuspension of samples (red=0, orange=2, yellow=3.5, lime=5, green=7.5, blue=10.5, purple=16, pink=28 min pre-incubation). An AR/P assay of remaining activity (30°C, 571 nm, 3 mM BZ, 3 replicates) was performed on titrated samples and linear regression calculated. **(b)** Comparison of the slopes (mOD/min/nM) calculated in (a) across time incubated (min). Non-linear regression gave a slope, -0.0025, which was not significantly different from zero ( $CI_{95} = -0.013 - 0.0085$ ;  $p = 0.5971$ ;  $r^2 = 0.04932$ ). **(c)** Comparison of the y-intercept from (a) across time incubated (min; open circle is -PLZ control and closed circle (overlapped by -PLZ point) is +PLZ control). Data fit to an equation for one phase exponential decay via nonlinear regression, excluding “0 time” incubation, gave a  $t_{1/2}$  of 4.4 min (Prism7;  $r^2 = 0.9952$ ). **(d)** Replots of y-intercepts versus x-intercepts from (a); 0 min excluded from linear regression (Prism7;  $r^2 = 0.9893$ ).

When PLZ (25 mM) was incubated with MAO-B in parallel experiments, the results were very different. First, as previously seen in Figure 5.6, the rate of activity dropped by 70% due solely to prior, fleeting exposure of enzyme to PLZ for “0 time”, but the concentration of active sites only decreased by 16% (red to orange line, Figure 5.11a). Comparison of the slopes obtained at increasing incubation times (Figure 5.11b) reveals that the loss of activity continued to be accompanied by a lower-than-expected loss of active sites, until a plateau was reached after 30 minutes pre-incubation. The half-life of inhibition of MAO-B by 25 mM PLZ was 2 minutes (Figure 5.11c), shorter than the 4.4 minutes observed for 25  $\mu$ M PLZ. However, titration with mofegiline suggested that around 28% (2.5 nM) of the active sites still remained after pre-incubation with 25 mM PLZ for 90 minutes, compared to just 16% remaining active sites after incubation with 25  $\mu$ M PLZ for 28 minutes. The relationship between the y- and x-axes reveals the scale of discrepancy between remaining activity and remaining active sites, respectively (Figure 5.11d).

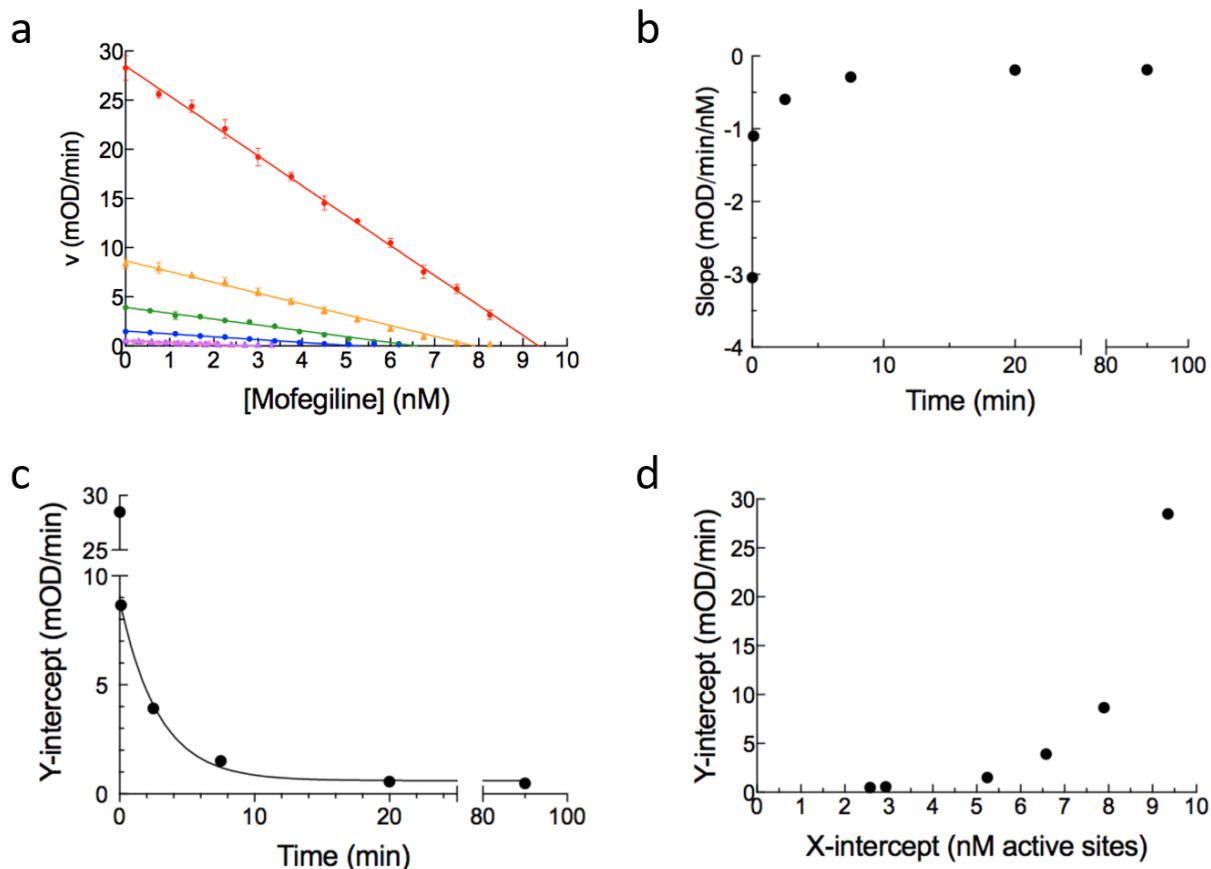


Figure 5.11 Inhibition of 16 nM MAO-B by high PLZ (25 mM) over time.

(a) Titration of active sites remaining in nominally 8.1 nM MAO-B by mofegiline (90 min at 30°C) after pre-incubation and resuspension of samples (red=0 PLZ; orange=0, green=2.5, blue=7.5, purple=20, pink=90 min pre-incubation). An AR/P assay of remaining activity (30°C, 571 nm, 3 mM BZ, 3 replicates) was performed on titrated samples and linear regression calculated (Prism7). (b) Comparison of the slopes (mOD/min/nM) calculated in (a) across time incubated (min). As time pre-incubated increased, the slope absolute value decreased before plateauing after 20 minutes (purple triangle). (c) Comparison of the y-intercept from (a) across time incubated (min). Data fit to one phase exponential decay curve via nonlinear regression, excluding “0 PLZ” incubation (Prism7;  $r^2 = 0.9972$ ), and  $t_{1/2}$  calculated to be 2 min ( $CI_{95} = 1.3\text{--}3.1$  min). (d) Comparison of the y-intercept to the x-intercept from (a), illustrating the non-linear relationship between initial remaining activity (y-axis) and mofegiline-titratable active site concentration (x-axis).

## 5.4. Discussion & Conclusion

When a fixed concentration of PLZ was incubated with a range of MAO-B concentrations, as the concentration of enzyme increased, the time it took to inactivate the enzyme decreased (Figure 5.1b) and the rate constant for inactivation increased (Figure 5.1c). This observation is consistent with competition between the inhibitory species, PEDz, and other ligands, such as PLZ, PED, and BZ, for binding to MAO-B. Competition would only occur if PEDz left the active site before returning to inhibit the enzyme. As well, the half-life for MAO-B inactivation by PLZ is increased at high concentrations of PLZ. This is also inconsistent with another criterion for mechanism-based inhibition, specifically that at a saturating concentration of inhibitor, inhibition of the enzyme population proceeds at the maximum possible rate ( $V_{max}$ ). This required further exploration to determine what is happening to MAO-B at high, presumably saturating, PLZ concentrations far higher than the  $IC_{50}$  of  $1.44 \mu\text{M}$  obtained from an inhibitor plot for PLZ (Figure 5.8) and also the  $K_D$  of around  $8 \mu\text{M}$  for the initial reversible interaction with MAO-B, determined in our laboratory (A. Holt, unpublished observation).

At  $25 \mu\text{M}$  PLZ,  $t_{1/2}$  was 6.2 minutes (Figure 5.9) and the decrease in activity over time mirrored the decrease in the number of mofegiline-titratable sites (Figure 5.10a), producing parallel slopes in mofegiline titration plots (Figure 5.10b). This is expected for time-dependent inhibitors, as the removal of active site from the population pool of enzyme by inactivation lowers the maximum possible activity for that population concomitantly, resulting in a loss of activity which corresponds directly to the loss of active sites.

At  $25 \text{ mM}$ , however, activity was lost much more quickly than were the active sites (Figure 5.11a), resulting in non-parallel lines of mofegiline titration (Figure 5.11b). Irreversible inhibition by PLZ results in the formation of a covalent adduct between FAD and a phenylethyl group derived

from PLZ, which prevents binding of substrate and subsequent catalytic activity. However, mofegiline titration identified a much greater number of active sites than might have been predicted, based on the level of activity remaining.

A decrease in activity of a single monomer, without loss of the active site in that monomer, might be explained by an allosteric modulation of catalytic efficiency by PLZ. Binding of PLZ to an allosteric site would result in either increased  $K_M$ , or decreased  $k_{cat}$ , or both, but could not physically block substrate or mofegiline access to the active site. The imidazoline  $I_2$  site in the substrate entrance channel of MAO-B has been identified as an allosteric modulatory site on hMAO-B (Bonivento et al., 2010; McDonald et al., 2010), but  $I_2$  site ligands block access of substrate, and of inhibitors such as mofegiline, to the active site. As such, binding of PLZ to the  $I_2$  site can not explain the loss of activity, but retention of active sites. Aside from the  $I_2$  site, no other allosteric site has been identified in hMAO-B to date.

MAO-B is a homodimeric protein, composed of two identical monomers. While, in the absence of evidence to the contrary, it has been believed that the monomers operate independently of one another, recent *in silico* simulation studies suggested that the redox state of one monomer may impact the ability of ligands to associate with, or dissociate from, the opposing monomer (H. B. L. Jones et al., 2019). In this way, it is possible that activity in the opposing monomers remains 180° out of phase, with one monomer participating in an oxidative half-reaction while the other participates in a reductive half-reaction, in a process known as flip-flopping (Curado-Carballada et al., 2019; Fielden et al., 1974; Waight et al., 1977) (Figure 5.12a,b).

Binding of PEDz to one monomer which is primed to catalyze an oxidative half-reaction, followed by inactivation of that monomer, may serve to impede the mechanism by which the monomers flip-flop in their respective redox states (Figure 5.12d). In this way, PEDz, and perhaps

also mofegiline (Figure 5.12c), may bind to the active site of one monomer, inactivating that monomer and preventing the opposing monomer from completing its catalytic cycle such that it is ready to participate in a new reaction cycle. In other words, binding of PEDz to only one monomer inactivates both subunits, implying that binding of a single mofegiline molecule to only one monomer of a dimer may also inactivate both subunits.

The opposing monomer may be impeded in its cycle by the absence of induced structural changes which facilitate ligand access to the active site. Contenders for residues involved in the transmission of structural changes from one monomer to the other include the gating residues Ile199 and Tyr 326, the movement of which forms the high-affinity I<sub>2</sub> site in the entrance channel (McDonald et al., 2010), and the substrate loop located just outside of the binding domain of the enzyme, comprised of residues 99-112 and responsible for the stabilization and admittance of ligands into the substrate binding domain (Allen & Bevan, 2011; Binda et al., 2004; H. B. L. Jones et al., 2019). Without access to the active site cavity, the subunit is rendered functionally inactive, despite no formal inactivation by modification of the active site itself.

If PLZ acts in the manner described, we would expect to see a loss of activity accompanied by a proportional loss of active sites titratable with mofegiline, and mofegiline titration plots obtained following incubation of PLZ with enzyme for different periods of time would be parallel. This is exemplified in Figure 5.10a, where PLZ (25 μM) was incubated with enzyme. As such, the process described above may reflect that occurring when hMAO-B is incubated with low concentrations of PLZ (Figure 5.12b).

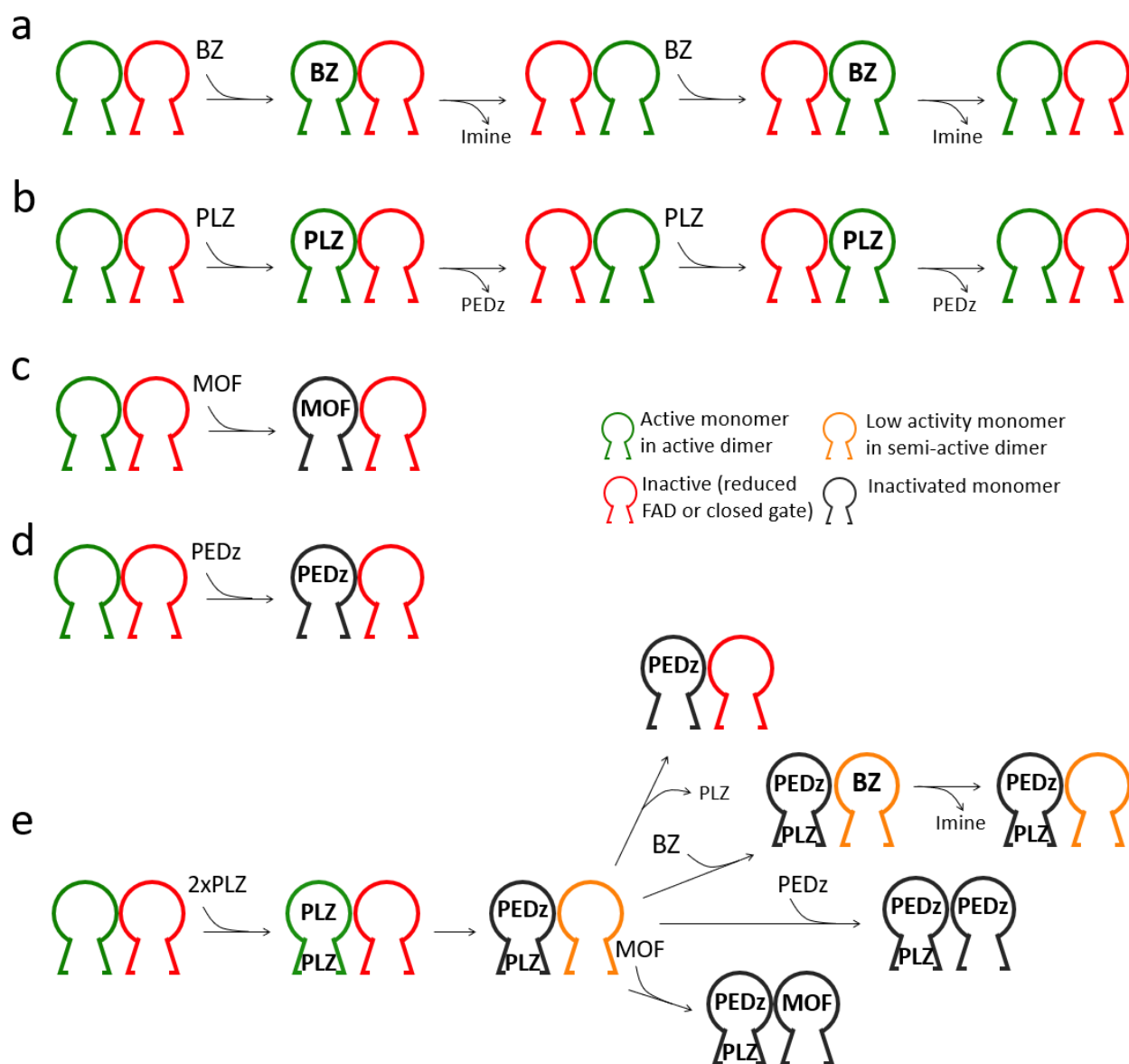


Figure 5.12 Proposal for mechanism of MAO-B inactivation via inter-subunit communication. (a) Normal monomer flip-flop with BZ as substrate; active and inactive monomers (green and red, respectively) alternate based on turnover of substrate. (b) In low PLZ incubations, PEDz is released from the active site during enzymatic turnover of PLZ, allowing for flip-flop. (c) Mofegiline binds irreversibly to one monomer (grey) and prevents re-activation of the second subunit (red), resulting in permanent inactivation of the dimer. (d) Rebinding of PEDz to an oxidized (green) active site similarly prevents re-activation of the inactive monomer (red). (e) Binding of PLZ to the active site, followed by binding of a second molecule of PLZ to the entrance channel of the active (green) subunit inactivates that monomer (grey), possibly due to *in-situ* formation of PEDz followed by cofactor reoxidation, but allows the second subunit (yellow) to retain partial activity. Dissociation of PLZ from the entrance channel would result in loss of this partial activity, rendering the second, low-activity monomer inactive. Otherwise, this semi-active dimer can metabolize substrate, albeit with lowered catalytic efficiency, or it can be completely inhibited by binding of PEDz or mofegiline at the low-activity monomer (yellow).

In contrast, when hMAO-B is incubated with high concentrations of PLZ, loss of activity is not accompanied by a proportional loss in mofegiline-accessible active sites. This might be explained if PLZ-mediated inactivation of one monomer changes the catalytic efficiency in the second monomer without compromising access to the active site for mofegiline to bind. Preliminary data from our laboratory (A. Holt, unpublished results) had revealed a significant increase in the  $K_M$  for BZ following pre-incubation of MAO-B with high PLZ and removal of unreacted, unbound PLZ (Figure 5.13), which is consistent with this theory.

Figure 5.13a shows remaining activity, in relative fluorescence units per second (RFU/s; determined by measuring resorufin fluorescence, rather than absorbance), for MAO-B which had been pre-incubated with various concentrations of PLZ, plotted against the concentration of BZ used to assess the remaining activity after centrifugation and resuspension of the enzyme, and the data fitted to one-site binding equations by nonlinear regression to obtain the  $K_M$ . Figure 5.13b shows the increases in  $K_M$  for BZ after pre-incubation as a function of the concentration of PLZ during pre-incubation, evidence that the catalytic efficiency of the enzyme decreased with increased concentration of PLZ.

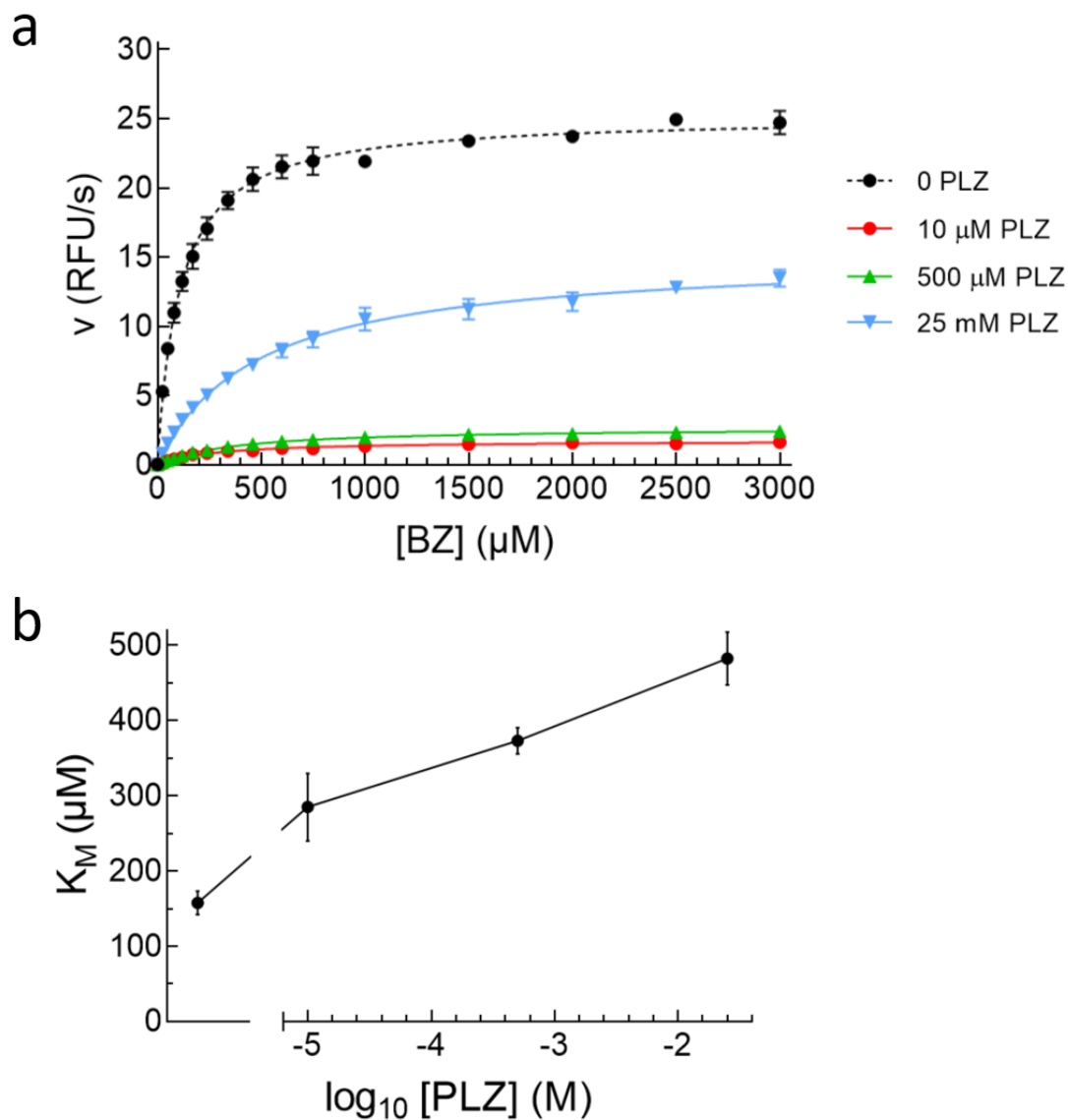


Figure 5.13 Increase in  $K_M$  for BZ after pre-incubation of MAO-B with PLZ.

(a) Remaining activity in MAO-B ( $v$ ; RFU/s) versus a range of BZ concentrations following pre-incubation of MAO-B with 10  $\mu\text{M}$  (red circles), 500  $\mu\text{M}$  (green triangles), and 25 mM (blue inverted triangles) PLZ compared to control (0 PLZ; black circles). Data fitted to one-site binding equations by nonlinear regression (Prism7) in order to obtain the  $K_M$  at each [PLZ]. (b) Replot of  $K_M$  values obtained from (a).

If inactivation of one monomer by PEDz results in a complete loss of activity in the opposing monomer, the inclusion of high concentrations of PLZ must presumably result in a modification of the inactivation response in the second subunit. We propose that low-affinity binding of a second molecule of PLZ to the already-inactive subunit lowers catalytic efficiency in the second subunit, through modifying movement of residues that respond to occupation of the active site by PLZ or PEDz and communication of information to the second subunit regarding the redox state of the first.

In this regard, we further propose that following occupation of the active site by PLZ, a second PLZ occupies the entrance channel, at the imidazoline I<sub>2</sub> binding site on the same subunit (Figure 5.12e). Binding of the second PLZ can not be to the second subunit, as occupation of either the active site or the entrance channel would prevent substrate and mofegiline access and would cause complete inhibition. The imidazoline I<sub>2</sub> ligand 2-BFI has been shown to modify MAO-B inactivation by PEA, an endogenous MAO-B substrate and PLZ analog, increasing the rate of inactivation of MAO-B by PEA (McDonald et al., 2010). As well, 2-BFI has been noted to modify inactivation of MAO-B by PLZ by altering the number of turnovers prior to inactivation and the half-life of inactivation (A. Holt, unpublished results).

In this scenario, we would expect to observe an initial fall in activity, associated with the inactivation of one monomer with full catalytic competence, accompanied by the renewed availability (via flip-flop) of the active site on the second monomer, but with lower catalytic efficiency. Further, there would be no initial loss of mofegiline accessibility associated with this lowered level of activity, consistent once again with the idea that one mofegiline molecule is sufficient to inhibit activity completely in an unmodified enzyme dimer. These events would be observed after a very brief exposure of the enzyme to PLZ as a mofegiline titration plot of reduced

slope but unaltered X-intercept. Thereafter, as times for preincubation of PLZ with MAO-B increased, titration of the second monomer with mofegiline would be accompanied by a concomitant decrease in activity, and a series of parallel mofegiline titration plots obtained with increasing incubation times, as mofegiline inactivated the second subunit. This is consistent with data presented in Figure 5.11a.

The present data do not confirm that low concentrations of PLZ are able, via generation of PEDz, to cause covalent inactivation of one monomer and complete (allosteric) inactivation of the other. If inactivation of one monomer by PEDz renders the second monomer available for catalysis with unmodified catalytic efficiency, data obtained would be indistinguishable from those shown in Figure 5.10a. However, what seems not to be in doubt is the ability of a single mofegiline molecule to render both monomers inactive (Figure 5.12c), based on the observations of reduced slopes in mofegiline titration plots following preincubation with high PLZ concentrations.

Should the effect of high concentrations of PLZ on inactivation of hMAO-B be one of allosteric modulation of inter-subunit communication, it would be one more blow to the notion that PLZ is a mechanism-based inhibitor, as defined by Silverman (1995b), as inhibitor stoichiometry would not apply at these high concentrations of PLZ. These findings represent the first direct evidence for inter-subunit communication, as well as evidence that PLZ is not a mechanism-based inhibitor and does not inhibit MAO-B according to the forked mechanism.

## Chapter 6

### General Discussion and Future Directions

#### 6.1. Summary of Novel Findings

##### 6.1.1. What We Have Learned About PLZ

The work presented in this thesis has contributed to the understanding of the mechanism of inhibition of hMAO-B by PLZ. The overarching theme of these findings is that the reactive intermediate PEDz leaves the active site after formation from MAO-B metabolism of PLZ. Using HDX, evidence was obtained to support the proposal that PEDz is the sole metabolite of PLZ oxidation (Chapter 2), a theory which had been suggested in older studies (Patek & Hellerman, 1974; Yu & Tipton, 1989). It is proposed that production of PEH as a major metabolite of PLZ, as established by Matveychuk (2015), occurs after release of PEDz from the active site, where it then reorganizes in bulk solvent to form PEH.

Release from the active site was demonstrated as occurring during inhibition by PEDz, due to the requirement for molecular oxygen ( $O_2$ ) to re-oxidize the reduced flavin cofactor before the diazene can form a covalent adduct with the N(5) atom of the isoalloxazine ring of FAD (Chapter 3), as it had been previously suggested that diazenes cannot interact with reduced flavin (Nagy et al., 1979). The other requirement for  $O_2$  in inhibition of MAO-B by PEDz as evidenced in Chapter 3 is radicalization of the diazene intermediate, which couples with an oxidized active site and results in a permanently inhibited enzyme. The data obtained can not confirm that the radical derived from PEDz is incapable of reacting with reduced flavin, though observation of dissociation of PEDz from the enzyme offers indirect support of that contention. Jones et al. (2019) found evidence of transient oxygen channels which extend from the surface of the globular protein to the

active site, and which become active in response to structural changes to the enzyme brought on by catalytic turnover. These oxygen channels may allow for re-oxidation of FAD without PEDz having to dissociate from the active site, resulting in a pseudo-*in situ* inactivation as described by the forked mechanism (Binda et al., 2008), but it is unknown the extent to which this pathway is utilized. Given the near-stoichiometric generation of PEH from PLZ (Matveychuk, 2015), it appears likely that dissociation is the norm.

Further discussion for the role of oxygen in inactivation of MAO-B by PLZ is presented in Chapter 3. The redox dye DCPIP replaced oxygen in anaerobic conditions, allowing for the re-oxidation of FAD reduced during oxidation of PLZ to PEDz, and resulting in a half-life of inactivation ( $t_{1/2}$ ) of 1.86 minutes, compared to 6.26 minutes in the absence of DCPIP, when oxygen and substrate were introduced into the anaerobic reaction vessel (Figures 3.9c and 3.9d, respectively). However, that inhibition did not occur under anaerobic conditions suggests a further role for oxygen: radicalizing the diazene to prompt interaction between PEDz and oxidized FAD.

Another surprising characteristic of PEDz exemplified in this thesis is the capacity of the diazene to be protected from degradation by removal of  $Fe^{3+}$  from the incubation. As shown in Chapter 4, ascorbate and DTPA are both capable of removing iron from solution, through reduction to  $Fe^{2+}$  or chelation, respectively, which served to drastically reduce  $t_{1/2}$  when included in the incubation of MAO-B and PLZ. This suggests that the redox environment is more important in determining the rate and extent of MAO-B inactivation by PLZ than previously thought.

The release of PEDz from the active site after formation introduces an element of competition not previously addressed; while there is competition in initial binding of PLZ to the active site *in vivo*, competition for re-binding between PEDz, PLZ, and PEH presents new understanding of the use of, and side effects of, PLZ in treating various psychiatric conditions. Use

of PLZ as a prodrug for PEH would therefore benefit from high doses of PLZ, since competition with PLZ would prevent PEDz from accessing and inactivating the oxidized enzyme, resulting in prolonged generation of PEDz, and subsequent PEH formation. However, rare instances of hepatotoxicity (Robinson & Kurtz, 1987) could be linked to the very reactive diazene which has been noted to inhibit cytochrome P450 enzymes (Jaladanki et al., 2017), among other effects (Nelson et al., 1976). Increased concentration of PLZ means increased release of PEDz which may degrade at varying rates, depending on the redox environment (iron and ascorbate concentrations for instance), and which may result in increased interactions with other cellular components.

#### 6.1.2. What We Have Learned About MAO-B

This understanding of the life of PEDz is inconsistent with the popular forked mechanism, which states that PEDz and PEH are both immediate, alternate products of PLZ metabolism by MAO-B, where formation of PEDz leads to *in situ* inactivation of the reduced enzyme while formation and release of PEH is reminiscent of normal substrate oxidation (Binda et al., 2008). Combined, these traits define a drug with a high partition ratio which is mechanism-based in its inhibition (Silverman, 1995b). However, PEDz leaving the active site after formation disqualifies PLZ from being a mechanism-based inhibitor, as inactivation does not usually occur *in situ*. Previous observations from our laboratory that the half-life of inactivation of hMAO-B by PLZ is shorter at higher enzyme concentrations further argue against *in situ* inactivation. Instead, the results from this thesis support the stepwise mechanism.

Another surprising finding from this thesis came from Chapter 5, in which the activity remaining in MAO-B after pre-incubation for a short period of time with high concentrations of PLZ was not proportional to the active sites lost to irreversible inactivation when titrated with mofegiline. This is the first evidence of the subunits of MAO-B responding to inhibition in

different ways from each other, reminiscent of half-sites reactivity as suggested over 25 years ago (Silverman, 1995a). The mechanism by which the homodimer has been proposed to act is through subunit flip-flop, in which only one monomer is active at any time (H. B. L. Jones et al., 2019); the reduction of the flavin of one monomer signals to the other flavin to switch from a partially-reduced (semiquinone) state to an oxidized state in preparation for the next substrate binding event. When only one monomer is active at any time, inhibition of the whole dimer can arise from inactivation of one monomer preventing the signal being transmitted to (or perhaps received by) the second monomer, as seems to be the case with mofegiline inhibition. It appears that the gears which facilitate the flip-flop in monomer activity can become seized following inactivation of one monomer by at least some inhibitors, while PLZ, at millimolar concentrations, acts as a lubricant to overcome the gear seizure to some degree, allowing flip-flop activation of the opposing monomer, albeit with a reduced catalytic efficiency.

## **6.2. Limitations and Future Directions**

### **6.2.1. Chapter 2**

This experiment showed significant results in terms of degree of deuterium incorporation into metabolic PEH, but there are limitations to be addressed. First and foremost was the single-quad mass spectrometer used to acquire the data, which had a mass-to-charge ratio ( $m/z$ ) resolution of 1 unit. Due to the structural similarities between PLZ and PEH (Figure 2.2), they differ in  $m/z$  by barely 2 units ( $m/z = 136.9$  and  $134.8$ , respectively). Given that each instance of HDX within a molecule confers an additional  $m/z$  unit to that molecule, instances of multiply-deuterated PEH (PEH that underwent more than one instance of HDX) would be impossible to distinguish from PLZ or D-PLZ ( $137.9$ ). Analysis by tandem MS, in which fragments from the previous MS

analysis are further fragmented and analyzed by another MS, would result in smaller, more unique fragments of these compounds which may allow for discrimination between PLZ and D,D-PEH (136.9), or D-PLZ and D,D,D-PEH (137.9).

The second limitation was the absence of a quenching step during the preparation of the deuterated samples for analysis. Rapidly decreasing both the temperature and the pH of the samples before analysis lowers the rate at which HDX occurs, minimizing deuteration of the C<sub>18</sub> column during the separation of analytes, as well as back exchange of hydrogens in deuterated PEH (Walters et al., 2012). In not including this step, the column was heavily contaminated by deuterium early on in the study, and non-deuterated controls performed later on in the study produced deuterated signals. It is also possible that early %HDX values were underestimated due to back exchange. While these considerations do not negate the conclusions drawn from this study, they do highlight the need for optimization of the experiment in order to collect consistently reproducible data, both of which were obstacles faced over the course of this study.

### 6.2.2. Chapter 3

Limitations in this study include the assay used to measure remaining MAO-B activity. Because DCPIP has a peak absorbance of 604 nm, the more sensitive Amplex Red/peroxidase assay (571 nm peak) could not be performed. However, there was also spectral overlap between DCPIP and benzaldehyde at 254 nm, such that changes observed at this wavelength were due to a combination of an increase in benzaldehyde production and a decrease in absorbance as DCPIP was reduced, preventing quantitation of the extent of the effect of DCPIP on MAO-B activity. Complicating matters further, DCPIP also interacted with PLZ at 604 nm in a concentration-dependent manner (Figure 3.4), necessitating the study be carried out at lower PLZ concentrations to minimize that effect.

In an effort to address these spectral considerations for absorbance, monitoring of resorufin fluorescence (560/591 nm) rather than absorbance had been explored as a way of measuring remaining activity via the Amplex Red assay. Although this approach encountered challenging technical difficulties early on and was neither pursued nor discussed in this thesis, with some optimization, this could offer a viable way to assess the extent of inhibition. Another potential approach is stopped-flow analysis of the anaerobic reaction between MAO-B and PLZ in the presence of DCPIP. Stopped-flow software is capable of parsing out individual contributions of ligands and proteins to multiple spectra recorded over a period of time, such as the case of the opposite contributions of DCPIP and benzaldehyde to the absorbance at 254 nm, and provides rate constants for these steps. However, preliminary assessments suggested that the high-energy lamp required for measurements in the UV region caused photodegradation of a component of the solvent in which purified MAO-B was eluted and stored, creating large spectral changes that masked any associated with oxidation of PLZ (A. Holt, unpublished observations). Circumventing this issue, although possible, would have been a time-consuming process, and optimization of this technique ultimately was not pursued.

#### 6.2.3. Chapter 4

The primary limitation early on was the interaction between ascorbate and both PLZ and Amplex Red reagent, in the presence and absence of DTPA, resulting in an over-estimation of the remaining activity as measured by the Amplex Red/peroxidase assay. This was circumvented by using preparations of enzyme embedded in outer mitochondrial membrane particles instead of detergent-soluble enzyme preparations, allowing for the removal of unreacted PLZ after pre-incubation via centrifugation, producing cleaner assay results.

In the short term, obtaining a more comprehensive inhibition plot for DTPA would do a lot to help explain or clarify some of the more surprising results from this study. For instance, inclusion of DTPA in pre-incubations of MAO-B and PLZ in the presence of ascorbate resulted in a half-life of inactivation which was double that of reactions which did not include DTPA ( $t_{1/2} = 3.5$  minutes and 1.7 minutes, respectively). This is despite DTPA being a chelator for iron, removing these contaminants from the phosphate buffer as does ascorbate, thereby avoiding the oxidation of ascorbate to its radical form. Therefore, examining the influence of a range of DTPA concentrations on the inhibition of MAO-B by PLZ or by PLZ and ascorbate may help develop a better understanding of ascorbate's role in greatly enhancing inactivation by PLZ, and how that differs from the contribution of DTPA to this effect.

Future directions for this study include measuring remaining MAO-B activity after incubation using radiolabelled benzylamine as substrate. This would eliminate the need to account for spectral interferences, a problem which has arisen in each chapter of this thesis thus far.

#### 6.2.4. Chapter 5

A limitation of this study was again the interaction between PLZ and ascorbate, which prevented analysis of inhibition by very high PLZ concentrations via the more-sensitive Amplex Red/peroxidase assay for remaining enzyme activity. The solution to this was again to centrifuge membrane particles, allowing for the use of much higher PLZ concentrations than have been tested previously.

Future directions include assessing the viability of the hypothesis that MAO-B regulates its activity through cross-talk between its monomers, an idea that was first suggested in 1995 (Silverman, 1995a). Formation of the I<sub>2</sub> site due to movement of some key residues within the entrance channel, including Ile199 (McDonald et al., 2010), may confer a structural change which

alters the binding of substrate or inhibitor in the same or opposite monomer's active site. In fact, recent computer modeling of MAO-B in complex with various ligands suggested the formation of transient oxygen channels from the surface of the protein to the active site upon binding of substrate to the opposing monomer and movement of Ile199 and other side chains (H. B. L. Jones et al., 2019), which may allow oxygen to access the active site and facilitate re-oxidation of the flavin cofactor before product is released from the active site. As well, the study by Jones et al. showed evidence of an asymmetry in substrate access to the active site of MAO-B. Binding of amine substrate to one monomer influences formation of substrate access tunnels within both monomers, such that the likelihood of substrate binding is increased for the unbound monomer and decreased for the bound monomer. In this way, the activity of the dimer is modulated by conformational changes to either monomer.

To date, experimental evidence to support flip-flop behaviour in MAO has not been published, in part because obtaining such direct evidence is technically and conceptually demanding. Future kinetic studies to increase our understanding of the rate and extent of inactivation of MAO by PLZ, mofegiline, and perhaps other inhibitors, and assessments of the stoichiometry of binding of [<sup>3</sup>H]PLZ to MAO-B, may provide indirect confirmation of communication between subunits.

Another future direction for this study is in understanding how PLZ behaves with MAO-A, the MAO isozyme which is more relevant in cancer, neurodegenerative diseases, and psychiatric conditions. The interaction between MAO-A and PLZ may inform on the enzymatic mechanism in a similar way as described here with MAO-B. The existence of an imidazoline binding site has been proposed in MAO-A (Jones et al., 2007), and it is possible that this site may prove important as an allosteric modulatory site of MAO-A activity.

## Bibliography

- Allen, W. J., & Bevan, D. R. (2011). Steered molecular dynamics simulations reveal important mechanisms in reversible monoamine oxidase B inhibition. *Biochemistry*, *50*(29), 6441–6454. <https://doi.org/10.1021/bi200446w>
- Anderson, M. C., Hasan, F., McCrodden, J. M., & Tipton, K. F. (1993). Monoamine oxidase inhibitors and the cheese effect. *Neurochemical Research*, *18*(11), 1145–1149. <https://doi.org/10.1007/BF00978365>
- Bach, A. W., Lan, N. C., Johnson, D. L., Abell, C. W., Bembenek, M. E., Kwan, S. W., Seeburg, P. H., & Shih, J. C. (1988). cDNA cloning of human liver monoamine oxidase A and B: Molecular basis of differences in enzymatic properties. *Proceedings of the National Academy of Sciences*, *85*(13), 4934–4938. <https://doi.org/10.1073/pnas.85.13.4934>
- Bai, Y., Milne, J. S., Mayne, L., & Englander, S. W. (1993). Primary structure effects on peptide group hydrogen exchange. *Proteins: Structure, Function, and Genetics*, *17*(1), 75–86. <https://doi.org/10.1002/prot.340170110>
- Baker, G. B., & Reynolds, G. P. (1989). Biogenic amines and their metabolites in Alzheimer's disease: Noradrenaline, 5-hydroxytryptamine and 5-hydroxyindole-3-acetic acid depleted in hippocampus but not in substantia innominata. *Neuroscience Letters*, *100*(1–3), 335–339. [https://doi.org/10.1016/0304-3940\(89\)90709-X](https://doi.org/10.1016/0304-3940(89)90709-X)
- Baker, G. B., Wong, J. T. F., Yeung, J. M., & Coutts, R. T. (1991). Effects of the antidepressant phenelzine on brain levels of  $\gamma$ -aminobutyric acid (GABA). *Journal of Affective Disorders*, *21*(3), 207–211. [https://doi.org/10.1016/0165-0327\(91\)90041-P](https://doi.org/10.1016/0165-0327(91)90041-P)
- Baker, G., Matveychuk, D., MacKenzie, E. M., Holt, A., Wang, Y., & Kar, S. (2019). Attenuation of the effects of oxidative stress by the MAO-inhibiting antidepressant and carbonyl scavenger phenelzine. *Chemico-Biological Interactions*, *304*, 139–147. <https://doi.org/10.1016/j.cbi.2019.03.003>
- Basile, L., Pappalardo, M., Guccione, S., Milardi, D., & Ramsay, R. R. (2014). Computational comparison of imidazoline association with the I<sub>2</sub> binding site in human monoamine oxidases. *Journal of Chemical Information and Modeling*, *54*(4), 1200–1207. <https://doi.org/10.1021/ci400346k>
- Battioni, P., Mahy, J.-P., Delaforge, M., & Mansuy, D. (1983). Reaction of monosubstituted hydrazines and diazenes with rat-liver cytochrome P450. Formation of ferrous-diazene and ferric sigma-alkyl complexes. *European Journal of Biochemistry*, *134*(2), 241–248. <https://doi.org/10.1111/j.1432-1033.1983.tb07557.x>
- Benson, C. A., Wong, G., Tenorio, G., Baker, G. B., & Kerr, B. J. (2013). The MAO inhibitor phenelzine can improve functional outcomes in mice with established clinical signs in experimental autoimmune encephalomyelitis (EAE). *Behavioural Brain Research*, *252*, 302–311. <https://doi.org/10.1016/j.bbr.2013.06.019>
- Bevc, S., Konc, J., Stojan, J., Hodošček, M., Penca, M., Praprotnik, M., & Janežič, D. (2011). ENZO: A web tool for derivation and evaluation of kinetic models of enzyme catalyzed reactions. *PLoS ONE*, *6*(7), e22265. <https://doi.org/10.1371/journal.pone.0022265>

- Binda, C., Hubálek, F., Li, M., Edmondson, D. E., & Mattevi, A. (2004). Crystal structure of human monoamine oxidase B, a drug target enzyme monotonically inserted into the mitochondrial outer membrane. *FEBS Letters*, *564*(3), 225–228. [https://doi.org/10.1016/S0014-5793\(04\)00209-1](https://doi.org/10.1016/S0014-5793(04)00209-1)
- Binda, C., Li, M., Hubalek, F., Restelli, N., Edmondson, D. E., & Mattevi, A. (2003). Insights into the mode of inhibition of human mitochondrial monoamine oxidase B from high-resolution crystal structures. *Proceedings of the National Academy of Sciences*, *100*(17), 9750–9755. <https://doi.org/10.1073/pnas.1633804100>
- Binda, C., Newton-Vinson, P., Hubálek, F., Edmondson, D. E., & Mattevi, A. (2002). Structure of human monoamine oxidase B, a drug target for the treatment of neurological disorders. *Nature Structural Biology*, *9*(1), 22–26. <https://doi.org/10.1038/nsb732>
- Binda, C., Wang, J., Li, M., Hubalek, F., Mattevi, A., & Edmondson, D. E. (2008). Structural and mechanistic studies of arylalkylhydrazine inhibition of human monoamine oxidases A and B. *Biochemistry*, *47*(20), 5616–5625. <https://doi.org/10.1021/bi8002814>
- Bodkin, J. A., & Amsterdam, J. D. (2002). Transdermal selegiline in major depression: A double-blind, placebo-controlled, parallel-group study in outpatients. *American Journal of Psychiatry*, *159*(11), 1869–1875. <https://doi.org/10.1176/appi.ajp.159.11.1869>
- Bonivento, D., Milczek, E. M., McDonald, G. R., Binda, C., Holt, A., Edmondson, D. E., & Mattevi, A. (2010). Potentiation of ligand binding through cooperative effects in monoamine oxidase B. *Journal of Biological Chemistry*, *285*(47), 36849–36856. <https://doi.org/10.1074/jbc.M110.169482>
- Brugger, D., Krondorfer, I., Zahma, K., Stoisser, T., Bolivar, J. M., Nidetzky, B., Peterbauer, C. K., & Haltrich, D. (2014). Convenient microtiter plate-based, oxygen-independent activity assays for flavin-dependent oxidoreductases based on different redox dyes. *Biotechnology Journal*, *9*(4), 474–482. <https://doi.org/10.1002/biot.201300336>
- Buckley, N. A., Dawson, A. H., & Isbister, G. K. (2014). Serotonin syndrome. *BMJ*, *348*(feb19 6), g1626–g1626. <https://doi.org/10.1136/bmj.g1626>
- Buettner, G. R. (1988). In the absence of catalytic metals ascorbate does not autoxidize at pH 7: Ascorbate as a test for catalytic metals. *Journal of Biochemical and Biophysical Methods*, *16*(1), 27–40. [https://doi.org/10.1016/0165-022X\(88\)90100-5](https://doi.org/10.1016/0165-022X(88)90100-5)
- Buettner, G. R. (1990). Ascorbate oxidation: UV absorbance of ascorbate and ESR spectroscopy of the ascorbyl radical as assays for iron. *Free Radical Research Communications*, *10*(1–2), 5–9. <https://doi.org/10.3109/10715769009145927>
- Buettner, G. R., & Czapski, Prof. G. (1986). Ascorbate autoxidation in the presence of iron and copper chelates. *Free Radical Research Communications*, *1*(6), 349–353. <https://doi.org/10.3109/10715768609051638>
- Bullock, D. H., & Irvine, O. R. (1956). A chromatographic study of cheddar cheese ripening. *Journal of Dairy Science*, *39*(9), 1229–1235. [https://doi.org/10.3168/jds.S0022-0302\(56\)94840-8](https://doi.org/10.3168/jds.S0022-0302(56)94840-8)
- Burke, W. (2004). Neurotoxicity of MAO metabolites of catecholamine neurotransmitters: Role in neurodegenerative diseases. *NeuroToxicology*, *25*(1–2), 101–115.

[https://doi.org/10.1016/S0161-813X\(03\)00090-1](https://doi.org/10.1016/S0161-813X(03)00090-1)

- Burke, W. J., Li, S. W., Williams, E. A., Nonneman, R., & Zahm, D. S. (2003). 3,4-Dihydroxyphenylacetaldehyde is the toxic dopamine metabolite in vivo: Implications for Parkinson's disease pathogenesis. *Brain Research*, 989(2), 205–213. [https://doi.org/10.1016/S0006-8993\(03\)03354-7](https://doi.org/10.1016/S0006-8993(03)03354-7)
- Chen, K., Maley, J., & Yu, P. H. (2006). Potential implications of endogenous aldehydes in  $\beta$ -amyloid misfolding, oligomerization and fibrillogenesis. *Journal of Neurochemistry*, 99(5), 1413–1424. <https://doi.org/10.1111/j.1471-4159.2006.04181.x>
- Clineschmidt, B. V., & Horita, A. (1969). The monoamine oxidase catalyzed degradation of phenelzine-1-<sup>14</sup>C, an irreversible inhibitor of monoamine oxidase—I. *Biochemical Pharmacology*, 18(5), 1011–1020. [https://doi.org/10.1016/0006-2952\(69\)90104-X](https://doi.org/10.1016/0006-2952(69)90104-X)
- Cruz, F., & Edmondson, D. E. (2007). Kinetic properties of recombinant MAO-A on incorporation into phospholipid nanodisks. *Journal of Neural Transmission*, 114(6), 699–702. <https://doi.org/10.1007/s00702-007-0673-0>
- Curado-Carballada, C., Feixas, F., Iglesias-Fernández, J., & Osuna, S. (2019). Hidden conformations in *Aspergillus niger* monoamine oxidase are key for catalytic efficiency. *Angewandte Chemie International Edition*, 58(10), 3097–3101. <https://doi.org/10.1002/anie.201812532>
- De Colibus, L., Li, M., Binda, C., Lustig, A., Edmondson, D. E., & Mattevi, A. (2005). Three-dimensional structure of human monoamine oxidase A (MAO A): Relation to the structures of rat MAO A and human MAO B. *Proceedings of the National Academy of Sciences*, 102(36), 12684–12689. <https://doi.org/10.1073/pnas.0505975102>
- Dostert, P. L., Benedetti, M. S., & Tipton, K. F. (1989). Interactions of monoamine oxidase with substrates and inhibitors. *Medicinal Research Reviews*, 9(1), 45–89. <https://doi.org/10.1002/med.2610090104>
- Ebadi, M., Sharma, S., Shavali, S., & El Refaey, H. (2002). Neuroprotective actions of selegiline. *Journal of Neuroscience Research*, 67(3), 285–289. <https://doi.org/10.1002/jnr.10148>
- Edmondson, D. E., Binda, C., Wang, J., Upadhyay, A. K., & Mattevi, A. (2009). Molecular and mechanistic properties of the membrane-bound mitochondrial monoamine oxidases. *Biochemistry*, 48(20), 4220–4230. <https://doi.org/10.1021/bi900413g>
- Fabbri, M., Rosa, M. M., Abreu, D., & Ferreira, J. J. (2015). Clinical pharmacology review of safinamide for the treatment of Parkinson's disease. *Neurodegenerative Disease Management*, 5(6), 481–496. <https://doi.org/10.2217/nmt.15.46>
- Fiedorowicz, J. G., & Swartz, K. L. (2004). The role of monoamine oxidase inhibitors in current psychiatric practice. *Journal of Psychiatric Practice*, 10(4), 239–248. <https://doi.org/10.1097/00131746-200407000-00005>
- Fielden, E. M., Roberts, P. B., Bray, R. C., Lowe, D. J., Mautner, G. N., Rotilio, G., & Calabrese, L. (1974). The mechanism of action of superoxide dismutase from pulse radiolysis and electron paramagnetic resonance. Evidence that only half the active sites function in catalysis. *Biochemical Journal*, 139(1), 49–60. <https://doi.org/10.1042/bj1390049>

- Figuerola-Méndez, R., & Rivas-Arancibia, S. (2015). Vitamin C in health and disease: Its role in the metabolism of cells and redox state in the brain. *Frontiers in Physiology*, *6*. <https://doi.org/10.3389/fphys.2015.00397>
- Fitzpatrick, P. F. (2010). Oxidation of amines by flavoproteins. *Archives of Biochemistry and Biophysics*, *493*(1), 13–25. <https://doi.org/10.1016/j.abb.2009.07.019>
- Fowler, C. J., Callingham, B. A., Mantle, T. J., & Tipton, K. F. (1978). Monoamine oxidase A and B: A useful concept? *Biochemical Pharmacology*, *27*(1), 97–101. [https://doi.org/10.1016/0006-2952\(78\)90262-9](https://doi.org/10.1016/0006-2952(78)90262-9)
- Fowler, J. (2002). Monoamine oxidase: Radiotracer development and human studies. *Methods*, *27*(3), 263–277. [https://doi.org/10.1016/S1046-2023\(02\)00083-X](https://doi.org/10.1016/S1046-2023(02)00083-X)
- Fowler, J. S., Volkow, N. D., Logan, J., Wang, G. J., MacGregor, R. R., Schyler, D., Wolf, A. P., Pappas, N., Alexoff, D., & Shea, C. (1994). Slow recovery of human brain MAO B after L-deprenyl (Selegeline) withdrawal. *Synapse (New York, N.Y.)*, *18*(2), 86–93. <https://doi.org/10.1002/syn.890180203>
- Fowler, J. S., Volkow, N. D., Wang, G.-J., Logan, J., Pappas, N., Shea, C., & MacGregor, R. (1997). Age-related increases in brain monoamine oxidase B in living healthy human subjects. *Neurobiology of Aging*, *18*(4), 431–435. [https://doi.org/10.1016/S0197-4580\(97\)00037-7](https://doi.org/10.1016/S0197-4580(97)00037-7)
- Frébort, I., Toyama, H., Matsushita, K., & Adachi, O. (1995). Half-site reactivity with p-nitrophenylhydrazine and subunit separation of the dimeric copper-containing amine oxidase from *Aspergillus niger*. *Biochemistry and Molecular Biology International*, *36*(6), 1207–1216.
- Galzigna, L., Maina, G., & Rumney, G. (1971). Role of L-ascorbic acid in the reversal of the monoamine oxidase inhibition by caffeine. *Journal of Pharmacy and Pharmacology*, *23*(4), 303–305. <https://doi.org/10.1111/j.2042-7158.1971.tb08664.x>
- Geha, R. M., Chen, K., Wouters, J., Ooms, F., & Shih, J. C. (2002). Analysis of conserved active site residues in monoamine oxidase A and B and their three-dimensional molecular modeling. *Journal of Biological Chemistry*, *277*(19), 17209–17216. <https://doi.org/10.1074/jbc.M110920200>
- Gillman, P. K. (2011). Advances pertaining to the pharmacology and interactions of irreversible nonselective monoamine oxidase inhibitors. *Journal of Clinical Psychopharmacology*, *31*(1), 66–74. <https://doi.org/10.1097/JCP.0b013e31820469ea>
- Gillman, P. K. (2018). A reassessment of the safety profile of monoamine oxidase inhibitors: Elucidating tired old tyramine myths. *Journal of Neural Transmission*, *125*(11), 1707–1717. <https://doi.org/10.1007/s00702-018-1932-y>
- Gillman, P. K., Feinberg, S. S., & Fochtmann, L. J. (2020). Revitalizing monoamine oxidase inhibitors: A call for action. *CNS Spectrums*, *25*(4), 452–454. <https://doi.org/10.1017/S1092852919001196>
- Glasoe, P. K., & Long, F. A. (1960). Use of glass electrodes to measure acidities in deuterium oxide. *The Journal of Physical Chemistry*, *64*(1), 188–190. <https://doi.org/10.1021/j100830a521>

- Goren, T., Adar, L., Sasson, N., & Weiss, Y. M. (2010). Clinical pharmacology tyramine challenge study to determine the selectivity of the monoamine oxidase type B (MAO-B) inhibitor rasagiline. *The Journal of Clinical Pharmacology*, *50*(12), 1420–1428. <https://doi.org/10.1177/0091270010369674>
- Grady, M. M., & Stahl, S. M. (2012). Practical guide for prescribing MAOIs: Debunking myths and removing barriers. *CNS Spectrums*, *17*(1), 2–10. <https://doi.org/10.1017/S109285291200003X>
- Grimsby, J., Chen, K., Wang, L. J., Lan, N. C., & Shih, J. C. (1991). Human monoamine oxidase A and B genes exhibit identical exon-intron organization. *Proceedings of the National Academy of Sciences*, *88*(9), 3637–3641. <https://doi.org/10.1073/pnas.88.9.3637>
- Halliwell, B. (1978). Superoxide-dependent formation of hydroxyl radicals in the presence of iron chelates: Is it a mechanism for hydroxyl radical production in biochemical systems? *FEBS Letters*, *92*(2), 321–326. [https://doi.org/10.1016/0014-5793\(78\)80779-0](https://doi.org/10.1016/0014-5793(78)80779-0)
- Hare, M. L. C. (1928). Tyramine oxidase. *Biochemical Journal*, *22*(4), 968–979. <https://doi.org/10.1042/bj0220968>
- Hill, R. L., Singh, I. N., Wang, J. A., & Hall, E. D. (2017). Time courses of post-injury mitochondrial oxidative damage and respiratory dysfunction and neuronal cytoskeletal degradation in a rat model of focal traumatic brain injury. *Neurochemistry International*, *111*, 45–56. <https://doi.org/10.1016/j.neuint.2017.03.015>
- Holt, A. (2018). On the practical aspects of characterising monoamine oxidase inhibition in vitro. *Journal of Neural Transmission*, *125*(11), 1685–1705. <https://doi.org/10.1007/s00702-018-1943-8>
- Holt, A., Alton, G., Scaman, C. H., Loppnow, G. R., Szpacenko, A., Svendsen, I., & Palcic, M. M. (1998). Identification of the quinone cofactor in mammalian semicarbazide-sensitive amine oxidase. *Biochemistry*, *37*(14), 4946–4957. <https://doi.org/10.1021/bi9729231>
- Huang, R. Y.-C., & Chen, G. (2014). Higher order structure characterization of protein therapeutics by hydrogen/deuterium exchange mass spectrometry. *Analytical and Bioanalytical Chemistry*, *406*(26), 6541–6558. <https://doi.org/10.1007/s00216-014-7924-3>
- Jaladanki, C. K., Shaikh, A., & Bharatam, P. V. (2017). Biotransformation of isoniazid by cytochromes P450: Analyzing the molecular mechanism using density functional theory. *Chemical Research in Toxicology*, *30*(11), 2060–2073. <https://doi.org/10.1021/acs.chemrestox.7b00129>
- Janes, S. M., Mu, D., Wemmer, D., Smith, A. J., Kaur, S., Maltby, D., Burlingame, A. L., & Klinman, J. P. (1990). A new redox cofactor in eukaryotic enzymes: 6-Hydroxydopa at the active site of bovine serum amine oxidase. *Science*, *248*(4958), 981–987. <https://doi.org/10.1126/science.2111581>
- Johnston, J. P. (1968). Some observations upon a new inhibitor of monoamine oxidase in brain tissue. *Biochemical Pharmacology*, *17*(7), 1285–1297. [https://doi.org/10.1016/0006-2952\(68\)90066-X](https://doi.org/10.1016/0006-2952(68)90066-X)

- Jones, H. B. L., Crean, R. M., Mullen, A., Kendrick, E. G., Bull, S. D., Wells, S. A., Carbery, D. R., MacMillan, F., van der Kamp, M. W., & Pudney, C. R. (2019). Exposing the interplay between enzyme turnover, protein dynamics, and the membrane environment in monoamine oxidase B. *Biochemistry*, 58(18), 2362–2372. <https://doi.org/10.1021/acs.biochem.9b00213>
- Jones, T. Z. E., Giurato, L., Guccione, S., & Ramsay, R. R. (2007). Interactions of imidazoline ligands with the active site of purified monoamine oxidase A: Imidazoline binding in the MAO-A active site. *FEBS Journal*, 274(6), 1567–1575. <https://doi.org/10.1111/j.1742-4658.2007.05704.x>
- Karayannis, M. I., Samios, D. N., & Gousetis, C. P. (1977). A study of the molar absorptivity of ascorbic acid at different wavelengths and pH values. *Analytica Chimica Acta*, 93(1), 275–279. [https://doi.org/10.1016/0003-2670\(77\)80032-9](https://doi.org/10.1016/0003-2670(77)80032-9)
- Kline, N. S. (1958). Clinical experience with iproniazid (Marsilid). *Journal of Clinical and Experimental Psychopathology*, 19(2, Suppl. 1), 72–78; discussion 78-79.
- Klinman, J. P. (1996). Mechanisms whereby mononuclear copper proteins functionalize organic substrates. *Chemical Reviews*, 96(7), 2541–2562. <https://doi.org/10.1021/cr950047g>
- Knoll, J., & Magyar, K. (1972). Some puzzling pharmacological effects of monoamine oxidase inhibitors. *Advances in Biochemical Psychopharmacology*, 5, 393–408.
- Latorre-Moratalla, M. L., Bover-Cid, S., Veciana-Nogués, M. T., & Vidal-Carou, M. C. (2012). Control of biogenic amines in fermented sausages: Role of starter cultures. *Frontiers in Microbiology*, 3. <https://doi.org/10.3389/fmicb.2012.00169>
- Leung, G., Sun, W., Zheng, L., Brookes, S., Tully, M., & Shi, R. (2011). Anti-acrolein treatment improves behavioral outcome and alleviates myelin damage in experimental autoimmune encephalomyelitis mouse. *Neuroscience*, 173, 150–155. <https://doi.org/10.1016/j.neuroscience.2010.11.018>
- Li, M., Binda, C., Mattevi, A., & Edmondson, D. E. (2006). Functional role of the “aromatic cage” in human monoamine oxidase B: Structures and catalytic properties of Tyr435 mutant proteins. *Biochemistry*, 45(15), 4775–4784. <https://doi.org/10.1021/bi051847g>
- Lyles, G. A. (1996). Mammalian plasma and tissue-bound semicarbazide-sensitive amine oxidases: Biochemical, pharmacological and toxicological aspects. *The International Journal of Biochemistry & Cell Biology*, 28(3), 259–274. [https://doi.org/10.1016/1357-2725\(95\)00130-1](https://doi.org/10.1016/1357-2725(95)00130-1)
- Lyles, G. A., & Callingham, B. A. (1982). In vitro and in vivo inhibition by benserazide of clorgyline-resistant amine oxidases in rat cardiovascular tissues. *Biochemical Pharmacology*, 31(7), 1417–1424. [https://doi.org/10.1016/0006-2952\(82\)90037-5](https://doi.org/10.1016/0006-2952(82)90037-5)
- Lyles, G. A., & Chalmers, J. (1992). The metabolism of aminoacetone to methylglyoxal by semicarbazide-sensitive amine oxidase in human umbilical artery. *Biochemical Pharmacology*, 43(7), 1409–1414. [https://doi.org/10.1016/0006-2952\(92\)90196-P](https://doi.org/10.1016/0006-2952(92)90196-P)
- MacKenzie, E. M. (2009). Neurochemical and neuroprotective aspects of phenelzine and its active metabolite  $\beta$ -phenylethylidenehydrazine. *PhD Thesis, University of Alberta*. <https://doi.org/10.7939/R35W24>

- MacKenzie, E. M., Fassihi, A., Davood, A., Chen, Q.-H., Rauw, G., Rauw, G., Knaus, E. E., & Baker, G. B. (2008). N-Propynyl analogs of  $\beta$ -phenylethylidenehydrazines: Synthesis and evaluation of effects on glycine, GABA, and monoamine oxidase. *Bioorganic & Medicinal Chemistry*, 16(17), 8254–8263. <https://doi.org/10.1016/j.bmc.2008.07.027>
- MacKenzie, E. M., Grant, S. L., Baker, G. B., & Wood, P. L. (2008). Phenzelzine causes an increase in brain ornithine that is prevented by prior monoamine oxidase inhibition. *Neurochemical Research*, 33(3), 430–436. <https://doi.org/10.1007/s11064-007-9448-0>
- Mahy, J.-P., Gaspard, S., Delaforge, M., & Mansuy, D. (1994). Reactions of prostaglandin H synthase with monosubstituted hydrazines and diazenes. Formation of iron(II)-diazene and iron(III)-sigma-alkyl or iron(III)-sigma-aryl complexes. *European Journal of Biochemistry*, 226(2), 445–457. <https://doi.org/10.1111/j.1432-1033.1994.tb20069.x>
- Mann, J. J. (1989). A controlled study of the antidepressant efficacy and side effects of (-)-deprenyl: A selective monoamine oxidase inhibitor. *Archives of General Psychiatry*, 46(1), 45. <https://doi.org/10.1001/archpsyc.1989.01810010047007>
- Matveychuk, D. (2015). Novel properties of the multifaceted drug phenzelzine and its metabolite  $\beta$ -phenylethylidenehydrazine. *PhD Thesis, University of Alberta*. <https://doi.org/10.7939/R3FT8DQ4H>
- Matveychuk, D., MacKenzie, E. M., Kumpula, D., Song, M.-S., Holt, A., Kar, S., Todd, K. G., Wood, P. L., & Baker, G. B. (2021). Overview of the neuroprotective effects of the MAO-inhibiting antidepressant phenzelzine. *Cellular and Molecular Neurobiology*. <https://doi.org/10.1007/s10571-021-01078-3>
- McDonald, G. R., Hudson, A. L., Dunn, S. M. J., You, H., Baker, G. B., Whittal, R. M., Martin, J. W., Jha, A., Edmondson, D. E., & Holt, A. (2008). Bioactive contaminants leach from disposable laboratory plasticware. *Science (New York, N.Y.)*, 322(5903), 917. <https://doi.org/10.1126/science.1162395>
- McDonald, G. R., Olivieri, A., Ramsay, R. R., & Holt, A. (2010). On the formation and nature of the imidazoline I<sub>2</sub> binding site on human monoamine oxidase-B. *Pharmacological Research*, 62(6), 475–488. <https://doi.org/10.1016/j.phrs.2010.09.001>
- Meyer, J. H., Matveychuk, D., Holt, A., Santhirakumar, A., & Baker, G. B. (2021). Monoamine oxidase inhibitors in depressive disorders. In P. Riederer, G. Laux, T. Nagatsu, W. Le, & C. Riederer (Eds.), *NeuroPsychopharmacotherapy* (pp. 1–33). Springer International Publishing. [https://doi.org/10.1007/978-3-319-56015-1\\_98-1](https://doi.org/10.1007/978-3-319-56015-1_98-1)
- Meyer, J. M. (2017). A concise guide to monoamine oxidase inhibitors: A better understanding of the risks can lead to increased use of these highly effective agents. *Current Psychiatry*, 16(12), 14+. Gale Academic OneFile.
- Milczek, E. M., Binda, C., Roviada, S., Mattevi, A., & Edmondson, D. E. (2011). The ‘gating’ residues Ile199 and Tyr326 in human monoamine oxidase B function in substrate and inhibitor recognition: Gating residue function in human MAO B. *FEBS Journal*, 278(24), 4860–4869. <https://doi.org/10.1111/j.1742-4658.2011.08386.x>

- Milczek, E. M., Bonivento, D., Binda, C., Mattevi, A., McDonald, I. A., & Edmondson, D. E. (2008). Structural and mechanistic studies of mofegiline inhibition of recombinant human monoamine oxidase B. *Journal of Medicinal Chemistry*, *51*(24), 8019–8026. <https://doi.org/10.1021/jm8011867>
- Moenne-Loccoz, P., Nakamura, N., Steinebach, V., Duine, J. A., Mure, M., Klinman, J. P., & Sanders-Loehr, J. (1995). Characterization of the topa quinone cofactor in amine oxidase from *Escherichia coli* by resonance Raman spectroscopy. *Biochemistry*, *34*(21), 7020–7026. <https://doi.org/10.1021/bi00021a013>
- Musgrave, T., Benson, C., Wong, G., Browne, I., Tenorio, G., Rauw, G., Baker, G. B., & Kerr, B. J. (2011). The MAO inhibitor phenelzine improves functional outcomes in mice with experimental autoimmune encephalomyelitis (EAE). *Brain, Behavior, and Immunity*, *25*(8), 1677–1688. <https://doi.org/10.1016/j.bbi.2011.06.011>
- Nagy, J., Kenney, W. C., & Singer, T. P. (1979). The reaction of phenylhydrazine with trimethylamine dehydrogenase and with free flavins. *The Journal of Biological Chemistry*, *254*(8), 2684–2688.
- Nair, N. P., Ahmed, S. K., & Kin, N. M. (1993). Biochemistry and pharmacology of reversible inhibitors of MAO-A agents: Focus on moclobemide. *Journal of Psychiatry & Neuroscience: JPN*, *18*(5), 214–225.
- Nelson, S. D., Mitchell, J. R., Timbrell, J. A., Snodgrass, W. R., & Corcoran, G. B. (1976). Isoniazid and iproniazid: Activation of metabolites to toxic intermediates in man and rat. *Science*, *193*(4256), 901–903. <https://doi.org/10.1126/science.7838>
- Nelson, T. J., & Boor, P. J. (1982). Allylamine cardiotoxicity—IV. *Biochemical Pharmacology*, *31*(4), 509–514. [https://doi.org/10.1016/0006-2952\(82\)90152-6](https://doi.org/10.1016/0006-2952(82)90152-6)
- Panneton, W. M., Kumar, V. B., Gan, Q., Burke, W. J., & Galvin, J. E. (2010). The neurotoxicity of DOPAL: Behavioral and stereological evidence for its role in Parkinson disease pathogenesis. *PLoS ONE*, *5*(12), e15251. <https://doi.org/10.1371/journal.pone.0015251>
- Paslawski, T., Knaus, E., Iqbal, N., Coutts, R. T., & Baker, G. B. (2001).  $\beta$ -Phenylethylidenehydrazine, a novel inhibitor of GABA transaminase. *Drug Development Research*, *54*(1), 35–39. <https://doi.org/10.1002/ddr.1202>
- Paslawski, T., Treit, D., Baker, G. B., George, M., & Coutts, R. T. (1996). The antidepressant drug phenelzine produces antianxiety effects in the plus-maze and increases in rat brain GABA. *Psychopharmacology*, *127*(1–2), 19–24. <https://doi.org/10.1007/BF02805970>
- Patek, D. R., & Hellerman, L. (1974). Mitochondrial monoamine oxidase. Mechanism of inhibition by phenylhydrazine and by aralkylhydrazines. Role of enzymatic oxidation. *The Journal of Biological Chemistry*, *249*(8), 2373–2380.
- Pizzinat, N., Copin, N., Vindis, C., Parini, A., & Cambon, C. (1999). Reactive oxygen species production by monoamine oxidases in intact cells. *Naunyn-Schmiedeberg's Archives of Pharmacology*, *359*(5), 428–431. <https://doi.org/10.1007/PL00005371>
- Popov, N., & Matthies, H. (1969). Some effects of monoamine oxidase inhibitors on the metabolism of gamma-aminobutyric acid in rat brain. *Journal of Neurochemistry*, *16*(6), 899–907. <https://doi.org/10.1111/j.1471-4159.1969.tb08978.x>

- Precious, E., & Lyles, G. A. (1988). Properties of a semicarbazide-sensitive amine oxidase in human umbilical artery. *Journal of Pharmacy and Pharmacology*, 40(9), 627–633. <https://doi.org/10.1111/j.2042-7158.1988.tb05322.x>
- Pross, A., & Sternhell, S. (1970). Oxidation of hydrazones with iodine in the presence of base. *Australian Journal of Chemistry*, 23(5), 989. <https://doi.org/10.1071/CH9700989>
- Raddatz, R., Parini, A., & Lanier, S. M. (1995). Imidazoline/guanidinium binding domains on monoamine oxidases. *Journal of Biological Chemistry*, 270(46), 27961–27968. <https://doi.org/10.1074/jbc.270.46.27961>
- Raddatz, R., Parini, A., & Lanier, S. M. (1997). Localization of the imidazoline binding domain on monoamine oxidase B. *Molecular Pharmacology*, 52(4), 549–553. <https://doi.org/10.1124/mol.52.4.549>
- Ramsay, R. R. (1991). Kinetic mechanism of monoamine oxidase A. *Biochemistry*, 30(18), 4624–4629. <https://doi.org/10.1021/bi00232a038>
- Ramsay, R. R., Basile, L., Maniquet, A., Hagenow, S., Pappalardo, M., Saija, M. C., Bryant, S. D., Albrecht, A., & Guccione, S. (2020). Parameters for irreversible inactivation of monoamine oxidase. *Molecules*, 25(24), 5908. <https://doi.org/10.3390/molecules25245908>
- Ramsay, R. R., Koerber, S. C., & Singer, T. P. (1987). Stopped-flow studies on the mechanism of oxidation of N-methyl-4-phenyltetrahydropyridine by bovine liver monoamine oxidase B. *Biochemistry*, 26(11), 3045–3050. <https://doi.org/10.1021/bi00385a015>
- Ramsay, R. R., Olivieri, A., & Holt, A. (2011). An improved approach to steady-state analysis of monoamine oxidases. *Journal of Neural Transmission*, 118(7), 1003–1019. <https://doi.org/10.1007/s00702-011-0657-y>
- Renouard, A., Widdowson, P. S., & Cordi, A. (1993). [<sup>3</sup>H]-idazoxan binding to rabbit cerebral cortex recognises multiple imidazoline I<sub>2</sub>-type receptors: Pharmacological characterization and relationship to monoamine oxidase. *British Journal of Pharmacology*, 109(3), 625–631. <https://doi.org/10.1111/j.1476-5381.1993.tb13618.x>
- Ricken, R., Ulrich, S., Schlattmann, P., & Adli, M. (2017). Tranylecypromine in mind (Part II): Review of clinical pharmacology and meta-analysis of controlled studies in depression. *European Neuropsychopharmacology*, 27(8), 714–731. <https://doi.org/10.1016/j.euroneuro.2017.04.003>
- Riederer, P., Danielczyk, Walter, & Grunblatt, Edna. (2004). Monoamine oxidase-B inhibition in Alzheimer's disease. *NeuroToxicology*, 25(1–2), 271–277. [https://doi.org/10.1016/S0161-813X\(03\)00106-2](https://doi.org/10.1016/S0161-813X(03)00106-2)
- Riederer, P., Konradi, C., Schay, V., Kienzl, E., Birkmayer, G., Danielczyk, W., Sofic, E., & Youdim, M. B. (1987). Localization of MAO-A and MAO-B in human brain: A step in understanding the therapeutic action of L-deprenyl. *Advances in Neurology*, 45, 111–118.
- Robinson, D. S., & Kurtz, N. M. (1987). What is the degree of risk of hepatotoxicity for depressed patients receiving phenelzine therapy? Is the risk sufficient to require that we modify the written advice (as to diet and risks) that we regularly give our patients before we institute this therapy?: *Journal of Clinical Psychopharmacology*, 7(1), 61. <https://doi.org/10.1097/00004714-198702000-00034>

- Rojas, R. J., Edmondson, D. E., Almos, T., Scott, R., & Massari, M. E. (2015). Reversible and irreversible small molecule inhibitors of monoamine oxidase B (MAO-B) investigated by biophysical techniques. *Bioorganic & Medicinal Chemistry*, 23(4), 770–778. <https://doi.org/10.1016/j.bmc.2014.12.063>
- Sankar, M., Nowicka, E., Carter, E., Murphy, D. M., Knight, D. W., Bethell, D., & Hutchings, G. J. (2014). The benzaldehyde oxidation paradox explained by the interception of peroxy radical by benzyl alcohol. *Nature Communications*, 5, 3332. <https://doi.org/10.1038/ncomms4332>
- Sheehan, D. V. (1980). Treatment of endogenous anxiety with phobic, hysterical, and hypochondriacal symptoms. *Archives of General Psychiatry*, 37(1), 51. <https://doi.org/10.1001/archpsyc.1980.01780140053006>
- Shen, J., Griffiths, P. T., Campbell, S. J., Utinger, B., Kalberer, M., & Paulson, S. E. (2021). Ascorbate oxidation by iron, copper and reactive oxygen species: Review, model development, and derivation of key rate constants. *Scientific Reports*, 11(1), 7417. <https://doi.org/10.1038/s41598-021-86477-8>
- Sherif, F., Gottfries, C. G., Alafuzoff, I., & Oreland, L. (1992). Brain gamma-aminobutyrate aminotransferase (GABA-T) and monoamine oxidase (MAO) in patients with Alzheimer's disease. *Journal of Neural Transmission - Parkinson's Disease and Dementia Section*, 4(3), 227–240. <https://doi.org/10.1007/BF02260906>
- Silverman, R. B. (1995a). Chapter 2 Radical thoughts about the life of MAO. In *Progress in Brain Research* (Vol. 106, pp. 23–31). Elsevier. [https://doi.org/10.1016/S0079-6123\(08\)61198-X](https://doi.org/10.1016/S0079-6123(08)61198-X)
- Silverman, R. B. (1995b). Mechanism-based enzyme inactivators. *Methods in Enzymology*, 249, 240–283. [https://doi.org/10.1016/0076-6879\(95\)49038-8](https://doi.org/10.1016/0076-6879(95)49038-8)
- Singh, I. N., Gilmer, L. K., Miller, D. M., Cebak, J. E., Wang, J. A., & Hall, E. D. (2013). Phenelzine mitochondrial functional preservation and neuroprotection after traumatic brain injury related to scavenging of the lipid peroxidation-derived aldehyde 4-hydroxy-2-nonenal. *Journal of Cerebral Blood Flow & Metabolism*, 33(4), 593–599. <https://doi.org/10.1038/jcbfm.2012.211>
- Sparks, D. L., Woeltz, V. M., & Markesbery, W. R. (1991). Alterations in brain monoamine oxidase activity in aging, Alzheimer's disease, and Pick's disease. *Archives of Neurology*, 48(7), 718–721. <https://doi.org/10.1001/archneur.1991.00530190064017>
- Stein, D. J., Cameron, A., Amrein, R., & Montgomery, S. A. (2002). Moclobemide is effective and well tolerated in the long-term pharmacotherapy of social anxiety disorder with or without comorbid anxiety disorder: *International Clinical Psychopharmacology*, 17(4), 161–170. <https://doi.org/10.1097/00004850-200207000-00002>
- Steinebach, V., Groen, B. W., Wijmenga, S. S., Niessen, W. M. A., Jongejan, J. A., & Duine, J. A. (1995). Identification of topaquinone, as illustrated for pig kidney diamine oxidase and *Escherichia coli* amine oxidase. *Analytical Biochemistry*, 230(1), 159–166. <https://doi.org/10.1006/abio.1995.1451>

- Suva, R. H., & Abeles, R. H. (1978). Studies on the mechanism of action of plasma amine oxidase. *Biochemistry*, *17*(17), 3538–3545. <https://doi.org/10.1021/bi00610a018>
- Tan, A. K., & Ramsay, R. R. (1993). Substrate-specific enhancement of the oxidative half-reaction of monoamine oxidase. *Biochemistry*, *32*(9), 2137–2143. <https://doi.org/10.1021/bi00060a003>
- Tipton, K. F., Boyce, S., O’Sullivan, J., Davey, G. P., & Healy, J. (2004). Monoamine oxidases: Certainties and uncertainties. *Current Medicinal Chemistry*, *11*(15), 1965–1982. <https://doi.org/10.2174/0929867043364810>
- Tipton, K. F., & Spires, I. P. C. (1971). The kinetics of phenethylhydrazine oxidation by monoamine oxidase. *Biochemical Journal*, *125*(2), 521–524. <https://doi.org/10.1042/bj1250521>
- Todd, K. G., & Baker, G. B. (1995). GABA-elevating effects of the antidepressant/antipanic drug phenelzine in brain: Effects of pretreatment with tranylcypromine, (–)-deprenyl and clorgyline. *Journal of Affective Disorders*, *35*(3), 125–129. [https://doi.org/10.1016/0165-0327\(95\)00056-9](https://doi.org/10.1016/0165-0327(95)00056-9)
- Votyakova, T. V., & Reynolds, I. J. (2004). Detection of hydrogen peroxide with Amplex Red: Interference by NADH and reduced glutathione auto-oxidation. *Archives of Biochemistry and Biophysics*, *431*(1), 138–144. <https://doi.org/10.1016/j.abb.2004.07.025>
- Waight, R. D., Leff, P., & Bardsley, W. G. (1977). Steady-state kinetic studies of the negative cooperativity and flip-flop mechanism for *Escherichia coli* alkaline phosphatase. *Biochemical Journal*, *167*(3), 787–798. <https://doi.org/10.1042/bj1670787>
- Waldmeier, P. C., Amrein, R., & Schmid-Burgk, W. (1994). Pharmacology and pharmacokinetics of brofaromine and moclobemide in animals and humans. In *Clinical Advances in Monoamine Oxidase Inhibitor Therapies* (pp. 33–59). American Psychiatric Press.
- Walters, B. T., Ricciuti, A., Mayne, L., & Englander, S. W. (2012). Minimizing back exchange in the hydrogen exchange-mass spectrometry experiment. *Journal of the American Society for Mass Spectrometry*, *23*(12), 2132–2139. <https://doi.org/10.1007/s13361-012-0476-x>
- Wang, S. X., Mure, M., Medzihradsky, K. F., Burlingame, A. L., Brown, D. E., Dooley, D. M., Smith, A. J., Kagan, H. M., & Klinman, J. P. (1996). A crosslinked cofactor in lysyl oxidase: Redox function for amino acid side chains. *Science (New York, N.Y.)*, *273*(5278), 1078–1084. <https://doi.org/10.1126/science.273.5278.1078>
- Wang, W., Gao, C., Hou, X., Liu, Y., Zong, Y., & Zhang, G. (2004). Activation and involvement of JNK1/2 in hydrogen peroxide-induced neurotoxicity in cultured rat cortical neurons. *Acta Pharmacologica Sinica*, *25*(5), 630–636.
- Westlund, K., Denney, R., Kochersperger, L., Rose, R., & Abell, C. (1985). Distinct monoamine oxidase A and B populations in primate brain. *Science*, *230*(4722), 181–183. <https://doi.org/10.1126/science.3875898>
- Westlund, K. N., Denney, R. M., Rose, R. M., & Abell, C. W. (1988). Localization of distinct monoamine oxidase a and monoamine oxidase B cell populations in human brainstem. *Neuroscience*, *25*(2), 439–456. [https://doi.org/10.1016/0306-4522\(88\)90250-3](https://doi.org/10.1016/0306-4522(88)90250-3)

- Williams, T., McCaul, M., Schwarzer, G., Cipriani, A., Stein, D. J., & Ipser, J. (2020). Pharmacological treatments for social anxiety disorder in adults: A systematic review and network meta-analysis. *Acta Neuropsychiatrica*, 32(4), 169–176. <https://doi.org/10.1017/neu.2020.6>
- Willis, G. L., & Kennedy, G. A. (2004). The implementation of acute versus chronic animal models for treatment discovery in Parkinson's disease. *Reviews in the Neurosciences*, 15(1). <https://doi.org/10.1515/REVNEURO.2004.15.1.75>
- Wood, P. L., Khan, M. A., Moskal, J. R., Todd, K. G., Tanay, V. A. M. I., & Baker, G. (2006). Aldehyde load in ischemia–reperfusion brain injury: Neuroprotection by neutralization of reactive aldehydes with phenelzine. *Brain Research*, 1122(1), 184–190. <https://doi.org/10.1016/j.brainres.2006.09.003>
- Yang, L., Omori, K., Otani, H., Suzukawa, J., & Inagaki, C. (2003). GABA<sub>C</sub> receptor agonist suppressed ammonia-induced apoptosis in cultured rat hippocampal neurons by restoring phosphorylated BAD level: GABA<sub>C</sub> receptor agonist restores phospho-BAD levels. *Journal of Neurochemistry*, 87(3), 791–800. <https://doi.org/10.1046/j.1471-4159.2003.02069.x>
- Yang, L., Omori, K., Suzukawa, J., & Inagaki, C. (2004). Calcineurin-mediated BAD Ser155 dephosphorylation in ammonia-induced apoptosis of cultured rat hippocampal neurons. *Neuroscience Letters*, 357(1), 73–75. <https://doi.org/10.1016/j.neulet.2003.12.032>
- Youdim, M. B. H., Edmondson, D., & Tipton, K. F. (2006). The therapeutic potential of monoamine oxidase inhibitors. *Nature Reviews Neuroscience*, 7(4), 295–309. <https://doi.org/10.1038/nrn1883>
- Yu, P. H., & Tipton, K. F. (1989). Deuterium isotope effect of phenelzine on the inhibition of rat liver mitochondrial mono amine oxidase activity. *Biochemical Pharmacology*, 38(23), 4245–4251. [https://doi.org/10.1016/0006-2952\(89\)90522-4](https://doi.org/10.1016/0006-2952(89)90522-4)
- Yu, P. H., Wright, S., Fan, E. H., Lun, Z.-R., & Gubisne-Harberle, D. (2003). Physiological and pathological implications of semicarbazide-sensitive amine oxidase. *Biochimica et Biophysica Acta (BBA) - Proteins and Proteomics*, 1647(1–2), 193–199. [https://doi.org/10.1016/S1570-9639\(03\)00101-8](https://doi.org/10.1016/S1570-9639(03)00101-8)
- Zapata-Torres, G., Fierro, A., Barriga-González, G., Salgado, J. C., & Celis-Barros, C. (2015). Revealing monoamine oxidase B catalytic mechanisms by means of the quantum chemical cluster approach. *Journal of Chemical Information and Modeling*, 55(7), 1349–1360. <https://doi.org/10.1021/acs.jcim.5b00140>
- Zeller, E. A. (1938). Über den enzymatischen abbau von histamin und diaminen. 2. Mitteilung. *Helvetica Chimica Acta*, 21(1), 880–890. <https://doi.org/10.1002/hlca.193802101115>